

DISCERNING THE CHEMICAL REACTIVITY OF COVALENT
SURFACE-FUNCTIONALIZED ORDERED MESOPOROUS
CARBON NANOPARTICLES THROUGH OXIDATIVE
COUPLING AND ORGANOLITHIUM
MEDIATED APPROACHES

by

Nolan Christopher Kovach

© Copyright by Nolan Christopher Kovach, 2024

All Rights Reserved

A thesis submitted to the Faculty and the Board of Trustees of the Colorado School of Mines in partial fulfillment of the requirements for the degree of Doctor of Philosophy (Applied Chemistry).

Golden, Colorado

Date _____

Signed: _____

Nolan Christopher Kovach

Signed: _____

Dr. Brian G. Trewyn
Thesis Advisor

Golden, Colorado

Date _____

Signed: _____

Dr. Thomas Gennett
Professor and Chemistry Department Head
Applied Chemistry

ABSTRACT

Porous carbons materials are particularly attractive to study and utilize due to their high surface area, chemical resistance towards high and low pHs, and inherent thermal & electrical conductivity. However, many porous carbons are relatively devoid of reactive surface chemical functionality, primarily comprising sp^2 C-C bonds (both planar or strained/curved) and sp^3 C-H bonds, being both inherently hydrophobic and nonreactive towards chemical attack.

Post-synthetic modifications instill new chemical groups on carbon surfaces to imbue new functionality. Covalently modified carbons are preferred to retain surface functionality over time relative to leachable non-covalently surface bound adsorbates. Catalyst and adsorbent regeneration, as well as operating conditions for electrodes call for the immersion of carbon into acid or base at concentrations which can degrade some material surfaces. Despite there being many covalently modified carbon materials, there is a dearth of knowledge regarding pH ranges which these can operate while retaining surface functionality.

Ordered mesoporous carbon (OMC) hard templated from mesoporous silica nanoparticles were selected for primary amine surface modification by two methods—wet chemical oxidation and organolithium activation—to explore differences in etheric and carbon-carbon surface bonding. The former method installs surface hydroxyls through the Fenton reaction which then undergo a Williamson ether-like synthesis to furnish ether bonds. The latter technique furnishes C-C bonds by means of an alkyllithium to deprotonate C-H moieties on the carbon surface followed by an S_N2 reaction with an electrophile.

OMC and hydroxylated OMC were reacted with haloethylamines, giving rise to surface ethylamine groups appended by C-C and C-O-C bonds, respectively. Particle stability and surface amine presence were examined before and after immersion in pH 14 (in sodium

hydroxide) and pH 0-3 (in hydrochloric acid). Particle physical characterization included nitrogen sorption, low-angle X-ray diffraction, and both scanning and transmission electron microscopy. The primary amine moiety was qualitatively identified by point-of-zero charge and quantified by a 4-nitrobenzaldehyde colorimetric assay, enabling the amine density on the OMC materials to be calculated. The aminated OMCs were proven to retain catalytic activity over multiple reaction cycles as a heterogeneous base catalyst for the Knoevenagel condensation reaction. Most importantly, the acid and base immersion results directly inform which pH environments these types of covalently modified OMC materials can, and cannot be used in. Knowledge from this dissertation's research campaign may inspire scientists developing other types of functional carbon materials to consider their work beyond the scope of a singular application.

TABLE OF CONTENTS

ABSTRACT	iii
LIST OF FIGURES.....	vii
LIST OF TABLES	x
LIST OF ABBREVIATIONS	xi
ACKNOWLEDGMENTS.....	xiii
CHAPTER 1 STRATEGIES FOR POST-SYNTHETIC FUNCTIONALIZATION OF MESOPOROUS CARBON NANOMATERIAL SURFACES	1
1.1 Abstract.....	1
1.2 Introduction.....	2
1.3 Physisorption Processes	9
1.4 Chemisorption Chemistry	21
1.5 Conclusion and Outlook.....	29
1.6 References.....	31
CHAPTER 2 OMC AMINATION BY ORGANOLITHIUM ACTIVATION TO CONFER C-C LINKAGES WITH PENDANT PRIMARY AMINES	44
2.1 Abstract.....	44
2.2 Introduction.....	45
2.3 Material Synthesis.....	49
2.4 Physicochemical Characterizations.....	50
2.5 Results and Discussion	54
2.6 Conclusion	67
2.7 References.....	68
CHAPTER 3 ASSESSING THE ACIDIC AND ALKALINE STABILITY OF COVALENTLY BOUND SURFACE AMINES ON ORDERED MESOPOROUS CARBON SCAFFOLDS	74
3.1 Abstract.....	74
3.2 Introduction.....	75
3.3 Experimental Section	79
3.4 Material Characterization.....	80
3.5 Results and Discussion	82
3.6 Conclusion	101

3.7	References.....	102
CHAPTER 4 EXPOUNDING THE APPLIED SCOPE OF THE ORGANOLITHIUM AND HYDROXYLATION-ETHERIZATION METHODS.....107		
4.1	Abstract.....	107
4.2	Improvements to the Organolithium Method.....	107
4.3	Improvements to Hydroxylation-Etherization	110
4.4	Final Remarks	118
4.5	References.....	119
APPENDIX A PERMISSIONS FROM PUBLISHERS124		
APPENDIX B PHYSISORPTIVE DECORATION OF OMC BY N,N,N,N-TETRAOCTYLDIGLYCOAMIDE FOR F-ELEMENT SEQUESTRATION.....127		
B.1	Introduction.....	127
B.2	Probing Eu ³⁺ Uptake on TODGA Modified OMC	128
B.3	Towards the Covalent Grafting of f-Element Extractants.....	132
B.4	References.....	134
APPENDIX C RAW DATA FOR PREVIOUS CHAPTER MEASUREMENTS136		

LIST OF FIGURES

Figure 1.1.	(a) A simplified model illustrating a Stone-Wales defect formation (b) Single point defect producing a highly strained, bent system with a characteristic “dangling bond” depicted by the dashed red line. (c) Double point defect morphing a flat carbon frame into a strained system alike to that made from single point defect. 5	5
Figure 1.2.	Molecular depiction of the most typical oxygen moieties found on carbon surfaces. For aesthetic purposes, oxygen (O) functional groups are pinned to the distal edge of the carbon and all reside within the page plane. 8	8
Figure 1.3.	Electron microscopy images depicting MC synthesis routes which highlights the diversity of possible architectures that can be made from different synthetic techniques. Scale bar is 1 μm for all images. (From top to bottom, all with permission) Adapted from Ref. 43. Copyright: Elsevier 2009. Adapted from Ref. 126. Copyright: ACS 2016. Adapted from Ref. 44. Copyright: Wiley 2011. Adapted from Ref. 45. Copyright: Elsevier: 2019. Adapted from Ref. 46. Copyright: ACS 2018. Reprinted from Ref. 47. 10	10
Figure 1.4.	TEM images depicting MNPs deposited using an <i>ex situ</i> MNP synthesis (A), and MNP prepared by liquid immersion (B). (A) Reproduced from Ref. 85 with permission. Copyright: Elsevier 2020. (B) Adapted from Ref. 86 with permission. Copyright: Springer Nature 2020..... 16	16
Figure 1.5.	Surface hydroxyl functionalization with functional trialkoxysilanes. 24	24
Figure 1.6.	Schematic of an EDC coupling of a peptide to an MC support. Reprinted with permission from Ref. 126. Copyright: Elsevier 2019. 25	25
Figure 1.7.	Two-step process for grafting a bipyridine (Bpy) ligand onto MC through organolithium C–H activation. Reproduced with permission from Ref. 130. Copyright: American Chemical Society 2014. 26	26
Figure 2.1.	Elementary depiction of the Knoevenagel condensation between an aldehyde and an “active” methylene reactant containing electron withdrawing groups (EWG)..... 45	45
Figure 2.2.	Nitrogen sorption isotherms for OMC (solid black trace) and EtNH ₂ @OMC (dotted red trace) materials with a BJH desorption pore size distribution plot (inset)..... 55	55
Figure 2.3.	Scanning electron micrographs showing particle morphology preservation between the MSN-10 template (left) and OMC (right). Scale bar: 1 μm 56	56
Figure 2.4.	Transmission electron micrographs of OMC (left) and EtNH ₂ @OMC (right)..... 57	57
Figure 2.5.	Powder XRD patterns of OMC and EtNH ₂ @OMC. Step size: 0.002°; scan rate: 0.50 sec/step..... 58	58
Figure 2.6.	FTIR-ATR spectra obtained for unfunctionalized OMC and EtNH ₂ @OMC highlighting motifs pertaining to the amination..... 60	60
Figure 2.7.	Thermogravimetric traces obtained for OMC (black trace) and EtNH ₂ @OMC (dotted red trace) under 10 °C · min ⁻¹ ramp rate. 61	61
Figure 2.8.	TGA and DTG curves for EtNH ₂ @OMC..... 62	62

Figure 2.9.	Conversion to benzylidenemalononitrile using various solid porous catalysts. Reaction conditions: benzaldehyde (2 mmol), malononitrile (3 mmol), MeOH (6.0 mL), 550 rpm, 40 °C, 4 h.....	64
Figure 2.10.	Proposed mechanism of the Knoevenagel condensation mediated by surface-bound primary amine groups on OMC involving an imine formation to initiate the abstraction of the acidic malononitrile hydrogen.....	65
Figure 2.11.	Catalyst conversion over five cycles for EtNH ₂ @OMC.....	66
Figure 2.12.	Initial rates of product formation for three rounds of catalysis.....	67
Figure 3.1.	Methods for selective hydroxylation of carbon surfaces by means of (A) Fenton reaction using FeSO ₄ ·7H ₂ O and 30% H ₂ O ₂ , (B) Nitric acid oxidation followed by sodium aluminum hydride reduction, and (C) Sodium aluminate surface complexation followed by NaOH hydrolysis.....	78
Figure 3.2.	Point of zero charge assessment by the pH drift method.....	83
Figure 3.3.	Boehm titration results for NaOH treated oxOMC using 0.01N Na ₂ CO ₃ as the titrant solution.....	84
Figure 3.4.	Nitrogen adsorption isotherms for OMC (A) and oxOMC (B) materials before and after functionalization, and after acid and base exposure.....	86
Figure 3.5.	Nitrogen sorption isotherms with BJH desorption pore size distribution inset for EtNH ₂ @oxOMC tested at pH 1, 2, and 3.....	87
Figure 3.6.	Low-angle X-ray diffractograms for the tested OMC materials before and after acid and base testing.....	90
Figure 3.7.	Bright field transmission electron micrographs showing particle size and shape similarity for OMC (A) and oxOMC (B), as well as the aminated versions, EtNH ₂ @OMC (C) and EtNH ₂ @oxOMC (D). Scale bar = 100 nm.....	92
Figure 3.8.	Transmission electron microscope images showing preservation of parallel mesopores after acid exposure (left) and base exposure (right) for EtNH ₂ @OMC (top) and EtNH ₂ @oxOMC (bottom). Scale bar = 100 nm.....	93
Figure 3.9.	Thermogravimetric decomposition for OMC, oxOMC, EtNH ₂ @OMC, and EtNH ₂ @oxOMC performed under air flow.....	95
Figure 3.10.	FTIR spectra exhibiting signals for methylene-CH motions (top) and N-H bending and aryl C-H motions (bottom) for OMC and EtNH ₂ @OMC.....	97
Figure 3.11.	Curve-fitted XPS spectra of the C 1s core level for EtNH ₂ @oxOMC and EtNH ₂ @OMC, post HCl and post NaOH treatment. On the right, overlaid C 1s and O 1s of EtNH ₂ @oxOMC and EtNH ₂ @OMC spectra that has been background subtracted and normalized at peak maximum to emphasize differences due to treatment.....	99
Figure 3.12.	Boehm titration NaHCO ₃ and Na ₂ CO ₃ trial results for oxOMC.....	105
Figure 3.13.	N 1s spectra of EtNH ₂ @oxOMC and EtNH ₂ @OMC, both post HCl and post NaOH... 106	106
Figure 4.1.	Proposed reactions for preparation of the amine-enriched fly ash sorbent.....	113

Figure 4.2.	Introduction of phenyl esters, carboxylic acids or methyl ethers by utilizing hydroxyl surface groups of a reduced carbon as nucleophiles.....	114
Figure 4.3.	Mechanism of ethylamine surface cleavage occurring at the etheric oxygen.....	115
Figure 4.4.	Mechanism for amine liberation by means of SN2 attack by the etheric oxygen.....	116
Figure 4.5.	Mechanism of deamination from chloride SN2 attack on the amine α carbon.....	116

LIST OF TABLES

Table 1.1.	Examples of MNP deposition conditions onto MC supports. U=Ultrasonication.	18
Table 1.2.	A list of non-covalently appended polymers to MC supports.....	19
Table 1.3.	A list of recently reported diaza-linked molecules onto MC substrates.....	27
Table 2.1.	Nitrogen sorption-derived BET surface area ($0.10 < P/P_0 < 0.22$) and BJH desorption pore volume and pore size distributions.....	54
Table 2.2.	Elemental microanalysis (wt. %) for the analyzed elements. Nitrogen content obtained by the Dumas method.....	63
Table 3.1.	Nitrogen sorption derived porosity metrics for all materials, before and after testing. The BET SA was calculated between 0.02 and 0.18 P/P ₀ . *BJH desorption branch derived values.	85
Table 3.2.	Porosity metrics for EtNH ₂ @oxOMC exposed to pH 1, 2, and 3.....	88
Table 3.3.	Results from the 4-Nitrobenzaldehyde colorimetric assay for materials at all stages.....	95
Table 3.4.	Detected wt. % of selected elements by elemental combustion microanalysis.....	101

LIST OF ABBREVIATIONS

Mesoporous Carbon	MC
X-ray Diffraction	XRD
Low-Angle X-ray Diffraction	LA-XRD
Secondary Ion Mass Spectrometry	SIMS
X-ray Photoelectron Spectroscopy	XPS
Temperature-Programmed Desorption	TPD
Fourier-Transform Infrared Spectroscopy	FTIR
Metal Nanoparticle	MNP
Metal-Organic Framework	MOF
Incipient Wetness	IW
Differential Scanning Calorimetry	DSC
Energy Dispersive X-ray	EDX
Chemical Vapor Deposition	CVD
Acetylacetone	acac
Azobisisobutylnitrile	AIBN
Polyvinylpyrrolidone	PVP
1,2-Distearoyl-sn-glycero-3-phosphoethanolamine-Poly(ethylene glycol)	DSPE-PEG
Polyethyleneimine	PEI
1-Ethyl-3-(3-dimethylaminopropyl)carbodiimide	EDC
N-hydroxysuccinimide	NHS
2-(N-morpholino)-Ethanesulfonic Acid	MES
Tetrahydrofuran	THF
Single-stranded DNA	ssDNA
Carbon Nanotubes	CNTs
Bipyridine	bpy
Electrochemical Reduction	ER
Solid-State Nuclear Magnetic Resonance	ssNMR
N,N,N,N-Tetraoctyldiglycoamide	TODGA
Small-Angle X-ray Scattering	SAXS

Wide-Angle X-ray Scattering	WAXS
Ordered Mesoporous Carbon	OMC
N-(2-hydroxyethyl)ethylenediamine-N,N',N'-triacetic acid.	HEDTA
Electron Withdrawing Group	EWG
Graphitic Carbon Nitride	gCN
Mesoporous Silica Nanoparticle	MSN
Brunauer-Emmett-Teller	BET
Barrett-Joyner-Helenda	BJH
4-Nitrobenzaldehyde	4-NB
Scanning Electron Microscopy	SEM
Transmission Electron Microscopy	TEM
Highly-Oriented Pyrolytic Graphite.	HOPG
Polymer-derived Carbon.	PDC
P,P'-di(2-ethylhexyl)methanediphosphonic acid.	DIPEX
Octylphenyl-N,N-diisobutyl Carbamoylphosphine Oxide	CMPO

ACKNOWLEDGMENTS

The appreciation for the support provided from a gamut of amazing individuals throughout my Ph.D. journey is unparalleled. To my family: Despite being more than a thousand miles away, you have remained steadfastly in my heart and have only shown me unconditional love throughout my PhD journey; I am eternally grateful for you all. To my friends: Thank you for empowering me to develop as an adult. Your emotional and financial aid will never be forgotten. To my committee members: Thank you for your undying support through all phases of my doctorate journey. My growth as an independent researcher is largely due to your assistance, critiques, and conversations, and I will always have a warm spot in my heart for you.

CHAPTER 1 STRATEGIES FOR POST-SYNTHETIC FUNCTIONALIZATION OF MESOPOROUS CARBON NANOMATERIAL SURFACES

Modified from a paper published in *Microporous and Mesoporous Materials*¹

Nolan C. Kovach^{2,3}, Glory A. Russell-Parks³, Brian G. Trewyn^{4,5}

1.1 Abstract

Most widely used carbon-based materials feature a bulk framework tolerant of extreme pH and temperature conditions while maintaining physical robustness, electrical conductivity, and biological relevance due to its inherent nontoxicity. At the nanoscale, the study of porous carbons has been of interest because of the enhanced accessible surface area relative to nonporous analogues. The evolution of synthetic techniques has developed structural allotropes with tunable internal pore diameter averages spanning from sub-nanometer to micron-plus sizes. Within the mesopore range, surface chemical phenomena abide by a kinetic-limited ruleset (ignoring the effects of bulk diffusion, as they do not pertain to this size regime). Further, mesopores provide sufficient volume and surface area for hosting relatively large guest species, including metal nanoparticles, polymers, organic molecules, and biomolecules like enzymes and DNA. These two unique features of mesoporous carbon drive interest in surface modifications to create new physicochemical functionality to these systems and their hosted species. As a result, the evolution of mesoporous carbon surface modification techniques has been scattered to disparate niches across the literature. Being the case, a large burden is placed into the hands of

¹ Reprinted with permission of Elsevier 2023. *Microporous Mesoporous Mater.* **2022**, 329, 111453.

² Primary researcher and author

³ Graduate student, Chemistry Dept., Colorado School of Mines

⁴ Associate Professor, Chemistry Dept., Colorado School of Mines

⁵ Research Joint Appointment, National Renewable Energy Laboratory (NREL)

applied mesoporous carbon material researchers to be thorough with literature precedent knowledge.

There exist considerable differences between applied research fields when it comes to the conditions—be it temperature, pressure, or pH—in which functionalized mesoporous carbons are used. Additionally, the structure of modern research often relies on project funding to study a singular application, thereby forcing researchers to study functionalized materials in a limited scope. This dissertation chapter is structured to inform the reader on recent (within about a decade) publications of post-synthetically functionalized mesoporous carbon materials that are categorized by the surface chemical structures they possess, rather than the application in which they are studied. Abiding by the core tenet of chemistry being, “structure derives function”, the compilation of functionalized mesoporous carbon references by their functionalized surface structure is intended to enable researchers to take that information and utilize it for their own applications.

1.2 Introduction

The motivation to develop materials that can effectively address energy and environmental needs on the global scale is evermore necessary given the worsening inequity for humans on Earth. Among these material solutions reside the application of surface-modified mesoporous carbons. The shift away from polluting energy sources steered research towards flavors of advanced energy like H₂ production/storage, Li/Na-S batteries, fuel cells, solar devices and bioreactors. The scarcity of clean water continues to pervade the world, as only 71% of the global population had access to potable water in 2017 according to the World Health Organization.¹ To remediate this pervasive issue, water desalination with solid phase sorbents is currently undergoing a research revolution.²⁻⁴ Mesoporous carbon (MC) has been shown to sorb

recalcitrant organic pollutants that cannot be effectively removed by other carbonaceous structures,⁵⁻⁷ as well as behave as an electrode for microbe remediation from potable water streams, leveraging the uniquely inherent conductivity of carbon.⁸ Also, the Earth's atmosphere is amassing record amounts of greenhouse gases whose negative effects will continue to deleteriously affect both nature and humanity. The environmental sequestration of the most harmful gases (like methane, carbon dioxide, and nitrogen oxides) into inert species *via* sorption or valorization are two modernly applied functionalized mesoporous carbon techniques.^{9, 10} The oil and gas industry implements solid phase sorbents at large scale, used for sweetening (removal of hydrogen sulfide and carbon dioxide),¹¹ desulfurization (removal of sulfur-based gas components),^{12, 13} and demercuration¹⁴ processing steps. Moreover, modern medical research relies heavily on biocompatible composites for the improvement of theranostic imaging¹⁵ and targeted drug delivery.¹⁶ Amongst these global concerns, MCs also find use in other niche applications such as *f*-element separation,¹⁷⁻¹⁹ microwave absorbers,²⁰ chemical warfare agent deactivation,²¹ *in vivo* sensing^{22, 23} and commodity gas purifications.²⁴ Each of these, and even more, research paths have a technological bleeding edge relying on the surface functionalization of mesoporous carbon nanomaterials.

Chemical Features of Carbon in 3-D Allotropes

The shape, size, topology and ordering of pores vastly differ amongst the types of MC nanomaterials. The different surface chemistries of MC materials are discussed in terms of commonly shared, exploitable carbon chemical functionalities imbued into a mesoporous scaffold. For most macromolecular carbon systems, the framework is composed of highly conjugated sp^2 carbons in a mix of hexagonal and pentagonal arrangements.^{25, 26} The aromatized, planar constituents of the surface impart electrical conductivity to the framework; departure from

this flatness derives the 3-D topology and, oftentimes, a cylindrical pore network. The delocalized nature of the sp^2 electrons present on the surfaces have a tendency to sorb hydronium (H_3O^+) ions.²⁷ Defects impinge flatness *via* sp^3 carbon sites. To note, these defects are non-crystallographic; MC materials exhibit amorphousness under high angle X-ray diffraction (XRD) analysis ($20-35^\circ 2\theta$). Low-angle XRD (LA-XRD) elucidates the presence of mesopore ordering ($0.25-5^\circ 2\theta$), and thus a signal can be obtained for this feature, though it is important to note that this does not imply crystallinity, only pore ordering. Carbon defects range from Stone-Wales (non-substitutional geometric rearrangement) and single point defects to multiple point defects and line dislocations (Figure 1.1).²⁸

A Stone-Wales defect is defined by a 90° twist in the central carbons, resulting in formation of two 5-membered and two 7-membered rings from four 6-membered rings whilst maintaining planarity, yet increasing strain. Single point defects impart buckling and exist as surface protrusions.²⁹ These surface features are also hydrophobic but hamper electron mobility through the bulk material. Note the energy required to create two defects is only marginally higher than that for a single; double point defects are more common, as the average energy to induce a vacancy is about half of that for a single defect. C-H defects tend to be dispersed evenly throughout and preferentially at pore edges, providing points for potential functionalization *via* C-H activation chemistry. These energetic sites may quench with the carbon itself (creating a localized surface disruption) or combine with ambient oxygen (effectively doping the surface with oxygen in some form) which will be discussed later.

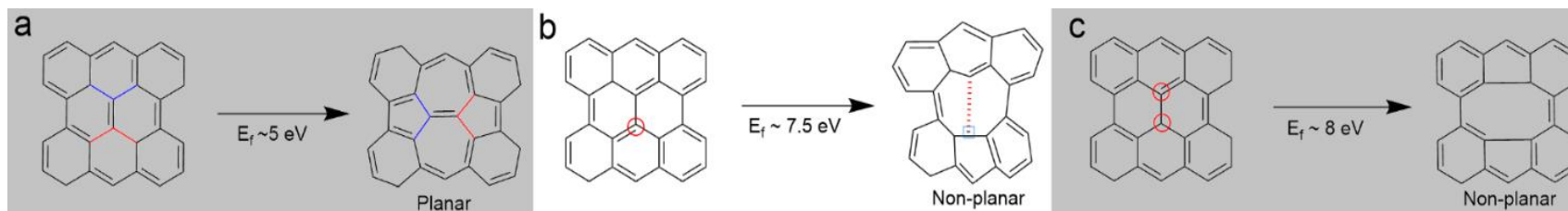


Figure 1.1. (a) A simplified model illustrating a Stone-Wales defect formation (b) Single point defect producing a highly strained, bent system with a characteristic “dangling bond” depicted by the dashed red line. (c) Double point defect morphing a flat carbon frame into a strained system alike to that made from single point defect.

Investigating the physiochemical properties of MCs often necessitates the combination of multiple characterization methods, with each technique providing another layer of information. Raman spectroscopy noninvasively probes the presence of disordered (D, sp^3) and graphitic (G, sp^2) carbons in a sample, which give rise to strong adsorption peaks centered around 1350 cm^{-1} and 1594 cm^{-1} , respectively. The ratio of the peak intensities (I_D/I_G) elucidates the structural rigidity of the bulk material. Disorder and defects are more prominent with a higher D/G ratio; features that disrupt aromaticity, reducing electrical conductivity.^{28, 30} Likewise, thermal conductivity is attenuated by the tendency of phonons to scatter at the defect sites. Secondary ion mass spectrometry (SIMS) presents similar information but relies on surface ablation of the sample to be ejected to a detector. The production of C_2^- and C_2H^- is inferred to arise from interior, planar carbons and edge, defect site carbons, respectively. Though considered quasi-destructive, a SIMS experiment can provide insight on the relative polyaromaticity of the surface by the C_2H^-/C_2^- ratio, where a smaller value indicates a more planar surface.²⁶ If available, low-pressure nitrogen sorption allows for the determination of graphitic order. To obtain such data, a sorption instrument would need to be outfitted with transducers that can register low partial pressures (P/P_0), as low as 10^{-7} , where monolayer formation is observed. Manipulation of the original isotherm into its corresponding adsorption potential distribution allows for an accurate determination of the surface adsorption potential.^{31, 32} For carbons, this tends to fall between 4-10 $\text{kJ} \cdot \text{mol}^{-1}$, with lower values indicating less graphitization. From a physical standpoint, the atomic roughness imparted by defects prohibits the packing of the dosed nitrogen. X-ray photoelectron spectroscopy (XPS) deconvolution of the parent C peak elucidates an averaged coordination environment of topical carbons. To obtain the most accurate carbon XPS information, the collected peak must be fit to the number of possible C-X bonding environments,

where X should include H, C and O, and any other element that could be present in the carbon matrix. Synthetically, nearly all engineered carbon fabrication methods rely on high temperature/pressure conditions; carbons produced at higher temperatures exhibit greater graphitization and thus conductivity at the cost of frame embrittlement and energy input.

Surface Oxygen Speciation

MC materials can contain a number of different oxygen moieties, typically as an inhomogeneous mixture in varying limited quantities (typically less than 10 at%). Both identity and amount of oxygenation are largely dependent on the methods of post synthetic treatment. A crowded representation of oxygen functional groups that occupy MC surfaces (Figure 1.2). The collection of functionalities is comprised of both acidic (red) and basic sites (blue). Surface basicity of a porous carbon replete of surface oxide has been measured as $0.59 \text{ meq} \cdot \text{g}^{-1}$.³³ Oxygenation can incorporate within the surface, increasing topical roughness, hydrophilicity and polarity.

Porous carbons characterized with CO temperature-programmed desorption (TPD) can speciate carboxylic anhydrides, phenols, carbonyls, quinones and etheric components present while CO₂ TPD elucidates carboxyl and lactone functionality.³⁴ The Boehm titration method provides a handle to measure the acidity derived from phenols, lactones and carboxyls.

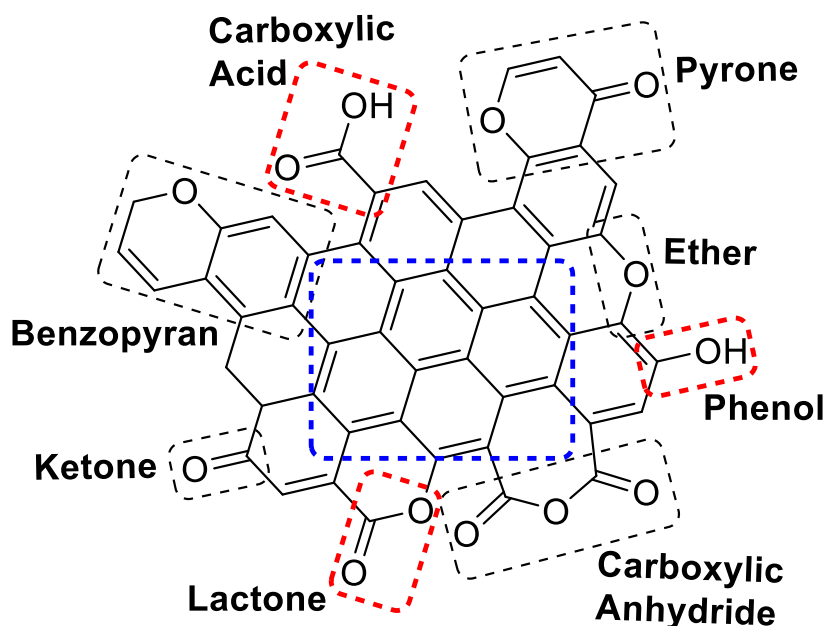


Figure 1.2. Molecular depiction of the most typical oxygen moieties found on carbon surfaces. For aesthetic purposes, oxygen (O) functional groups are pinned to the distal edge of the carbon and all reside within the page plane.

The precursors for MC and synthetic conditions dictate the degree of oxygenation of the final product, as well as post-synthetic protocols. The presence of oxygen on MC surfaces alters the hydrophilic nature and electron density of the material, which can influence overall performance. Unavoidably, oxygenation imparts topological deformation to the framework. As-made scaffolds commonly undergo an oxidation or reduction which changes the surface hydrophilicity. Acid chemical activation will tend to give rise to acidic functionality and imbue the carbon with increased micropore surface area. The quest to oxidize carbon nanomaterials with specific oxygen functionality in a single step is still being pursued; thus, most oxidations performed with current methods are considered “bulk” in that they incorporate multiple forms of oxygen groups into the carbon surface network. Determining which functional groups are present on a carbon surface is possible through a few characterization techniques.

Spectroscopically identifying O-groups in bulk carbon substrates can be determined through Fourier transform infrared spectroscopy (FTIR) to uncover hydroxyl ($\sim 3500\text{ cm}^{-1}$) and carbonyl ($\sim 1700\text{ cm}^{-1}$) motifs, which can elucidate phenolics, carboxyls, ethers and ketones. When available, oxygen XPS can corroborate and clarify bond lengths of oxygen present, verifying its functional contributions. TPD is a non-spectroscopic technique where a sample is heated under an inert gas flow and a downstream detector senses the presence of decomposition products of various O groups originating from the MC surface (typically CO or CO₂). There are reviews that detail carbon material oxidation and reduction, and these phenomena are beyond the scope of this review.^{27, 35, 36} Rather, this review will discuss the diversity of chemical transformations of common types of oxygen functional group found on MC surfaces and the implications in an applied scope.

1.3 Physisorption Processes

There exists a vast number of procedures to produce MC nanomaterials. The MC morphology, size, shape and surface chemical properties will all be unique to the given synthetic protocol (Figure 1.3).³⁶ What is similar in all of these different MC is the internal porosity that is comprised of interconnected networks, sometimes ordered, where pore diameters range between 2 nm and 50 nm.

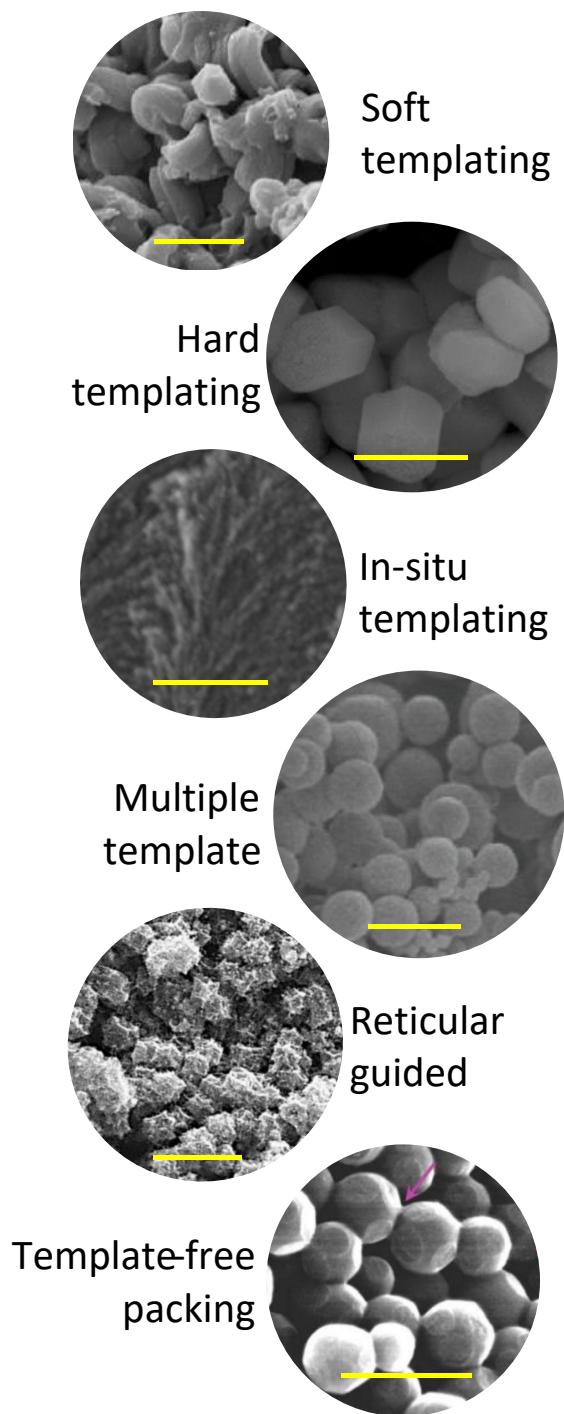


Figure 1.3. Electron microscopy images depicting MC synthesis routes which highlights the diversity of possible architectures that can be made from different synthetic techniques. Scale bar is 1 μm for all images. (From top to bottom, all with permission) Adapted from Ref. 43. Copyright: Elsevier 2009. Adapted from Ref. 126. Copyright: ACS 2016. Adapted from Ref. 44. Copyright: Wiley 2011. Adapted from Ref. 45. Copyright: Elsevier: 2019. Adapted from Ref. 46. Copyright: ACS 2018. Reprinted from Ref. 47.

The mesoporous size regime is suitable for the non-covalent incorporation of metal nanoparticles (MNPs), biomolecules and polymers with a MC framework. From an atomic viewpoint, there are no explicit bonds that form between the adsorbate and the MC surface, and intramolecular distance is limited by sterics or electrostatics. Hydrophobic substrates lend well to sorption resultant of favorable intramolecular van der Waals forces. Alternatively, physical defect sites can initiate nucleation for metal clusters forming *in situ* or behave as deposition sites for pre-synthesized MNPs due to localized surface energy disruption. Since many physicochemical (catalytic) properties of metals, metal oxides and alloys emerge at the nanoscale, MCs with varying pore diameters can accommodate MNPs imparting drastically different reactivity. Enzymes encapsulated within MC pore framework observe activity at non-biological conditions, which would otherwise deactivate the same unprotected enzyme. Macromolecular structures (polymers, metal-organic-frameworks (MOFs), covalent organic frameworks) are ubiquitous in applied science, and the fusion with MCs impart recyclability and durability to the guest structures (nanoparticles, metal clusters, DNA) akin to enzymes. In order to optimize the useful properties of physisorbed species, achieving monodispersion across the MC surface is key. Techniques utilized for achieving monodispersity will be discussed in later sections. Apart from conformally coated macromolecules, sorbed species must remain stationary on the surface; agglomeration due to surface mobility decreases the catalyst accessibility (activity), limiting the performance of the system. It is a known bottleneck for MC supported MNPs where the working conditions of these systems (requiring high temperatures, electrical potentials, extreme pH and/or biological duress) are also the conditions where nucleation/agglomeration arise. In other words, top performance has been demonstrated in

systems where the operating environment is very near the limits of physical deactivation of the adsorbate.

Surface Coverage with Small Organics

The ability of MCs to uptake and release bulky, 3-D molecular cargo is advantageous for many applications and is possible due to the tunable cavity dimensions of MC nanomaterials.³⁷⁻⁴⁷ The inherent lipophilicity of MC poises it as an ideal carrier for low water-soluble compounds such as pharmaceuticals. Small molecules are also utilized for decorating MC, though this phenomenon is not enabled or limited by the pore size. While small molecules diffuse through micropore networks, larger particles and molecules are restricted from diffusion into microporous (<2 nm diameter) materials. Unlike larger nanoparticles, which suffer substantially from intra-surface agglomeration, small molecules more often leach off the surface. For most applications with the exception of drug delivery, leaching is a hinderance to applied performance. In the case of multilayer sorption, the intermolecular π -stacking of the sorbent is in opposition to the molecule dissolution. Grafting onto unmodified MC nanomaterials, hydrophobic forces are tantamount to an adsorbates' tendency to avoid leaching. The loading of small organics into MC pores is corroborated by nitrogen sorption; an experimentally-backed model which uses Langmuir adsorption has been developed to provide an accurate determination of lipophilic drug loading into MC pores.³⁹ In contrast, the ability to sorb molecules makes MC nanoparticles ideal for water purification and for detecting trace organic compounds.^{48, 49} As no gas-phase depositions are known, loading small molecules is performed in solution.

Incipient wetness (IW) impregnation from a quantified (typically through ultraviolet-visible light spectrophotometry or GCMS) parent solution onto a suspension of MCs occurs following a period of equilibration between the surface concentration and solution concentration of deposited

analyte. Deposition from IW tends to be prescribed in aqueous solutions. Alternatively, evaporative drying takes a known amount of analyte dissolved in a volatile solution, introduces it to the MC material and mixes until evaporation is complete. Evaporative drying is analogous to IW loading, replacing the equilibration phase with solvent removal. In many cases, deliberate action is needed when performing aqueous IW depositions to pre-wet the MCs. Stirring samples over long periods of time (days) can achieve this, as can ultrasonication for hours. The wetting of mesoporous capillaries is understood through the Laplace equation, which established an inverse relationship between a pore diameter and the pressure drop along the liquid-solid interface.⁵⁰ Thus, adopting an IW method to a MC with a different pore diameter may require time adjustments to be made to the wetting step. Evaporative drying can avoid the wetting issue, permitting the analyte is sufficiently soluble in the non-aqueous solvent. Attempts to melt-cast compounds into MC pores have proven to be ineffective for two reasons: solid melts are too viscous to permit diffusion into the mesopores and the exterior-bound compounds tend to crystallize.⁵¹

Both techniques furnish non-crystalline deposits that can be easily identified with differential scanning calorimetry (DSC) and XRD, the absence of characteristic adsorbate peaks from the spectra deduces this claim. Typically, a crystalline signal implies its crystallinity outside of a MC pore, meaning the alleged pore-loaded MC is contaminated with exterior-bound adsorbate agglomerations. Changes in porous material nitrogen sorption measurements can infer small molecule pore occupation. Electron microscopy energy dispersive X-ray (EDX) can corroborate small molecule loading when detectable elements are present in the adsorbed species. High-resolution SEM and TEM can also identify exterior-bound agglomerates.

Metal Nanoparticle Modification

The presence of O-groups is vital for placing metal nanoparticles (MNP) onto MC surfaces. Here, MNP broadly encompasses zero-valent (metallic), metal-oxide, metal-nitride, metal phosphide and polymetallic alloys. Many routes can achieve this modification. The state-of-the-art for immobilizing MNPs is to integrate heteroatoms such as N, B and S within the carbon framework (referred to as heteroatom species in a carbon framework). The heteroatom islands serve as preferential nucleation points for common MNP precursors; the stabilization of metal salts to the heteroatom nodes reduces a growing particle's propensity to migrate.⁵² These doped materials are carbon-heteroatom composites which have been extensively reviewed and will not be discussed in this review.⁵²⁻⁵⁸

Nanoparticles synthesized *ex situ* can be introduced to a MC *via* post-grafting. Briefly, a suspension of MNPs is introduced to a MC host through an IW procedure. Penetration of the MNPs into a MC scaffolding relies on the MNP relative size to the host MC pore diameter. It is also to note that there is no evidence to show that the MNPs congregate at oxygen surface groups. Shape, size and composition of MNPs are synthetic handles that guide rational design for hybrid MNP-MC materials. While post-grafting methods rely on the same principle, nuances reside in preparing the MC and MNPs for implantation. Hydrophobically capped particles can be beneficial due to enhanced dispersion with the tradeoff of bulkiness. In order to remove any nanoparticle capping agents, inert atmosphere thermal treatment of post-grafted MNPs is used to strip those compounds.

In situ growth of MNPs has been developed through an extension of IW precursor loading. A MC support is immersed in liquid solution of metal salt precursor(s) where metal salts undergo a concurrent reduction and nanoparticle ripening. Liquid phase reduction or evaporative drying

type processes are followed. Liquid phase reduction employs chemical reductants (citric acid, NaBH₄, NaOH) for nanoparticle formation, with milder and nontoxic chemicals preferred for safety reasons. The surface hydrophilicity facilitates diffusion of aqueous reactants which enables MNP formation throughout the internal pore network. Methods for liquid phase reduction are commonly water or alcohol-based given the solubility of the metal precursors. Moreover, the relative size of nanoparticle to the MC support dimensions dictates the effectiveness of MNP dispersion. Electron microscopy illustrates MNP agglomerating and depositing outside of the pores for Pt₂CuNi (Figure 1.4A), because of the MNP diameters exceeding that of the pore network.⁸⁵ Alternatively (Figure 1.4B) shows ordered pores with no resolvable Pt nanoparticles.⁸⁶ Upon further inspection by EDX, it is shown that the impregnated Pt MNPs (from glutathione-capped Pt clusters) are distributed throughout the MC framework. All the claimed TEM observations were corroborated with nitrogen sorption data, showing a negligible reduction in average pore diameter with an attenuation in surface area and pore volume.

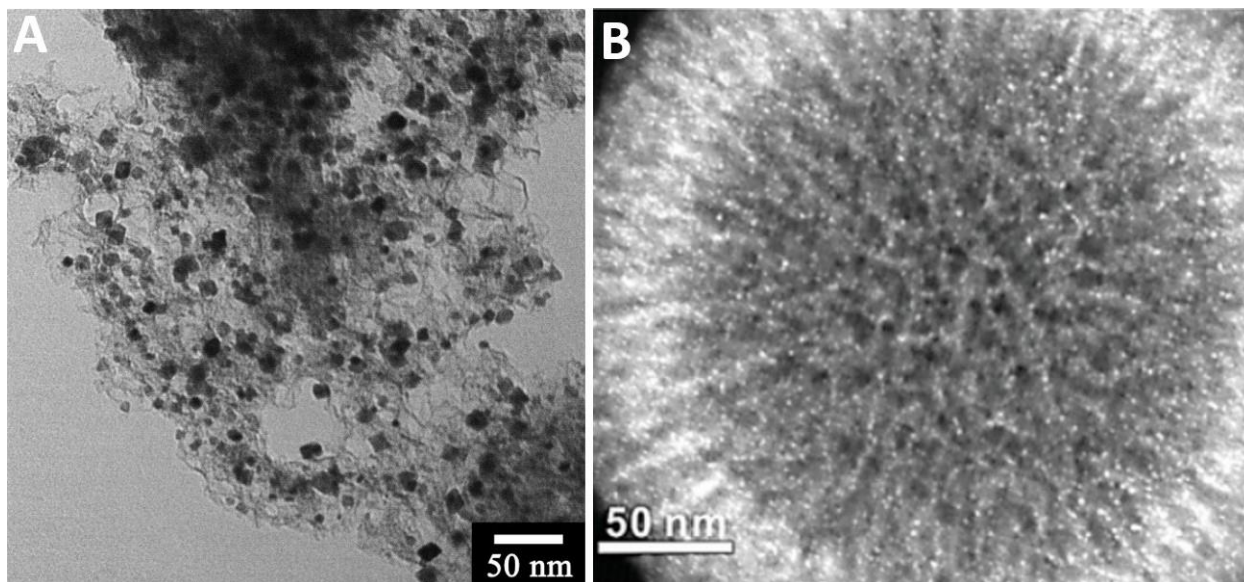


Figure 1.4. TEM images depicting MNPs deposited using an *ex situ* MNP synthesis (A), and MNP prepared by liquid immersion (B). (A) Reproduced from Ref. 85 with permission. Copyright: Elsevier 2020. (B) Adapted from Ref. 86 with permission. Copyright: Springer Nature 2020.

Alternatively, the precursor solution may evaporatively dry, blanketing the MC with atomic metal salts. In these cases, alcohols and low boiling point organics are used as liquid carriers for the precursor salt deposition onto the MC. The metal loaded MC is then subjected to thermal treatment (200-500 °C) for nanoparticle formation. Treatments tend to use He, Ar, N₂, or dilute H₂ atmospheres for the reduction of metal salts to yield metallic sites. Reduction under inert gases liberates the surface oxides at the known decomposition temperatures; oxide loss under a dilute hydrogen atmosphere occurs at lower temperatures. Argon and helium are preferred, as heat treating under nitrogen has shown to incorporate nitrogen into carbon frames on the order of <0.5 at. %.⁶² The target temperature for MNP formation is most critical in terms of particle size, dispersion and surface composition, all of which are quintessential for use in fields such as heterogeneous catalysis, biosensing and water treatment. A notable departure from this protocol reported the synthesis of CoS₂, FeS₂ and Co_{0.25}Fe_{0.75}S₂ onto a MC matrix. Prior to metal salt

incorporation, the MC was first immersed in a $\text{Na}_2\text{S}_2\text{O}_8$ oxidant for 8 hr. This was thermally treated at 240 °C in air to procure metal oxide species. The metal oxide-impregnated MC was then placed downstream from a crucible of elemental sulfur and heated to 350 °C to complete the sulfidation of the nanoparticles.⁶³ This report was unique in that the MNP sulfidation employed a chemical vapor deposition (CVD)-like reactor setup and is the sole literature example of employing a gas-phase deposition process. Gas phase physical/chemical vapor deposition material fabrication demands highly polished, flat, reactive surfaces. Even with the inhomogeneity and porosity exhibited by MCs, opportunity lays in gas-phase deposition; gas analytes aren't hindered by wetting and may enter the pores with less inhibition.

The chemical and physical robustness of MC supports enables *in situ* MNP formation under harsh environmental conditions like microwave irradiation and ultrasonication.⁶⁴⁻⁶⁸ Because of this, MNP decoration can be achieved with these well-developed particle growth techniques geared to cut down on reaction time. The most detailed reports are explicit describing the full specifications of the sonication or microwave systems used. This point tends to be excluded although microwaves and ultrasonicators can have greatly disparate power ratings (wattage) and operating frequencies (Hz). One group assessed the effects of microwave heating (900 W) versus thermal treatment (450 °C) on titania-precursor embedded MC.⁶⁷ Microwave sintering afforded smaller average particle size than thermal calcination. This study demonstrates that microwave heating can produce small <3 nm TiO_2 nanoparticles, and that with longer irradiation times, particle size increases due to nanoparticle migration. A chief finding from this study was that 7 MW irradiation gave rise to crystallites with fewer defects and strain in comparison to the nanoparticles produced with 14 MW power, a finding that was reported without a theoretical description. Working with other metal oxides is a logical extension to this method, as would

working with different performance rated microwaves. Influence of mesopore size for functionalization in sonicated or microwave irradiated environments has yet to be studied explicitly in these terms. A selection of diverse MNP functionalizations have been listed below (Table 1.1). Nanoparticle growth has been the main target, though other chemical conversions are expedited by the processes, namely polymer synthesis.

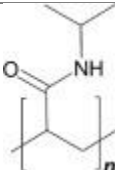
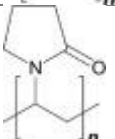
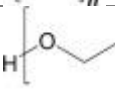
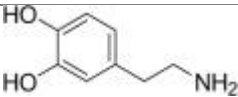
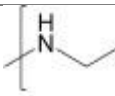
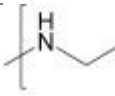
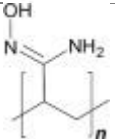
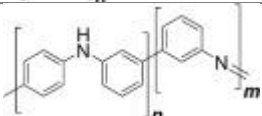
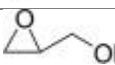
Table 1.1. Examples of MNP deposition conditions onto MC supports. U=Ultrasonication.

MNP Type	Metal Precursor	Deposition Solution	Drying	MNP Formation	Carrier Gas	MNP size
Ag ¹⁷⁸	Ag(acac)	Oleylamine/benzyl (1:2)	50 °C, overnight vacuum	LiBEt ₃ H, 30 min	N/A	4 nm
AgCu ⁹⁰	AgNO ₃ and Cu(NO ₃) ₂ 3H ₂ O	(U) Water, 1 h	60 °C, 8 h	500 °C, 1 h	10% H ₂ in Ar	2–9 nm
AgFe ⁹⁰	AgNO ₃ and Fe(NO ₃) ₃ 9H ₂ O	(U) Water, 1 h	60 °C, 8 h	500 °C, 1 h	10% H ₂ in Ar	3–10 nm
NiO ⁹¹	Ni(NO ₃) ₂ 6H ₂ O	(U) EtOH, 1 h	RT, until dry	350 °C, 6 h	Ar	NS
NiP ¹⁷⁹	Ni(NO ₃) ₂ 6H ₂ O	Water with (NH ₄) ₂ HPO ₄	110 °C, overnight	650 °C, 0 h	H ₂	10–30 nm
PdNiP ¹⁷⁹	Ni(NO ₃) ₂ 6H ₂ O and Pd(NO ₃) ₂ xH ₂ O	Water with (NH ₄) ₂ HPO ₄	110 °C, overnight	550 °C, 1 h	H ₂	5–15 nm
CeNi ¹⁸⁰	Ni(NO ₃) ₂ 6H ₂ O and Ce(NO ₃) ₂ 6H ₂ O	Water, overnight	RT, until dry	900 °C, 2 h	5% H ₂ in N ₂	5–10 nm
Ce ¹⁸¹	CeCl ₃	Water, NS	100 °C, 5 h	400 °C, 3 h	N ₂	11.2 nm
Pt₂CuNi ⁸⁵	Pt/Cu/Ni(acac) ₂	Chloroform	Vacuum	210 °C, 1 h	5% H ₂ in CO	6–10 nm
Pd ¹⁸²	H ₂ PdCl ₄	EtOH	80 °C, 12 h	300 °C, 4 h	10% H ₂ in Ar	1.2 nm
SnO₂ ⁹⁴	SnCl ₂ 2H ₂ O	(U) Water, 2 h	60 °C, 3 h vacuum	350 °C, 1 h	N/A	5 nm

Passivating with Polymers

Unlike the aforementioned techniques for dispersing particles, porous MC materials become coated with polymers in a conformal manner. Polymers exhibit different surface polarity and functionality than carbon surfaces and are thus used to enable drug molecule and enzyme loading, modulate biocompatibility enhance CO₂ capture, and imaging/sensing.^{46, 69-82} A non-exhaustive list of polymers used in creating MC-polymer hybrids is displayed below (Table 1.2).

Table 1.2. A list of non-covalently appended polymers to MC supports.

Polymer type	Structure	Loading conditions (Temp, time)	Polymerization conditions	Workup Conditions
Poly(N-isopropylacrylamide) ⁹⁷		N-isopropylacrylamide and AIBN in EtOH (RT, 2 h)	80 °C, 24 h	Chloroform EtOH, 80 °C
Polyvinylpyrrolidone ¹⁰⁰		Ascorbic acid, PVP in water (80 °C, 4 h)	N/A	Water 3x
Polyethyleneglycol ¹⁰⁰		DSPE-PEG in chloroform (<30 °C, 2 h)	N/A	Water 3x
Polydopamine ¹⁰⁹		Dopamine in tris buffer with bilirubin (Sonicate, 5 min)	Dark, RT, 15 min	Water NaOH in EtOH, Vacuum oven
Polyethylenimine ¹⁰¹		PEI in EDC and NHS in MES buffer (RT, 24 h)	N/A	Water 3x
Polyethylenimine ¹⁰²		PEI in MeOH (40 °C, 4 h)	N/A	Rotovap
Polyacrylamidoxime ¹⁰³		2-butenenitrile and AIBN in DCM (Lyophilize)	Dry, 120 °C, 8 h	TCM then EtOH, vacuum oven
Polyaniline ¹⁰⁶		Aniline in 1 M HCl (Sonicate, 2 h)	Added (NH ₄) ₂ S ₂ O ₈ , 0 °C, 12 h	Water then acetone
Polyglycerol ⁹³		Succinic anhydride in pyridine (U, 1 h)	140 °C, 24 h	Dialysis, ultrafiltration

The disparity in chemical functionality within different bulk polymers allows these tailored carbons to be utilized in multiple applied fields from next generation energy storage to stimuli-responsive drug delivery. Pre-made polymers of sufficiently small size (about 1 nm or smaller) to diffuse into the pores can be directly deposited onto MC surfaces. Otherwise, polymers are made *in situ*, atop the MC pore surface. Small sized monomers can infiltrate pores of the MC and produce composites which are best described as thin films passivating a MC core. Multi-tiered hybrid systems benefit with additional MNPs, enzymes and small molecules are built off polymer-MC composites, expanding the applied scope. Essentially every method of MC-polymer preparation begins with the adsorption of the to-be grafted monomer onto the carbon surface from a solution. Some syntheses call for lyophilization prior to initiation of the polymer on the MC. The polymerizations then proceed under necessary conditions (i.e. *sans* light for polydopamine⁸³ or pH < 3 for polyethyleneamine (PEI)⁷¹) and workup. Removing excess/unreacted precursors from the as-made materials vary in time, reagent demand and complexity. Centrifugation with neat solvent washes is most typical, though membrane dialysis is another viable technique. Solvent removal *via* lyophilization is ideal when the penultimate workup is done in water; air drying is ample for relatively hydrophobic polymers and those that require organic solvent workups.

Encapsulating Enzymes

A major advantage of MCs is the ability to confine biomolecules within its pores. Notably, enzymes are of great interest for their innate substrate selectivity and rapid kinetics at optimal conditions. Researchers in the biofuel cell community have found that enzymes retain significant catalytic performance when incorporated into MC as cargo. The carbon nanomaterials are latent with active surface area and improved electron transfer rates.⁸⁴ Bound enzymes also demonstrate

activity in non-biological conditions. It has been shown MC materials are robust carriers of therapeutic proteins and D/RNA strands. The purpose of MC for *in vitro* transportation of these biomolecules is to shelter them from biological deactivation, namely proteases and/or destructive labeling. Research on the biocompatibility of MC nanoparticles in human tissues has been conducted to delineate their effects on a systemic scale. To date, there are only a couple of noted examples of adsorptive protein loading on MC,⁸⁴⁻⁸⁹ perhaps due to the relatively weak attachment when compared to covalent linking. Enzymes loaded through IW will tend to maximize the contact of hydrophobic regions to the similarly polar carbon surface, which could hinder the accessibility of an active site located within the hydrophobic enzyme topology. One group found that an amide coupled lipase showed superior activity (31 U/g) over a physisorbed lipase deposited on the MC surface (8.6 U/g), likely due to the tendency for lipase to either dimerize or bury its active site into the carbon surface when physisorbed.⁹⁰ Another study showed that enzyme loading is optimized with larger (~20 nm) pore sizes compared with smaller (7 nm and 12.5 nm) pored monoliths.⁹¹ This observation has shifted the focus of much bioapplied research away from using physisorptive methods to incorporate enzyme into MC materials.

Despite the vast number of techniques for modifying MC materials through physisorptive means, there is a comparably large amount of research conducted on the covalent modification of the carbon surfaces.

1.4 Chemisorption Chemistry

Hugh S. Taylor introduced the term “activated adsorption” in the early 1930’s to support the observation that some gases only adsorb onto a surface at elevated temperatures.⁹² It was noted that the adsorbed gases were chemically bonded to the substrate. This observation led to the

emergence of the second surface phenomena relevant to MC decoration, chemisorption. Chemisorption implies covalency or covalent-like interactions between the adsorbent and adsorbate. Energetically, the activation energy associated with chemisorption falls between $40 \text{ kJ} \cdot \text{mol}^{-1}$ up to $400 \text{ kJ} \cdot \text{mol}^{-1}$. We see that MC surface reactions are derived from graphene (2-D) and carbon nanotube (1-D) science, where the surface chemistry is analogous, yet porosity and 3-D features are nonexistent. Chemically linked compounds may either graft off of oxygen groups or “activated” carbon centers (C^- or C^\bullet), which tend to be distributed across the MC topology uniformly, but in different concentrations. Reactions working with latent surface oxygens do one of two things, 1) chemically activate nucleophilic oxygens to couple with an electrophilic functionality present on the sorbate, or 2) convert the oxygen functional groups to a new moiety to undergo subsequent bond formation. Covalent attachment directly onto carbon centers has been realized through *in situ* diazonium and organolithium C-H activation pathways. Chemisorption is superior to physisorption in terms of the stability of sorbed species, at the cost of synthetic energy input. The diversity of oxygen groups on a carbon surface enables established solution phase chemical reactions to build off, which are outlined next.

Oxygen as a Nucleophile

Carboxylic acids and hydroxyl groups are the most commonly exploited oxygen groups when it comes to nucleophilicity—the former exhibiting both weak nucleophilic character relative to the electrophilic α -carbon. Perhaps the simplest conversion is the acidic workup of hydroxyls by way of sulfonation⁹³ or phosphorylation⁹⁴ over the timeframe of hours under reflux. Both procedures provide the intended inorganic acid group ($-\text{SO}_3\text{H}/-\text{PO}_3\text{H}$) but do so at the expense of adding other, different oxygen sites on the MC surface like hydroxyls, carboxylic acids and

aldehydes. For these reasons, oxidation is less used in an attempt to install inorganic acidic moieties in light of alternative, superior methods.

The nucleophilic nature of hydroxyls enable linkage to an electrophilic carbon center located on the adsorbate of interest. Recently, a group had shown a chlorinated diglycoester to undergo attachment at surface hydroxyls under chilled conditions in tetrahydrofuran (THF). This attachment involved a selective oxidation which yielded a relatively high amount of hydroxyl groups compared to carboxylic acids and aldehydes. These materials demonstrated loadings of 3% and 4.6% for two *f*-element complexants.¹⁹

Following silica research, derivatization of surface hydroxyls with organosilicates is useful in MC science.⁹⁵⁻⁹⁷ Unlike silica surfaces, the concentration of hydroxyls are magnitudes sparser on MCs. This scarcity means that trialkoxysilane linkers will likely only hydrolyze once; whereas hydroxyl dense silica surfaces allow for multiple hydrolyses, giving rise to more links between the surface and silica. Essentially all research using silane capped MC supports utilize the first linker for a second coupling.⁹⁸⁻¹⁰¹ There are still many functional silanes that have yet to be derivatized onto MC surfaces.

Silanes allow for functionalities to reside on MCs that would otherwise be nearly impossible to install with relative synthetic ease. Some studied MC-tethered silanes are shown (Figure 1.5), where the functional groups were utilized for subsequent transformations. Nonfunctional silanes could be explored to impart novel surface properties like reducing pore size with long hydrocarbon chains or improve lipophilicity.

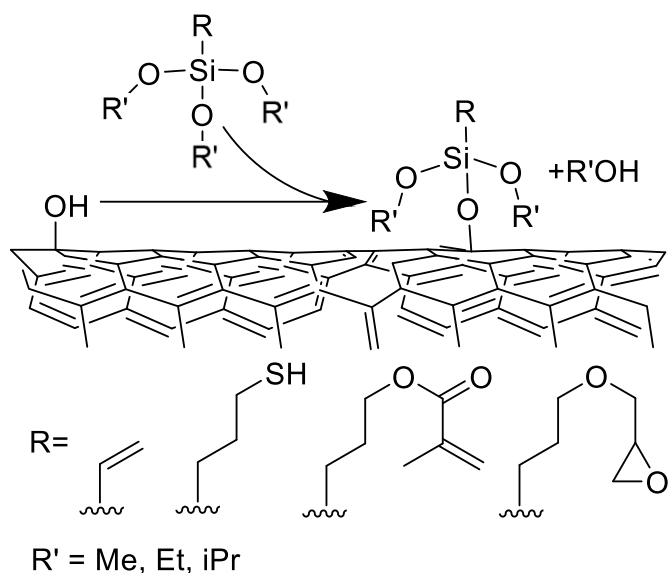


Figure 1.5. Surface hydroxyl functionalization with functional trialkoxysilanes.

Other Oxygen Transformations

Aside from the hydroxyls, carbonyl compounds offer potential for other reactions to proceed. The carboxylic acid group is especially useful in immobilizing biomolecules. It is known from decades of solution phase chemistry that N-terminal amino acids (e.g. lysine) on proteins can couple with a carboxyl functional group in the presence of 1-ethyl-3-(3-dimethylaminopropyl)carbodiimide (EDC) to form a stable amide bond. In the case of enzymatic attachment, it is beneficial that MC surface -COOH groups are dilute on most MC surfaces given their large size, as to prevent overcrowding. If the functional groups occur closer together, analyte accessibility would be impeded. This EDC chemistry is commonly used in a two-step process to furnish peptide coupling (Figure 1.6)¹⁰². A notable change in focus from enzymes in the bio realm is a recent report showing the covalent linking of single-stranded DNA (ssDNA); a hexylamine group was appended to the DNA to allow for amidation with the carboxylic acids.¹⁰³

The decorated MC outperformed its unmodified counterpart in Nd^{3+} adsorption, providing a proof of concept for rare earth element separations. Electrophilic activation of carboxyls *via* chlorination provide means for amidation, and this chemistry was used to grow covalent organic polymers (COPs) within carbon frames.¹⁰⁴ Expanding the set of COPs, MOFs or other coordination-framed materials grown from acyl-modified -COOH on MCs is a viable direction for this method due to the common use of primary amines in these compounds.

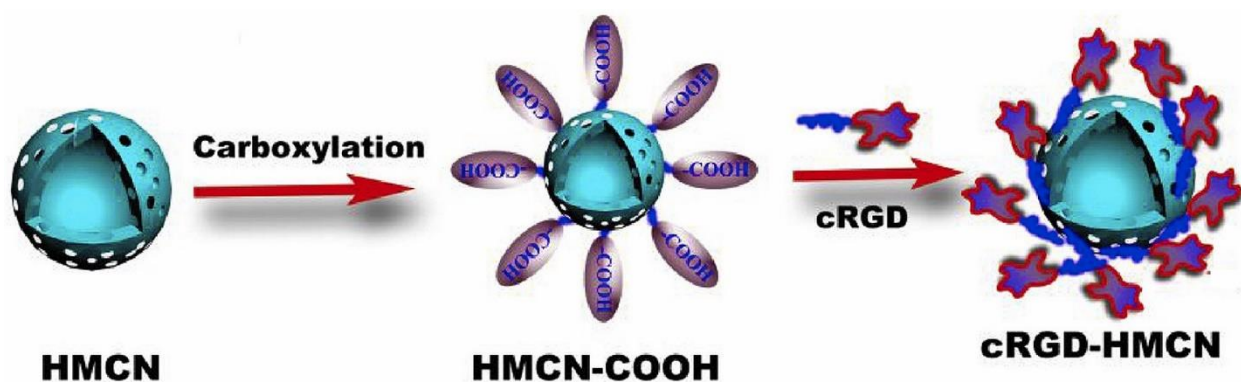


Figure 1.6. Schematic of an EDC coupling of a peptide to an MC support. Reprinted with permission from Ref. 126. Copyright: Elsevier 2019.

C-H Activation

In order to chemically build off of a carbon center, C-H activation with reductive organolithium agents or an *in situ* reduction with diazonium salts is necessitated. The first method is deemed a defect-mediated functionalization, as sp^3 and aryl defects on the MC are targeted by an added organolithium base such as *n*-butyllithium, or *n*-BuLi, performed in dry ether or THF. Next, a compound possessing an electrophilic center is dropped into solution, undergoing an $\text{S}_{\text{N}}2$ substitution at the base-generated carbanion site. This method originally showed grafting of electrophilic bromoethylamine onto *n*-BuLi treated carbon nanotubes

(CNTs).¹⁰⁵ A short time later, this reaction was applied to an MC substrate grafting a bromo-bipyridine (bpy) ligand (Figure 1.7).^{106, 107}

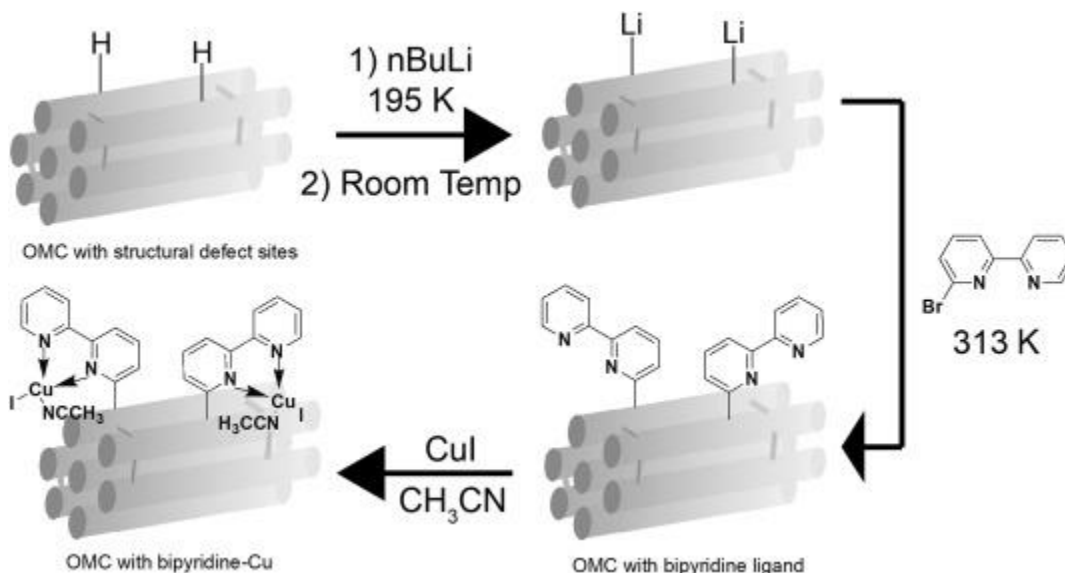


Figure 1.7. Two-step process for grafting a bipyridine (Bpy) ligand onto MC through organolithium C–H activation. Reproduced with permission from Ref. 130. Copyright: American Chemical Society 2014.

Only a few other embodiments of this C-H activating pathway have been reported, both for catalytic applications.^{108, 109} A hallmark of C-H activation procedures is the preservation of the morphological and structural integrity of the MC frame, contrary to coupling *via* oxidation. One potential drawback to this method, however, is the necessity for the grafted group to be soluble in dry ether. The nascence of defect-mediated C-H activation research in MC surface science opens doors for expanding the fundamental substrate scope of this route. A more studied method for C-H activation is anchoring by *in situ* diazotization. First reported in the late 20th century on glassy carbon electrodes, the electrochemical reduction (ER) of substituted aryl diazonium salts afforded covalent bonding to C-H defect sites.¹¹⁰ Unfortunately, surface quantification was not

possible due to a lack of knowledge on the structure of activated carbon. Around the same time, Cabot Corporation was granted a patent that enabled the method's use on a wide range of aryl and alkyl diaza salts and precursors. The electrical conductivity of MC is the primary driver for the advancement of the method. Nowadays, ER does not require use of expensive diazonium salts through the formation of the reactive diaza *in situ* from a solution of to-be-grafted amine and some acid source. The liberation of N₂ gas confirms the radical activation and concurrent attachment. Prior to the development of the ER method, sulfonation was only possible through harsh H₂SO₄ oxidation. The first report of ER grafting onto MC was in 2007; a mesoporous carbon substrate with 4-benzene-diazoniumsulfonate was immersed in cold water:ethanol bath. Addition of hypophosphorous acid afforded the final sulfonyl grafted MC.¹¹¹ There are some recent examples of *in situ* ER on MCs (Table 1.3), where a range of loading amounts have been achieved for various substrates.¹¹¹⁻¹¹⁹

Table 1.3. A list of recently reported diaza-linked molecules onto MC substrates.

Grafted group	Co-reagents	Reaction Conditions	Loading (mmol · g ⁻¹)
Sulfanilic acid ¹⁴⁵	NaNO ₂ , HCl	80 °C, 12 h	3.11
Sulfanilic acid ¹³⁸	NaNO ₂ , HCl	70 °C, 10 min	0.72
4-benzenediazonium sulfonate ¹³⁵	H ₃ PO ₂	4 °C, NS	1.93
4-benzenediazonium sulfonate ¹³⁶	HCl	5 °C, 3 h	1.49–1.72
4'(4-aminophenyl)-2,2':6',2'' terpyridine ¹³⁹	NaNO ₂ , HCl	0 °C, 1 h	NS
4-aminoacetophenone oxime ¹³⁷	Isoamyl nitrite	60 °C, 10 h	2.16
p-Aryl diazonium salts ¹³⁴	NaNO ₂ , HCl	ER in acetonitrile	NS

The ER method is superior to others with respect to reaction time, being less than an hour. The loadings using the ER method on MCs shows surface coverage of less than 5 mmol · g⁻¹ for most examples. The substrate scope, however, is constrained to diazonium salts which can stably adopt a radical charge; thus, it is unlikely that ER coupling would be viable with non-aromatic diaza salts.

Halogenation

Debatably the harshest of post-synthetic protocols from a chemical activation standpoint, halogenation has been studied. Imbuing a halogen (X) onto the surface of a MC frame yields marked material changes such as hydrophobicity without much structural compromise to the parent material. Examples of chlorinated^{120, 121}, brominated^{122, 123}, fluorinated^{124, 125} and even iodinated¹²⁶ MC materials are reported, with the latter largely incorporated into an N-doped MC. Halogenations proceed through energetic intermediates formed *in situ* at carbon sp³ defects, similar to that of *in situ* diazonium C-H functionalization. Many halogenated MC materials do exist, though they are formed during the synthetic step, where the carbon precursor material contains the choice dopant element.¹²⁷⁻¹³¹ There are many more examples of halogenation in the graphene (2-D) research realm,¹³²⁻¹⁴⁵ and these methods could likely to be translatable to MC science. EDX is usually chosen over solid-state ¹⁹F/³⁷Cl/⁷⁹Br nuclear magnetic resonance (ssNMR) to assess halogen coverage due to the availability of microscopes relative to ssNMR systems. The relative dearth of halogenated mesoporous carbon research will likely see a reversal in research focus as the surface properties of the materials can be more thoroughly understood.

1.5 Conclusion and Outlook

In just two decades, mesoporous carbon nanomaterial surface science has evolved to employ an arsenal of functionalization methods that consistently enhance many applied fields. The oil and gas processing industry are under intense scrutiny and has some technological flaws where MC could improve the state-of-the-art. Particularly, natural gas separations demand a series of (typically) tandem reactions that sequester non-hydrocarbon gases to purify the methane stream. Sorbed polymers in a controlled pore size MC could provide a more effective route to dehydration over hydrophobic surfaces. Acid gases like CO₂ and H₂S react readily near ambient conditions with Lewis acids as well as certain metals. Thiol or noble metal functionalized MC could be effective in the capture of trace Hg from natural gas which is a necessity for pipeline corrosion abatement.

Though not covered in this review, computational chemistry is an indispensable tool for predicting structures and benchmarking experimentally determined values (e.g. surface energies, bond lengths and topology metrics). There are a gamut of molecular models used, where the information gleaned from each primarily ranges in terms of dimension and time. For example, some commonly utilized computational tools for nanoparticle analysis (with associated space and timescales) include: Quantum mechanical methods (0.1-1 nm, ps), all-atom molecular dynamics/fluid dynamics/Monte Carlo simulations (1-10 nm, ns), coarse grained/dissipative particle dynamics modeling (10-100 nm, ns- μ s), and continuum based modeling (1-10 μ m, μ s-ms). As technology is on track to obey Moore's Law, larger unit cell volumes will be computable on timescales that are feasible in terms of cost, time, and accuracy for computational researchers. At the time of this dissertation's writing, published works leveraging computational chemistry to corroborate experimental data for mesoporous carbon materials are for ordered porous structures.

To this end, the utility of mesoporous material molecular modeling relies on structure knowledge derived from physicochemical measurements like electron microscopy, X-ray diffraction, and porosimetry. On one hand, ordered materials are simpler to model relative to disordered, randomly oriented porous structures. On the other hand, the lion's share of industrially applied porous materials comprise disorganized pore frameworks, so the applicability of computational methods for these particles are necessarily lacking.

Running two separate modifications, for example carboxyl coupling and then MNP physisorption, in succession is a relatively unexplored synthetic realm given the vast number of potential combinations that exist. Nanoparticle syntheses are advancing in terms of morphological control and scalability while remaining cost-competitive; this will only open more doors for nanoparticle anchoring onto MCs. A less exploited, yet inherent property of all carbon nanomaterials is photothermia, the transference of energy from visible light to the infrared regime is enabled from the relative size of MC pores to the impinging waves. Once absorbed, the heat can dissipate with ease given the thermal conductivity of MCs. Preferentially, heat could be transferred to surface sorbed nanoparticles, injecting hot electrons to drive select catalysis. Gas storage could be more feasible with MCs exploiting the photothermal effect, as desorption increases with temperature. The future of applied mesoporous carbon nanomaterials has immense opportunity given the diversity of surface modifications which enable their dominance in many relevant, globally impacting fields.

The state-of-the-art for mesoporous carbon fabrication and post-synthetic modification of these structures is well established experimentally, from which modern analytical techniques can readily assess on a range of physical and chemical scales. As researchers strive to optimize surface-functionalized mesoporous carbons for a given application, there is a dearth of

knowledge regarding the limitations of said materials *across* applied fields. While success is routinely achieved for a specific application, the concept of material optimization may be subject to the pitfall of Goodhart's Law, "when a measure becomes a target, it ceases to be a good measure". In other words, much of applied mesoporous material research is convergent towards only one studied function.

This dissertation aims to denude the aforementioned blinders unintentionally donned by mesoporous carbon material scientists. Given the growing number of published works for applied mesoporous carbon materials, there exists a need for greater communicability for said materials to be potentially utilized in different fields.

1.6 References

1. W. H. Organization, Drinking Water Fact Sheet. **2019**.
2. Sharma, K.; Kim, Y. H.; Gabitto, J.; Mayes, R. T.; Yiacoumi, S.; Bilheux, H. Z.; Walker, L. M. H.; Dai, S.; Tsouris, C., Transport of Ions in Mesoporous Carbon Electrodes during Capacitive Deionization of High-Salinity Solutions. *Langmuir* **2015**, 31 (3), 1038-1047.
3. Zbair, M.; Bottlinger, M.; Ainassaari, K.; Ojala, S.; Stein, O.; Keiski, R. L.; Bensitel, M.; Brahmi, R., Hydrothermal Carbonization of Argan Nut Shell: Functional Mesoporous Carbon with Excellent Performance in the Adsorption of Bisphenol A and Diuron. *Waste Biomass Valori*. **2020**, 11 (4), 1565-1584.
4. Duan, F.; Du, X.; Li, Y. P.; Cao, H. B.; Zhang, Y., Desalination Stability of Capacitive Deionization using Ordered Mesoporous Carbon: Effect of Oxygen-Containing Surface Groups and Pore Properties. *Desalination* **2015**, 376, 17-24.
5. Khalid, A.; Rowles, L. S.; Ateia, M.; Xiao, M. H.; Ramirez-Sanchez, I.; Bello, D.; Karanfil, T.; Saleh, N. B.; Apul, O. G., Mesoporous Activated Carbon Shows Superior Adsorption Affinity for 11-nor-9-carboxy- Δ -tetrahydrocannabinol in Water. *NPJ Clean Water* **2020**, 3 (1).
6. Li, Y.; Yuan, B.; Fu, J.; Deng, S. G.; Lu, X. Y., Adsorption of Alkaloids on Ordered Mesoporous Carbon. *J. Colloid Interf. Sci.* **2013**, 408, 181-190.
7. Kim, Y.; Bae, J.; Park, H.; Suh, J. K.; You, Y. W.; Choi, H., Adsorption Dynamics of Methyl Violet onto Granulated Mesoporous Carbon: Facile Synthesis and Adsorption Kinetics. *Water Res.* **2016**, 101, 187-194.

8. Cao, C. H.; Wu, X. F.; Zheng, Y. M.; Zhang, D. H.; Chen, J. H.; Chen, Y. F., Ordered Mesoporous Carbon with Chitosan for Disinfection of Water via Capacitive Deionization. *Nanomaterials-Basel* **2020**, 10 (3).
9. Källdström, M.; Kumar, N.; Murzin, D. Y., Valorization of Cellulose over Metal Supported Mesoporous Materials. *Catal. Today* **2011**, 167 (1), 91-95.
10. Haynes, T.; Bounouch, O.; Dubois, V.; Hermans, S., Preparation of Mesoporous Silica Nanocapsules with a High Specific Surface Area by Hard and Soft Dual Templating Approach: Application to Biomass Valorization Catalysis. *Microporous Mesoporous Mater.* **2020**, 306.
11. Lei, L. F.; Lindbråthen, A.; Zhang, X. P.; Favvas, E. P.; Sandru, M.; Hillestad, M.; He, X. Z., Preparation of Carbon Molecular Sieve Membranes with Remarkable CO/CH Selectivity for High-Pressure Natural Gas Sweetening. *J. Membrane Sci.* **2020**, 614.
12. Li, X. L.; Zhu, H. B.; Liu, C.; Yuan, P.; Lin, Z. X.; Yang, J. T.; Yue, Y. Y.; Bai, Z. S.; Wang, T. H.; Bao, X. J., Synthesis, Modification, and Application of Hollow Mesoporous Carbon Submicrospheres for Adsorptive Desulfurization. *Ind. Eng. Chem. Res.* **2018**, 57 (44), 15020-15030.
13. Qi, J. W.; Wei, G. P.; Sun, X. Y.; Wang, L. J.; Li, J. S., Enhanced Removal for H₂S by Cu-Ordered Mesoporous Carbon Foam. *J. Hazard. Mater.* **2020**, 396.
14. Ling, Y.; Man, X. K.; Zhang, W. B.; Wang, D. L.; Wu, J.; Liu, Q. Z.; Gu, M. Y.; Lin, Y. Y.; He, P.; Jia, T., Molybdenum Trioxide Impregnated Carbon Aerogel for Gaseous Elemental Mercury Removal. *Korean J. Chem. Eng.* **2020**, 37 (4), 641-651.
15. Zhou, L. B.; Jing, Y.; Liu, Y. B.; Liu, Z. H.; Gao, D. Y.; Chen, H. B.; Song, W. Y.; Wang, T.; Fang, X. F.; Qin, W. P.; Yuan, Z.; Dai, S.; Qiao, Z. A.; Wu, C. F., Mesoporous Carbon Nanospheres as a Multifunctional Carrier for Cancer Theranostics. *Theranostics* **2018**, 8 (3), 663-675.
16. Li, C. Y.; Qian, M.; Wang, S. S.; Jiang, H. L.; Du, Y. L.; Wang, J. X.; Lu, W. Y.; Murthy, N.; Huang, R. Q., Aptavalve-gated Mesoporous Carbon Nanospheres Image Cellular Mucin and Provide On-demand Targeted Drug Delivery. *Theranostics* **2017**, 7 (13), 3319-3325.
17. Bertelsen, E. R.; Kovach, N. C.; Reinhart, B. J.; Trewyn, B. G.; Antonio, M. R.; Shafer, J. C., Multiscale Investigations of Europium(III) Complexation with Tetra-octyl Diglycolamide Confined in Porous Solid Supports. *CrystEngComm* **2020**, 22 (41), 6886-6899.
18. Bertelsen, E. R.; Kovach, N. C.; Trewyn, B. G.; Antonio, M. R.; Shafer, J. C., Electrochemical Reduction of Europium(III) using Tetra-octyl Diglycolamide Functionalized Ordered Mesoporous Carbon Microelectrodes. *J. Mater. Chem. C* **2020**, 8 (20), 6689-6700.

19. Perreault, L. L.; Giret, S.; Gagnon, M.; Florek, J.; Larivière, D.; Kleitz, F., Functionalization of Mesoporous Carbon Materials for Selective Separation of Lanthanides under Acidic Conditions. *ACS Appl. Mater. Interfaces* **2017**, 9 (13), 12003-12012.
20. Cheng, Y.; Zhao, H. Q.; Zhao, Y.; Cao, J. M.; Zheng, J.; Ji, G. B., Structure-Switchable Mesoporous Carbon Hollow Sphere Framework Toward Sensitive Microwave Response. *Carbon* **2020**, 161, 870-879.
21. Giannakoudakis, D. A.; Barczak, M.; Florent, M.; Bandosz, T. J., Analysis of Interactions of Mustard Gas Surrogate Vapors with Porous Carbon Textiles. *Chem. Eng. J.* **2019**, 362, 758-766.
22. Li, X. X.; Liu, J. J.; Sun, M. M.; Sha, T. Z.; Bo, X. J.; Zhou, M., Amperometric Sensing of Ascorbic Acid by using a Glassy Carbon Electrode Modified with Mesoporous Carbon Nanorods. *Microchim. Acta* **2018**, 185 (10).
23. Wang, S. Y.; Guo, P.; Ma, G. S.; Wei, J.; Wang, Z. Y.; Cui, L.; Sun, L. L.; Wang, A. Y., Three-Dimensional Hierarchical Mesoporous Carbon for Regenerative Electrochemical Dopamine Sensor. *Electrochim. Acta* **2020**, 360.
24. Gibson, J. A. A.; Gromov, A. V.; Brandani, S.; Campbell, E. E. B., Comparison of Amine-Impregnated Mesoporous Carbon with Microporous Activated Carbon and 13X Zeolite for Biogas Purification. *J. Porous. Mat.* **2017**, 24 (6), 1473-1479.
25. Rodriguez-Reinoso, F.; Molina-Sabio, M., Textural and Chemical Characterization of Microporous Carbons. *Adv. Colloid Interface Sci.* **1998**, 271-294.
26. Darmstadt, H.; Roy, C.; Kaliaguine, S.; Kim, T. W.; Ryoo, R., Surface and Pore Structures of CMK-5 Ordered Mesoporous Carbons by Adsorption and Surface Spectroscopy. *Chem. Mater.* **2003**, 15 (17), 3300-3307.
27. Shafeeyan, M. S.; Daud, W. M. A. W.; Houshmand, A.; Shamiri, A., A Review on Surface Modification of Activated Carbon for Carbon Dioxide Adsorption. *J. Anal. Appl. Pyrol.* **2010**, 89 (2), 143-151.
28. Banhart, F.; Kotakoski, J.; Krasheninnikov, A. V., Structural Defects in Graphene. *ACS Nano* **2011**, 5 (1), 26-41.
29. Duplock, E. J.; Scheffler, M.; Lindan, P. J. D., Hallmark of Perfect Graphene. *Phys. Rev. Lett.* **2004**, 92 (22).
30. Liu, X. B.; Dong, H.; Li, Y.; Mei, N., Thermal Conductivity and Raman Spectra of Carbon Fibers. *Int. J. Thermophys.* **2017**, 38 (10).
31. Jaroniec, M.; Gadkaree, K. P.; Choma, J., Relation Between Adsorption Potential Distribution and Pore Volume Distribution for Microporous Carbons. *Colloids Surf. A Physicochem. Eng. Asp.* **1996**, 118 (3), 203-210.

32. Kruk, M.; Li, Z. J.; Jaroniec, M.; Betz, W. R., Nitrogen Adsorption Study of Surface Properties of Graphitized Carbon Blacks. *Langmuir* **1999**, 15 (4), 1435-1441.
33. Barton, S. S.; Evans, M. J. B.; Halliop, E.; MacDonald, J. A. F., Acidic and Basic Sites on the Surface of Porous Carbon. *Carbon* **1997**, 35 (9), 1361-1366.
34. Bleda-Martinez, M. J.; Lozano-Castello, D.; Morallon, E.; Cazorla-Amoros, D.; Linares-Solano, A., Chemical and Electrochemical Characterization of Porous Carbon Materials. *Carbon* **2006**, 44 (13), 2642-2651.
35. Ferri, M.; Campisi, S.; Carniti, P.; Gervasini, A.; Shen, J., Tunable Acidity in Mesoporous Carbons for Hydrolysis Reactions. *New J. Chem.* **2020**, 44 (15), 5873-5883.
36. Zhang, M.; He, L.; Shi, T.; Zha, R. H., Nanocasting and Direct Synthesis Strategies for Mesoporous Carbons as Supercapacitor Electrodes. *Chem. Mater.* **2018**, 30 (21), 7391-7412.
37. Wang, X. F.; Liu, P.; Tian, Y., Ordered Mesoporous Carbons for Ibuprofen Drug Loading and Release Behavior. *Microporous Mesoporous Mater.* **2011**, 142 (1), 334-340.
38. Fort, C. I.; Cotet, L. C.; Turdean, G. L.; Danciu, V., Meldola Blue Immobilised on Mesoporous Carbon Aerogel - New Electrode Material for NADH Electrocatalytic Oxidation. *Studia UBB Chemia* **2015**, 60 (3), 215-224.
39. Gao, Y. K.; Zhu, W. Q.; Liu, J.; Di, D. H.; Chang, D.; Jiang, T. Y.; Wang, S. L., A Geometric Pore Adsorption Model for Predicting the Drug Loading Capacity of Insoluble Drugs in Mesoporous Carbon. *Int. J. Pharmaceut.* **2015**, 485 (1-2), 25-30.
40. Wang, H.; Wang, K.; Mu, Q.; Stephen, Z. R.; Yu, Y.; Zhou, S.; Zhang, M., Mesoporous Carbon Nanoshells for High Hydrophobic Drug Loading, Multimodal Optical Imaging, Controlled Drug Release, and Synergistic Therapy. *Nanoscale* **2017**, 9 (4), 1434-1442.
41. Amreen, K.; Kumar, A. S., Highly Redox-Active Hematin-Functionalized Carbon Mesoporous Nanomaterial for Electrocatalytic Reduction Applications in Neutral Media. *ACS Appl. Nano. Mater.* **2018**, 1 (5), 2272-2283.
42. Gao, X. L.; Du, D. F.; Li, S.; Yan, X.; Xing, W.; Bai, P.; Xue, Q. Z.; Yan, Z. F., Outstanding Capacitive Performance of Ordered Mesoporous Carbon Modified by Anthraquinone. *Electrochim. Acta* **2018**, 259, 110-121.
43. Li, X.; Wang, X. D.; Sha, L. P.; Wang, D.; Shi, W.; Zhao, Q. F.; Wang, S. L., Thermosensitive Lipid Bilayer-Coated Mesoporous Carbon Nanoparticles for Synergistic Thermochemotherapy of Tumor. *ACS Appl. Mater. Interfaces* **2018**, 10 (23), 19386-19397.
44. Bertelsen, E. R.; Deodhar, G.; Kluherz, K. T.; Davidson, M.; Adams, M. L.; Trewyn, B. G.; Shafer, J. C., Microcolumn Lanthanide Separation using Bis-(2-

- ethylhexyl) Phosphoric Acid Functionalized Ordered Mesoporous Carbon Materials. *J. Chromatogr. A* **2019**, 1595, 248-256.
45. Fan, C. H.; Kong, F. H.; Shetti, D.; Zhang, B.; Yang, Y. G.; Wei, K., Resveratrol Loaded Oxidized Mesoporous Carbon Nanoparticles: A Promising Tool to Treat Triple Negative Breast Cancer. *Biochem. Bioph. Res. Co.* **2019**, 519 (2), 378-384.
 46. Hussain, A.; Guo, S. R., NIR-Triggered Release of DOX from Sphorolipid-Coated Mesoporous Carbon Nanoparticles with the Phase-Change Material 1-tetradecanol to Treat MCF-7/ADR cells. *J. Mater. Chem. B* **2019**, 7 (6), 974-985.
 47. Kannan, A.; Devi, K. S. S.; Dinesh, B.; Krishnan, U. M.; Gandhi, S., Tailoring the electrochemical interface of mesoporous carbon with ubiquinone for detection of parabens in cosmetics. *ChemistrySelect* **2020**, 5 (15), 4628-4636.
 48. Meng, Z.; You, N.; Fan, H. T., In-situ Sampling of Chlorophenols in Industrial Wastewater using Diffusive Gradients in Thin Films Technique Based on Mesoporous Carbon. *Chemosphere* **2019**, 232, 18-25.
 49. Regiart, M.; Magallanes, J. L.; Barrera, D.; Villarroel-Rocha, J.; Sapag, K.; Raba, J.; Bertolino, F. A., An Ordered Mesoporous Carbon Modified Electrochemical Sensor for Solid-Phase Microextraction and Determination of Triclosan in Environmental Samples. *Sensor Actuat. B* **2016**, 232, 765-772.
 50. Dujardin, E.; Ebbesen, T. W.; Hiura, H.; Tanigaki, K., Capillarity and Wetting of Carbon Nanotubes. *Science* 1994, 265 (5180), 1850-1852.
 51. Zhao, Q. F.; Lin, Y. Z.; Han, N.; Li, X.; Geng, H. J.; Wang, X. D.; Cui, Y.; Wang, S. L., Mesoporous Carbon Nanomaterials in Drug Delivery and Biomedical Application. *Drug Deliv.* **2017**, 24 (2), 94-107.
 52. Cao, Y. L.; Mao, S. J.; Li, M. M.; Chen, Y. Q.; Wang, Y., Metal/Porous Carbon Composites for Heterogeneous Catalysis: Old Catalysts with Improved Performance Promoted by N-Doping. *ACS Catal.* **2017**, 7 (12), 8090-8112.
 53. See, K. A.; Jun, Y. S.; Gerbec, J. A.; Sprafke, J. K.; Wudl, F.; Stucky, G. D.; Seshadri, R., Sulfur-Functionalized Mesoporous Carbons as Sulfur Hosts in Li-S Batteries: Increasing the Affinity of Polysulfide Intermediates to Enhance Performance. *ACS Appl. Mater. Interfaces* **2014**, 6 (14), 10908-10916.
 54. Zhang, J. T.; Dai, L. M., Heteroatom-Doped Graphitic Carbon Catalysts for Efficient Electrocatalysis of Oxygen Reduction Reaction. *ACS Catal.* **2015**, 5 (12), 7244-7253.
 55. Sun, Y. S.; Lin, C. F.; Luo, S. T.; Su, C. Y., Block-Copolymer-Templated Hierarchical Porous Carbon Nanostructures with Nitrogen-Rich Functional Groups for Molecular Sensing. *ACS Appl. Mater. Interfaces* **2017**, 9 (37), 31235-31244.

56. Varela, A. S.; Ju, W.; Bagger, A.; Franco, P.; Rossmeyl, J.; Strasser, P., Electrochemical Reduction of CO₂ on Metal-Nitrogen-Doped Carbon Catalysts. *ACS Catal.* **2019**, 9 (8), 7270-7284.
57. Veerakumar, P.; Sangili, A.; Manavalan, S.; Thanasekaran, P.; Lin, K. C., Research Progress on Porous Carbon Supported Metal/Metal Oxide Nanomaterials for Supercapacitor Electrode Applications. *Ind. Eng. Chem. Res.* **2020**, 59 (14), 6347-6374.
58. Zhang, P. F.; Zhang, J. S.; Dai, S., Mesoporous Carbon Materials with Functional Compositions. *Chem.-Eur. J.* **2017**, 23 (9), 1986-1998.
59. Wu, D. Z.; Shen, X. C.; Zhou, L. Q.; Nagai, T.; Pan, Y. B.; Yao, L. B.; Zulevi, B.; Lubers, A.; Jia, H. F.; Peng, Z. M., A Vacuum Impregnation Method for Synthesizing Octahedral Pt₂CuNi Nanoparticles on Mesoporous Carbon Support and the Oxygen Reduction Reaction Electrocatalytic Properties. *J. Colloid Interf. Sci.* **2020**, 564, 245-253.
60. Xu, H. Y.; Liu, Y. N.; Sun, G. W.; Kang, S. F.; Wang, Y. G.; Zheng, Z.; Li, X., Synthesis of Graphitic Mesoporous Carbon Supported Ce-doped Nickel Catalyst for Steam Reforming of Toluene. *Mater. Lett.* **2019**, 244, 123-125.
61. Wan, X. K.; Wu, H. B.; Guan, B. Y.; Luan, D. Y.; Lou, X. W., Confining Sub-Nanometer Pt Clusters in Hollow Mesoporous Carbon Spheres for Boosting Hydrogen Evolution Activity. *Adv. Mater.* **2020**, 32 (7).
62. Szabo, A.; Gyulavari, T.; Toth, Z. R.; Papa, Z.; Budai, J.; Hernadi, K., The Effect of Various Substrates and Catalyst Layer Deposition on the Incorporation of Nitrogen into Carbon Nanotube Forest Structures. *Thin Solid Films* **2020**, 709.
63. Huang, G. Q.; Xu, S. N.; Liu, Z. P.; Yuan, S. S.; Zhang, C.; Ai, J.; Li, N.; Li, X. T., Ultrafine Cobalt-Doped Iron Disulfide Nanoparticles in Ordered Mesoporous Carbon for Efficient Hydrogen Evolution. *ChemCatChem* **2020**, 12 (3), 788-794.
64. Zhu, S. M.; Zhou, H. A.; Hibino, M.; Honma, I.; Ichihara, M., Synthesis of MnO₂ Nanoparticles Confined in Ordered Mesoporous Carbon using a Sonochemical Method. *Adv. Funct. Mater.* **2005**, 15 (3), 381-386.
65. Zhou, J. H.; He, J. P.; Ji, Y. J.; Dang, W. J.; Liu, X. L.; Zhao, G. W.; Zhang, C. X.; Zhao, J. S.; Fu, Q. B.; Hu, H. P., CTAB Assisted Microwave Synthesis of Ordered Mesoporous Carbon Supported Pt Nanoparticles for Hydrogen Electro-oxidation. *Electrochim. Acta* **2007**, 52 (14), 4691-4695.
66. Qiao, H.; Li, J.; Fu, J. P.; Kumar, D.; Wei, Q. F.; Cai, Y. B.; Huang, F. L., Sonochemical Synthesis of Ordered SnO₂/CMK-3 Nanocomposites and Their Lithium Storage Properties. *ACS Appl. Mater. Interfaces* **2011**, 3 (9), 3704-3708.
67. Coromelci-Pastravanu, C.; Ignat, M.; Popovici, E.; Harabagiu, V., TiO₂-Coated Mesoporous Carbon: Conventional vs. Microwave-Annealing Process. *J. Hazard. Mater.* **2014**, 278, 382-390.

68. Li, Y. N.; Zhu, L.; Yao, T. H.; Liu, T.; Qian, R. F.; Li, F.; Han, X. G.; Yu, L. M.; Wang, H. K., Space-Confined Synthesis of Ultrasmall SnO₂ Nanodots within Ordered Mesoporous Carbon CMK-3 for High-Performance Lithium Ion Batteries. *Energ. Fuel* **2020**, 34 (6), 7709-7715.
69. Gisbert-Garzarán, M.; Berkmann, J. C.; Giasafaki, D.; Lozano, D.; Spyrou, K.; Manzano, M.; Steriotis, T.; Duda, G. N.; Schmidt-Bleek, K.; Charalambopoulou, G.; Vallet-Regí, M., Engineered pH-Responsive Mesoporous Carbon Nanoparticles for Drug Delivery. *ACS Appl. Mater. Interfaces* **2020**, 12 (13), 14946-14957.
70. Zhu, S. M.; Chen, C. X.; Chen, Z. X.; Liu, X. Y.; Li, Y.; Shi, Y.; Zhang, D., Thermo-Responsive Polymer-Functionalized Mesoporous Carbon for Controlled Drug Release. *Mater. Chem. Phys.* **2011**, 126 (1-2), 357-363.
71. Wu, L. D.; Ji, X.; Kong, J., Polymer-Coated Mesoporous Carbon as Enzyme Platform for Oxidation of Bisphenol A in Organic Solvents. *ACS Omega* **2019**, 4 (15), 16409-16417.
72. Ran, F.; Lei, W.; Cui, Y.; Jiao, J.; Mao, Y. L.; Wang, S. Y.; Wang, S. L., Size Effect on Oral Absorption in Polymer-Functionalized Mesoporous Carbon Nanoparticles. *J. Colloid Interf. Sci.* **2018**, 511, 57-66.
73. Orooji, Y.; Liang, F.; Razmjou, A.; Liu, G. P.; Jin, W. Q., Preparation of Anti-Adhesion and Bacterial Destructive Polymeric Ultrafiltration Membranes using Modified Mesoporous Carbon. *Sep. Purif. Technol.* **2018**, 205, 273-283.
74. Li, X. F.; Wang, L. Z.; She, L.; Sun, L. H.; Ma, Z. Q.; Chen, M.; Hu, P. W.; Wang, D.; Yang, F., Immunotoxicity Assessment of Ordered Mesoporous Carbon Nanoparticles Modified with PVP/PEG. *Colloid Surf. B* **2018**, 171, 485-493.
75. Mishra, G.; Mittal, N.; Sharma, A., Multifunctional Mesoporous Carbon Capsules and their Robust Coatings for Encapsulation of Actives: Antimicrobial and Anti-Bioadhesion Functions. *ACS Appl. Mater. Interfaces* **2017**, 9 (23), 19371-19379.
76. Orooji, Y.; Faghih, M.; Razmjou, A.; Hou, J. W.; Moazzam, P.; Emami, N.; Aghababaie, M.; Nourisfa, F.; Chen, V.; Jin, W. Q., Nanostructured Mesoporous Carbon Polyethersulfone Composite Ultrafiltration Membrane with Significantly Low Protein Adsorption and Bacterial Adhesion. *Carbon* **2017**, 111, 689-704.
77. Meng, Y.; Wang, S. S.; Li, C. Y.; Qian, M.; Yan, X. Y.; Yao, S. C.; Peng, X. Y.; Wang, Y.; Huang, R. Q., Photothermal Combined Gene Therapy Achieved by Polyethyleneimine-Grafted Oxidized Mesoporous Carbon Nanospheres. *Biomaterials* **2016**, 100, 134-142.
78. Wang, M.; Yao, L. W.; Wang, J. T.; Zhang, Z. X.; Qiao, W. M.; Long, D. H.; Ling, L. C., Adsorption and Regeneration Study of Polyethylenimine-Impregnated Millimeter-sized Mesoporous Carbon Spheres for Post-Combustion CO₂ capture. *Appl. Energ.* **2016**, 168, 282-290.

79. Wang, Y. X.; Guo, T.; Hu, X. D.; Hao, J.; Guo, Q. J., Mechanism and Kinetics of CO Adsorption for TEPA- Impregnated Hierarchical Mesoporous Carbon in the Presence of Water Vapor. *Powder Technol.* **2020**, 368, 227-236.
80. Rajkumar, C.; Nehru, R.; Chen, S. M.; Arumugam, S.; Qin-JinYeah; Sankar, R., A Chitosan Grafted Mesoporous Carbon Aerogel for Ultra-Sensitive Voltammetric Determination of Isoniazid. *Microchim. Acta* **2019**, 186 (7).
81. Shoja, Y.; Kermanpur, A.; Karimzadeh, F., Diagnosis of EGFR Exon21 L858R Point Mutation as Lung Cancer Biomarker by Electrochemical DNA Biosensor based on Reduced Graphene Oxide/Functionalized Ordered Mesoporous Carbon/Ni-oxytetracycline Metallopolymer Nanoparticles Modified Pencil Graphite Electrode. *Biosens. Bioelectron.* **2018**, 113, 108-115.
82. Kuang, Y.; Cao, Y.; Liu, M.; Zu, G. Y.; Zhang, Y. J.; Zhang, Y.; Pei, R. J., Geometrical Confinement of Gadolinium Oxide Nanoparticles in Poly(ethylene glycol)/Arginylglycylaspartic Acid-Modified Mesoporous Carbon Nanospheres as an Enhanced Magnetic Resonance Imaging Contrast Agent. *ACS Appl. Mater. Interfaces* **2018**, 10 (31), 26099-26107.
83. Huang, S. Y.; Zheng, J. T.; Zhang, Y. M.; Zheng, J.; Zhuang, Z. N.; Yang, Q.; Wang, F. X.; Chen, G. S.; Huang, S. M.; Ouyang, G. F., Polydopamine Decorated Ordered Mesoporous Carbon for Efficient Removal of Bilirubin under Albumin-rich Conditions. *J. Mater. Chem. B* **2020**, 8 (2), 290-297.
84. Lv, C. H.; Li, S. F.; Liu, L. X.; Zhu, X. Y.; Yang, X. W., Enhanced Electrochemical Characteristics of the Glucose Oxidase Bioelectrode Constructed by Carboxyl-Functionalized Mesoporous Carbon. *Sensors-Basel* **2020**, 20 (12).
85. Gellett, W.; Kesmez, M.; Schumacher, J.; Akers, N.; Minteer, S. D., Biofuel Cells for Portable Power. *Electroanal.* **2010**, 22 (7-8), 727-731.
86. Trifonov, A.; Herkendell, K.; Tel-Vered, R.; Yehezkeli, O.; Woerner, M.; Willner, I., Enzyme-Capped Relay-Functionalized Mesoporous Carbon Nanoparticles: Effective Bioelectrocatalytic Matrices for Sensing and Biofuel Cell Applications. *ACS Nano* **2013**, 7 (12), 11358-11368.
87. Korani, A.; Salimi, A.; Karimi, B., Guanine/Ionic Liquid Derived Ordered Mesoporous Carbon Decorated with AuNPs as Efficient NADH Biosensor and Suitable Platform for Enzymes Immobilization and Biofuel Cell Design. *Electroanal.* **2017**, 29 (11), 2646-2655.
88. Ramirez-Montoya, L. A.; Concheso, A.; Alonso-Buenaposada, I. D.; Garcia, H.; Menendez, J. A.; Arenillas, A.; Montes-Moran, M. A., Protein Adsorption and Activity on Carbon Xerogels with Narrow Pore Size Distributions Covering a Wide Mesoporous Range. *Carbon* **2017**, 118, 743-751.
89. Jahanbakhshi, M., Myoglobin Immobilized on Mesoporous Carbon Foam in a Hydrogel (Selep) Dispersant for Voltammetric Sensing of Hydrogen Peroxide. *Microchim. Acta* **2018**, 185 (2).

90. Reichardt, C.; Utgenannt, S.; Stahmann, K. P.; Klepel, O.; Barig, S., Highly Stable Adsorptive and Covalent Immobilization of *Thermomyces lanuginosus* Lipase on Tailor-made Porous Carbon Material. *Biochem. Eng. J.* **2018**, 138, 63-73.
91. Caldas, E. M.; Novatzky, D.; Deon, M.; de Menezes, E. W.; Hertz, P. F.; Costa, T. M. H.; Arenas, L. T.; Benvenuti, E. V., Pore Size Effect in the Amount of Immobilized Enzyme for Manufacturing Carbon Ceramic Biosensor. *Microporous Mesoporous Mater.* **2017**, 247, 95-102.
92. Taylor, H. S., Activated Adsorption of Hydrogen by Zinc and Chromium Oxides. *Nature* 1931, 128, 636-636.
93. Veerakumar, P.; Jeyapragasam, T.; Surabhi; Salamalai, K.; Maiyalagan, T.; Lin, K. C., Functionalized Mesoporous Carbon Nanostructures for Efficient Removal of Eriochrome Black-T from Aqueous Solution. *J. Chem. Eng. Data* **2019**, 64 (4), 1305-1321.
94. Lian, Q. Y.; Yao, L. G.; Ahmad, Z. U.; Konggidinata, M. I.; Zappi, M. E.; Gang, D. D. C., Modeling Mass Transfer for Adsorptive Removal of Pb(II) onto Phosphate Modified Ordered Mesoporous Carbon (OMC). *J. of Contam. Hydrol.* **2020**, 228.
95. Goscianska, J.; Olejnik, A., Dispersion Stability of the Aminosilane-grafted Mesoporous Carbons in Different Solvents. *Microporous Mesoporous Mater.* **2018**, 265, 149-161.
96. Goscianska, J.; Ciesielczyk, F., Lanthanum Enriched Aminosilane-grafted Mesoporous Carbon Material for Efficient Adsorption of Tartrazine Azo Dye. *Microporous Mesoporous Mater.* **2019**, 280, 7-19.
97. Goscianska, J.; Olejnik, A., Removal of 2,4-D Herbicide from Aqueous Solution by Aminosilane-grafted Mesoporous Carbons. *Adsorption* **2019**, 25 (3), 345-355.
98. Qin, L.; Shi, W. P.; Liu, W. F.; Yang, Y. Z.; Liu, X. G.; Xu, B. S., Surface Molecularly Imprinted Polymers Grafted on Ordered Mesoporous Carbon Nanospheres for Fuel Desulfurization. *RSC Adv.* **2016**, 6 (15), 12504-12513.
99. Chen, L.; Zheng, J.; Du, J. L.; Yu, S. P.; Yang, Y. Z.; Liu, X. G., Folic Acid-Conjugated Magnetic Ordered Mesoporous Carbon Nanospheres for Doxorubicin Targeting Delivery. *Mat. Sci. Eng. C-Mater.* **2019**, 104.
100. Simaioforidou, A.; Kostas, V.; Karakassides, M. A.; Louloudi, M., Surface Chemical Modification of Macroporous and Mesoporous Carbon Materials: Effect on Their Textural and Catalytic Properties. *Microporous Mesoporous Mater.* **2019**, 279, 334-344.
101. Yahaya, N.; Kamaruzaman, S.; Sanagi, M. M.; Ibrahim, W. A. W.; Mitome, T.; Nishiyama, N.; Nur, H.; Ghaffar, Z. A.; Aziz, M. Y.; Fauzi, H. M., Vinyl-functionalized Mesoporous Carbon for Dispersive Micro-Solid Phase Extraction

- of Azole Antifungal Agents from Aqueous Matrices. *Sep. Sci. Technol.* **2020**, *55* (17), 3102-3112.
102. Wang, J. J.; Tang, L.; Somasundaran, P.; Fan, W.; Zeng, G. M.; Deng, Y. C.; Zhou, Y. Y.; Wang, J. J.; Shen, Y., Highly Effective Antibacterial Activity by the Synergistic Effect of Three Dimensional Ordered Mesoporous Carbon-Lysozyme Composite. *J. Colloid Interf. Sci.* **2017**, *503*, 131-141.
103. Unsworth, C. E.; Kuo, C. C.; Kuzmin, A.; Khalid, S.; Saha, D., Adsorption of Rare Earth Elements onto DNA-Functionalized Mesoporous Carbon. *ACS Appl. Mater. Interfaces* **2020**, *12* (38), 43180-43190.
104. Mines, P. D.; Thirion, D.; Uthuppu, B.; Hwang, Y.; Jakobsen, M. H.; Andersen, H. R.; Yavuz, C. T., Covalent Organic Polymer Functionalization of Activated Carbon Surfaces through Acyl Chloride for Environmental Clean-up. *Chem. Eng. J.* **2017**, *309*, 766-771.
105. Tessonnier, J. P.; Villa, A.; Majoulet, O.; Su, D. S.; Schlogl, R., Defect-Mediated Functionalization of Carbon Nanotubes as a Route to Design Single-Site Basic Heterogeneous Catalysts for Biomass Conversion. *Angew. Chem. Int. Ed.* **2009**, *48* (35), 6543-6546.
106. Joglekar, M.; Pylypenko, S.; Otting, M. M.; Valenstein, J. S.; Trewyn, B. G., Universal and Versatile Route for Selective Covalent Tethering of Single-Site Catalysts and Functional Groups on the Surface of Ordered Mesoporous Carbons. *Chem. Mater.* **2014**, *26* (9), 2873-2882.
107. Joglekar, M.; Nguyen, V.; Pylypenko, S.; Ngo, C.; Li, Q. N.; O'Reilly, M. E.; Gray, T. S.; Hubbard, W. A.; Gunnoe, T. B.; Herring, A. M.; Trewyn, B. G., Organometallic Complexes Anchored to Conductive Carbon for Electrocatalytic Oxidation of Methane at Low Temperature. *J. Am. Chem. Soc.* **2016**, *138* (1), 116-125.
108. Savameri, A. H.; Izadbakhsh, A.; Zarenezhad, B., Study of the Performance of Amino-Functionalized Ordered Mesoporous Carbon in the Transesterification of Soybean Oil. *React. Kinet. Mech. Cat.* **2018**, *124* (1), 247-264.
109. Fretz, S. J.; Lyons, C. T.; Levin, E.; Chidsey, C. E. D.; Palmqvist, A. E. C.; Stack, T. D. P., Bromomethylation of High-Surface Area Carbons as a Versatile Synthon: Adjusting the Electrode-Electrolyte Interface in Lithium-Sulfur Batteries. *J. Mater. Chem. A* **2019**, *7* (34), 20013-20025.
110. Allongue, P.; Delamar, M.; Desbat, B.; Fagebaume, O.; Hitmi, R.; Pinson, J.; Saveant, J. M., Covalent Modification of Carbon Surfaces by Aryl Radicals Generated from the Electrochemical Reduction of Aiazonium Salts. *J. Am. Chem. Soc.* **1997**, *119* (1), 201-207.
111. Wang, X. Q.; Liu, R.; Waje, M. M.; Chen, Z. W.; Yan, Y. S.; Bozhilov, K. N.; Feng, P. Y., Sulfonated Ordered Mesoporous Carbon as a Stable and Highly Active Protonic Acid Catalyst. *Chem. Mater.* **2007**, *19* (10), 2395-2397.

112. Geng, L.; Wang, Y.; Yu, G.; Zhu, Y. X., Efficient Carbon-Based Solid Acid Catalysts for the Esterification of Oleic Acid. *Catal. Commun.* **2011**, 13 (1), 26-30.
113. Tian, G.; Geng, J. X.; Jin, Y. D.; Wang, C. L.; Li, S. Q.; Chen, Z.; Wang, H.; Zhao, Y. S.; Li, S. J., Sorption of Uranium(VI) Using Oxime-grafted Ordered Mesoporous Carbon CMK-5. *J. Hazard. Mater.* **2011**, 190 (1-3), 442-450.
114. Karimi, B.; Mirzaei, H. M.; Behzadnia, H.; Vali, H., Novel Ordered Mesoporous Carbon Based Sulfonic Acid as an Efficient Catalyst in the Selective Dehydration of Fructose into 5-HMF: the Role of Solvent and Surface Chemistry. *ACS Appl. Mater. Interfaces* **2015**, 7 (34), 19050-19059.
115. Ghasemi, E.; Alimardani, E.; Shams, E.; Koohmareh, G. A., Modification of Glassy Carbon Electrode with Iron-terpyridine Complex and Iron-terpyridine Complex Covalently Bonded to Ordered Mesoporous Carbon Substrate: Preparation, Electrochemistry and Application to H₂O₂ determination. *J. Electroanal. Chem.* **2017**, 789, 92-99.
116. Varmaghani, F.; Karimi, B.; Mallakpour, S., Stabilization of 4-Phenylurazole by Electrografting on a Nano-fibrillated Mesoporous Carbon Modified Electrode. Reactivity of Anchored Triazolinedione Groups against Michael-type Addition at Electrode/Electrolyte Interface. *Electrochim. Acta* **2018**, 269, 312-320.
117. Li, Y.; Murphy, I. A.; Chen, Y.; Lin, F.; Wang, X.; Wang, S. Y.; Hubble, D.; Jang, S. H.; Muller, K. T.; Wang, C. M.; Jen, A. K. Y.; Yang, J. H., A Multi-functional Interface derived from Thiol-modified Mesoporous Carbon in Lithium-Sulfur Batteries. *J. Mater. Chem. A* **2019**, 7 (21), 13372-13381.
118. Takahashi, Y.; Wanibuchi, M.; Kitazumi, Y.; Shirai, O.; Kano, K., Improved Direct Electron Transfer-type Bioelectrocatalysis of Bilirubin Oxidase using Porous Gold Electrodes. *J. Electroanal. Chem.* **2019**, 843, 47-53.
119. Zhang, Y.; Chen, T.; Zhang, G.; Wang, G. Y.; Zhang, H., Efficient Production of Isosorbide from Sorbitol Dehydration over Mesoporous Carbon-based Acid Catalyst. *Appl. Catal. A-Gen.* **2019**, 575, 38-47.
120. Perez-Cadenas, A. F.; Maldonado-Hodar, F. J.; Moreno-Castilla, C., On the Nature of Surface Acid Sites of Chlorinated Activated Carbons. *Carbon* **2003**, 41 (3), 473-478.
121. Zhu, J. Z.; Liang, H.; Fang, J.; Zhu, J. G.; Shi, B. C., Characterization of Chlorinated Tire-Derived Mesoporous Activated Carbon for Adsorptive Removal of Toluene. *Clean-Soil Air Water* **2011**, 39 (6), 557-565.
122. Barpanda, P.; Fanchini, G.; Amatucci, G. G., Structure, Surface, Morphology and Electrochemical Properties of Brominated Activated Carbons. *Carbon* **2011**, 49 (7), 2538-2548.
123. Rupp, E. C.; Wilcox, J., Mercury Chemistry of Brominated Activated Carbons - Packed-Bed Breakthrough Experiments. *Fuel* **2014**, 117, 351-353.

124. Parthiban, V.; Bhuvaneshwari, B.; Karthikeyan, J.; Murugan, P.; Sahu, A. K., Fluorine-enriched Mesoporous Carbon as Efficient Oxygen Reduction Catalyst: Understanding the Defects in Porous Matrix and Fuel Cell Applications. *Nanoscale Adv.* **2019**, 1 (12), 4926-4937.
125. Li, Z. J.; Del Cul, G. D.; Yan, W. F.; Liang, C. D.; Dai, S., Fluorinated Carbon with Ordered Mesoporous Structure. *J. Am. Chem. Soc.* **2004**, 126 (40), 12782-12783.
126. Jeon, I. Y.; Kim, C.; Kim, G.; Baek, J. B., Mechanochemically Driven Iodination of Activated Charcoal for Metal-free Electrocatalyst for Fuel Cells and Hybrid Li-air Cells. *Carbon* **2015**, 93, 465-472.
127. Long, P.; Feng, Y. Y.; Cao, C.; Li, Y.; Han, J. K.; Li, S. W.; Peng, C.; Li, Z. Y.; Feng, W., Self-Protective Room-Temperature Phosphorescence of Fluorine and Nitrogen Codoped Carbon Dots. *Adv. Funct. Mater.* **2018**, 28 (37).
128. Suresh, S. P.; Lekshmi, G. S.; Kirupha, S. D.; Ariraman, M.; Bazaka, O.; Levchenko, I.; Bazaka, K.; Mandhakini, M., Superhydrophobic Fluorine-modified Cerium-doped Mesoporous Carbon as an Efficient Catalytic Platform for Photo-degradation of Organic Pollutants. *Carbon* **2019**, 147, 323-333.
129. Wu, M. C.; Zhang, R. H.; Liu, K.; Sun, J.; Chan, K. Y.; Zhao, T. S., Mesoporous Carbon derived from Pomelo Peel as a High-performance Electrode Material for Zinc-Bromine Flow Batteries. *J. Power Sources* **2019**, 442.
130. Oschatz, M.; Thieme, S.; Borchardt, L.; Lohe, M. R.; Biemelt, T.; Brückner, J.; Althues, H.; Kaskel, S., A new Route for the Preparation of Mesoporous Carbon Materials with High Performance in Lithium-Sulphur Battery Cathodes. *Chem. Commun.* **2013**, 49 (52), 5832-5834.
131. Seok, J. Y.; Song, S. A.; Yang, I. Y.; Woo, K.; Park, S. Y.; Park, J. H.; Kim, S.; Kim, S. S.; Yang, M. Y., Hierarchically Porous Carbon Nanofibers with Controllable Porosity Derived from Iodinated Polyvinyl Alcohol for Supercapacitors. *Adv. Mater. Interfaces* **2020**, 7 (16).
132. Yao, Z.; Nie, H. G.; Yang, Z.; Zhou, X. M.; Liu, Z.; Huang, S. M., Catalyst-free Synthesis of Iodine-doped Graphene: a Facile Thermal Annealing Process and its use for Electrocatalytic Oxygen Reduction in an Alkaline Medium. *Chem. Commun.* **2012**, 48 (7), 1027-1029.
133. Simek, P.; Klimová, K.; Sedmidubsky, D.; Jankovsky, O.; Pumera, M.; Sofer, Z., Towards Graphene Iodide: Iodination of Graphite Oxide. *Nanoscale* **2015**, 7 (1), 261-270.
134. Zhang, X. Q.; Lu, G. X., The Spin-orbit Coupling Induced Spin Flip and its role in the Enhancement of the Photocatalytic Hydrogen Evolution over Iodinated Graphene Oxide. *Carbon* **2016**, 108, 215-224.

135. Chen, J.; Xu, M. W.; Wu, J. G.; Li, C. M., Center-Iodized Graphene as an Advanced Anode Material to Significantly Boost the Performance of Lithium-ion Batteries. *Nanoscale* **2018**, 10 (19), 9115-9122.
136. Marinoiu, A.; Raceanu, M.; Carcadea, E.; Varlam, M.; Stefanescu, L., Low Cost Iodine Intercalated Graphene for Fuel Cells Electrodes. *Appl. Surf. Sci.* **2017**, 424, 93-100.
137. Wang, A. Q.; Bok, S.; Mathai, C. J.; Gangopadhyay, K.; McFarland, J.; Maschmann, M. R.; Gangopadhyay, S., Stability study of Iodinated Reduced Graphene Oxide and its Application in Self-assembled Al/BiO Nanothermite Composites. *Nano Futures* **2020**, 4 (4).
138. Marinoiu, A.; Raceanu, M.; Carcadea, E.; Varlam, M.; Stefanescu, I., Iodinated Carbon Materials for Oxygen Reduction Reaction in Proton Exchange Membrane Fuel Cell. Scalable Synthesis and Electrochemical Performances. *Arab J. Chem.* **2019**, 12 (6), 868-880.
139. Marinoiu, A.; Raceanu, M.; Carcadea, E.; Varlam, M.; Soare, A.; Stefanescu, I., Doped Graphene as Non-Metallic Catalyst for Fuel Cells. *Mater. Sci.-Medzg.* **2017**, 23 (2), 108-113.
140. Poh, H. L.; Simek, P.; Sofer, Z.; Pumera, M., Halogenation of Graphene with Chlorine, Bromine, or Iodine by Exfoliation in a Halogen Atmosphere. *Chem.-Eur. J.* **2013**, 19 (8), 2655-2662.
141. Munaiah, Y.; Ragupathy, P.; Pillai, V. K., Single-Step Synthesis of Halogenated Graphene through Electrochemical Exfoliation and Its Utilization as Electrodes for Zinc Bromine Redox Flow Battery. *J. Electrochem. Soc.* **2016**, 163 (14), A2899-A2910.
142. Marinoiu, A.; Raceanu, M.; Carcadea, E.; Varlam, M.; Balan, D.; Ion-Ebrasu, D.; Stefanescu, I.; Enachescu, M., Iodine-Doped Graphene for Enhanced Electrocatalytic Oxygen Reduction Reaction in Proton Exchange Membrane Fuel Cell Applications. *J. Electrochem. Energy* **2017**, 14 (3).
143. Pumera, M.; Sofer, Z., Towards Stoichiometric Analogues of Graphene: Graphane, Fluorographene, Graphol, Graphene Acid and Others. *Chem. Soc. Rev.* **2017**, 46 (15), 4450-4463.
144. Jeon, I. Y.; Choi, H. J.; Choi, M.; Seo, J. M.; Jung, S. M.; Kim, M. J.; Zhang, S.; Zhang, L. P.; Xia, Z. H.; Dai, L. M.; Park, N.; Baek, J. B., Facile, Scalable Synthesis of Edge-Halogenated Graphene Nanoplatelets as Efficient Metal-free Electrocatalysts for Oxygen Reduction Reaction. *Sci. Rep.-UK* **2013**, 3.
145. Wu, K. H.; Wang, D. W.; Zeng, Q. C.; Li, Y.; Gentle, I. R., Solution Phase Synthesis of Halogenated Graphene and the Electrocatalytic Activity for Oxygen Reduction Reaction. *Chinese J. Catal.* **2014**, 35 (6), 884-890.

CHAPTER 2 OMC AMINATION BY ORGANOLITHIUM ACTIVATION TO CONFER C-C
LINKAGES WITH PENDANT PRIMARY AMINES

Manuscript submitted to *ChemCatChem*.

Nolan C. Kovach^{1,2}, Scott E. Massimi¹, Brian G. Trewyn^{3,4}

2.1 Abstract

Developing heterogeneous catalysts with more robust active sites that withstand numerous reaction cycles and/or strong conditions while maintaining original activity is key to realize these materials in many applications. We report the synthesis of ordered mesoporous carbon (OMC) nanoparticles functionalized with covalently bound ethylamine moieties (EtNH₂@OMC) that catalyze the Knoevenagel condensation reaction (90% conversion, >95% selectivity) between benzaldehyde and malononitrile under mild conditions in air. No benzoic acid oxidation side-product was detected for the amine-modified OMC reactions, attributed to the hydrophobic mesopore environment unique to OMC. Carbon surface modification was afforded by organolithium-mediated surface activation, presenting 0.4 wt% N content by elemental analysis and a confirmed coverage of 100 μmol · g⁻¹ -NH₂ by the 4-nitrobenzaldehyde colorimetric assay. We believe the confluence of surface chemistry and mesopore size enable the novel EtNH₂@OMC performance in the Knoevenagel condensation reaction. These studied aminated

¹ Graduate student, Chemistry Dept., Colorado School of Mines

² Primary researcher and author

³ Research Joint Appointment, National Renewable Energy Laboratory (NREL)

⁴ Associate Professor, Chemistry Dept., Colorado School of Mines

OMC scaffolds are explored further in the following chapter to ascertain a pH range for which they can be employed while maintaining the primary amine functionality.

2.2 Introduction

Carbon-carbon bond formation is an inordinately important reaction for fine chemical, pharmaceutical, cosmetic, and agrochemical industries.¹⁻⁴ Large scale manifestations often require high temperatures and pressures, highly corrosive reagents, and/or neurotoxic and geo-scarce metals.⁵⁻⁶ An attractive approach to ameliorate these hazards is by engineering novel catalysts employed in the Knoevenagel condensation pathway (Figure 2.1). Knoevenagel catalysts have multiple pathways to form carbon-carbon bond transformations. One pathway is by Lewis base catalyzed deprotonation of the active methylene reactant, enabling subsequent C-C bond formation with the aldehyde carbon. Another catalytic mechanism is to stabilize the reactant aldehyde oxygen, increasing the carbonyl susceptibility towards nucleophilic attack by a carbanionic methylene reactant.

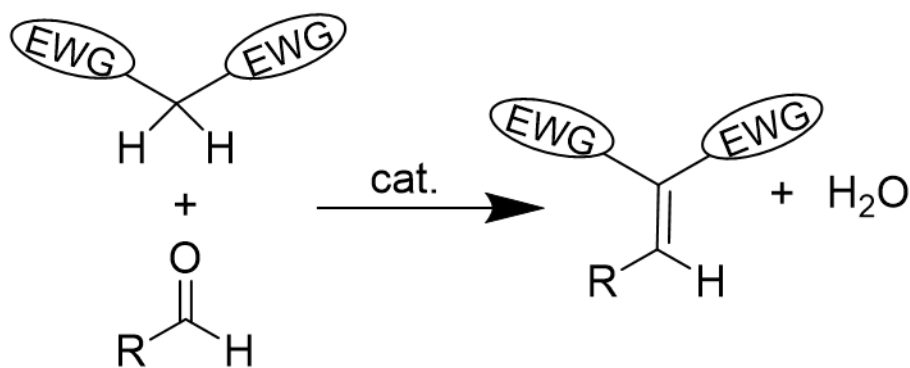


Figure 2.1. Elementary depiction of the Knoevenagel condensation between an aldehyde and an “active” methylene reactant containing electron withdrawing groups (EWG).

The Knoevenagel condensation reaction has been exemplified in industry using either pyridine or piperidine as a homogeneous catalyst to deprotonate the acidic methylene moiety or form a Schiff base (imine) to initiate the reaction. Cyclic amine toxicity and volatility have inspired researchers to look at various alternatives to these compounds.⁷

One perspective is to swap out amine catalysts with Lewis acidic metal chlorides like SnCl₂, CeCl₃, FeCl₃, InCl₃, or NbCl₅.⁸⁻¹² Using metal chlorides requires extra synthetic steps to segregate soluble metal catalysts from product streams, leading to a surge of interest in employing metal-containing solids. Ionic liquids benefit inherent solvent-catalyst dual behavior, maintain structure over multiple reaction runs, but often require distillation to separate catalysts from final products.¹³⁻¹⁶ Metal oxides show reasonable activity, yet the best performing examples use toxic HgCl₂ or CdCl₂.¹⁷⁻²⁰ Less-toxic solids like zeolites, clays, metal-organic-frameworks (MOFs), and metal nanoparticles embedded onto porous support surfaces are effective for the Knoevenagel condensation.²¹⁻²⁷ For many of these porous solid catalysts, internal pore dimensions can restrict reactant transport to active sites located through sufficiently narrow nanochannels, thereby limiting the activity of the catalyst. Thus, supports with larger pores are sought to improve upon the mass transfer inadequacies inherent to microporous scaffolds. Metal-contrived scaffolds used for Knoevenagel condensation have an extra hurdle to overcome, proving there is no leaching and/or nanoparticle agglomeration upon recycling. To circumvent these issues, mounting interest in using metal-free catalysts for Knoevenagel condensation reactions has emerged.

In 2012, metal-free heterogeneous catalysis was shown using platelet-shaped mesoporous graphitic carbon nitride (gCN) nanoparticles, hard templated from INC-2 mesoporous silica.²⁸ In the absence of any structure-directing-agent, gCN presents itself as nonporous stacked sheets.

The gCN research used microwave heating to promote reaction progress (90% conv, 99% sel., 0.2 hr, 120 °C). Despite impressive yields with such a short reaction time, irradiation greatly adds to the system cost and accessibility. The templating method for gCN has been realized with other mesoporous silica types like KIT-6 and SBA-15.²⁹⁻³⁰ Earlier reports attributed gCN catalytic activity to edge-localized primary amines, while later research pointed out the importance of the 1-amino/imino-1,2,4-triazole moiety that tends to dominate gCN structure when synthesized below 400 °C.³¹ Our understanding of nitrogen functionality on carbonaceous surfaces impacting Knoevenagel condensation catalysis is primarily from gCN—a majority of gCN compositions exhibit N/C ratios close to 1. Notably less Knoevenagel condensation research has been reported on nitrogen-doped carbon materials where and N/C ratio is often below 0.1. Perhaps the first example of nitrogen-doped ordered mesoporous carbon materials (NOMC) for Knoevenagel condensation catalysts was in 2018.³² Their NOMC reaction needed only a slight temperature elevation to react effectively (best: 87% conv., 99% sel., 4 h, 40 °C). The N-OMC comprised 3.6 nm mesopores measured by nitrogen sorption and presented lamellar planar stacking via TEM analysis. They posited graphitic nitrogen surface sites were responsible for the initial methylene activation in the Knoevenagel condensation, supported by XPS analysis. Albeit the fact graphitic nitrogen doping is thought to be a basic active site for KC activity, it has been demonstrated that primary amines functionalized atop carbon surfaces can impart basic activity.³³

The most applied functionalization route for porous carbon materials is wet chemical oxidation. Employing strong oxidants (like HNO₃, (NH₄)₂S₂O₈, and H₂O₂), chemical groups like hydroxyls, ketones, carboxylic acids, ethers, and lactones populate the surfaces exposed to the chemical treatment.³⁴⁻³⁷ These functionalities give rise to improved hydrophilicity which can

covalently react with subsequent compounds. Other materials with surface hydroxyls (i.e. zeolites, silicas, clays, metal oxides) have nucleophilic oxygen groups which condense with functional silicas. The pore space must be sufficiently large to sterically accommodate organosilanes, a common example being 3-aminopropyltriethoxysilane for introducing primary amine basicity.³⁸⁻⁴⁰ Wet chemical oxidation installs numerous functional groups at the expense of structural degradation in many, but not all cases.³⁴⁻³⁵, 41 On the standpoint of chemical stability, the Si-O-C bond is susceptible to basic and acidic hydrolysis.⁴²⁻⁴³ Another route for installing functional groups into OMC, organolithium C-H activation, was first realized in 2014, and the bipyridine-functionalized surface was used to chelate Pt²⁺ and Cu²⁺ for electro/catalytic applications.⁴⁴⁻⁴⁵

We sought to create a base-functionalized porous carbon material that would retain mesoporous structure following amination that would be effective for Knoevenagel condensation catalysis. Our OMC was templated by sucrose carbonized within mesoporous silica nanoparticles (MSN) comprising hexagonally packed mesopores (P3m crystallographic space group) interconnected by radial micropore tubules. The OMC pore walls are made up of hexagonally arranged carbon nanorods that were initially enshrouded by silica; likewise, the OMC pore space, being surrounded by carbonaceous rods, is the denuded volume that the silica solid originally resided. This hard-templated OMC exhibits both microporous and mesoporous features, with a surface able to undergo organolithium activation and subsequent electrophilic grafting of ethylamine groups. The concomitant introduction of acidic oxygen groups in proximity to the primary amines by the defect-mediated route enabled denuded activity on an OMC surface that showed no activity without such molecular decoration.

2.3 Material Synthesis

MSN were fabricated following a previous publication.⁴⁶ First, 7.0 g pluronic P104 surfactant was added to 225 mL 1.6M of aqueous HCl, stirred at 550 rpm for 1 h at 55 °C. To this clear solution, 10.4 mL TEOS was added rapidly, forming an opaque milky solution after a few minutes. After stirring for 24 h, the contents of the flask were transferred to an autoclave and placed in an air-convection oven at 150 °C for 24 h. The suspension filtrate was then filtered over a medium frit funnel, and the solid particles were dried in a 70 °C oven for 6 h. The dried material was then placed into a ceramic crucible and calcined at 550 °C for 6 h in a muffle furnace. The calcined silica was washed with water twice, then ethanol, and allowed to dry in an oven overnight.

Ordered Mesoporous Carbon Fabrication

Templating the mesoporous silica involves four successive wet impregnations of sucrose. Two grams of MSN were added to a ceramic crucible along with a certain amount of sucrose and dry mixed. Then, 14 mL Nanopure™ water was mixed to produce a slurry, to which 0.5 mL of 36% HCl was added. This suspension is placed in an air convection oven at 110 °C for 6 h then raised to 160 °C for 6 h. The amounts of sucrose added in each step was: 2.628 g, 1.614 g, 0.324 g and 0.446 g. Following this, the silica:carbon composite was placed into a quartz boat for carbonization in a tube furnace under 150 sccm Ar flow from RT to 600 °C in 1.5 h, from 600 °C to 900 °C ramped up over 6 h, and held at 900 °C for 6 h. The silica from the composite was then etched by splitting the sample into two polypropylene tubes and then adding 40 mL 10% HF, allowing to sit overnight after manual agitation. The etched material was then suspended in methanol and stirred at 550 rpm for 24 h to remove residual silica-fluoride salts. The as-made material was then centrifuged for 10 min at 4400 ×g and decanted, with wash/spin cycles

repeated three times with water and once with methanol. Finally, the OMC was dried at 70 °C overnight.

Covalent Ethylamine Functionalization

First, 0.250 g carbon was added to a 100 mL RBF outfitted with a short neck drop funnel with an applied nitrogen stream. The apparatus was submerged in 110 °C oil bath overnight. A chloroform/N₂ slurry was prepared to maintain -77 °C. Next, 25 mL diethyl ether was added to the RBF and stirred at 350 rpm for 5 min. The flask was sonicated in an ice bath for ~1 min to disaggregate the OMC. After returning to the cold bath, 2.5 mL 2.5 M *n*-BuLi in hexanes was added and allowed to stir to RT over the course of 5 h. Then, 3.0 mmol (0.13 g) of bromoethylamine hydrobromide was added and allowed to stir for 16 h. The product was then split into two polypropylene centrifuge tubes and spun at 4400 ×g for 10 min and decanted. The materials were then washed thrice with methanol and dried at 70 °C overnight.

2.4 Physicochemical Characterizations

Nitrogen Adsorption Isotherms

Nitrogen sorption measurements were recorded on a monthly-calibrated Micromeritics Tristar II gas adsorption tool to determine specific surface area and porosity predicated by outgassing at 150 °C for 6 h using a Micromeritics SmartPrep unit under N₂ flow. Experiments were conducted at 77 K with N₂ probe gas. Specific surface area was measured following the Brunauer-Emmett-Teller (BET) method assessing the partial pressure (P/P_0) range of 0.10-0.22. While the BET method fails to accurately model monolayer adsorption for materials containing micropores, the validity of the theory stands for mesopores with pore widths greater than 4 nm. The studied OMCs are predominantly mesoporous with a relatively small (~10% of total surface

area) contribution from micropore domains. For this experimentation, the BET surface area values are assumed to mostly reflect the changes to the mesopore space in the OMCs and will be interpreted as such. All mesopore pore size distributions and mesopore volumes were calculated by the Barrett-Joyner-Halenda (BJH) method on the isotherm desorption branch. The t-plot analysis can provide an estimate on the extent of micropore functionalization.

Scanning Electron Microscopy

Scanning electron micrographs were obtained on native samples (no Au sputtering coat) using an Amray 3300 Field Emission Scanning Electron Microscope by a secondary electron detector. OMC samples were imaged using a high tension of 20 kV. For imaging the silica template, a lower operating voltage of 10 kV was necessary to avoid charging artifacts.

Transmission Electron Microscopy

An FEI Talos F200X field emission scanning/transmission electron microscope was used to collect all TEM images. Samples were measured on Ni grids with lacy carbon.

4-Nitrobenzaldehyde Assay

Surface-functionalized primary amines were assessed by the 4-nitrobenzaldehyde (4-NB) assay modified to accommodate 15 mL polypropylene centrifuge tubes.⁴⁷ All samples were assessed in triplicate. Approximately 5 mg of carbon was added to a 15 mL tube to which 2 mL of 50 mg · mL⁻¹ 4-NB in methanol was added and shaken in an incubator-shaker at 45 °C at 350 rpm for at least 8 h. Then, the carbon was separated by centrifugation at 4400 ×g for 5 min. The carbon was then rinsed thrice with 10 mL methanol to remove excess, unreacted 4-NB, waiting at least an hour after initial contact. Finally, surface-reacted 4-NB (in the form of a Schiff base)

was hydrolyzed three times by immersing the carbon in 10 mL of 50:50 methanol:water. The supernatant from each hydrolysis was subjected to UV-Vis spectroscopy to monitor the $n \rightarrow \pi^*$ transition of 4-NB.⁴⁸

Elemental Analysis

Carbon samples were analyzed for C, H, O and N by combustion elemental microanalysis contracted by Hazen Research, Inc. (Golden, CO) following a 6 h degassing at 100 °C. Nitrogen content was assessed by the Dumas method.

Thermogravimetric Analysis

A QA Instruments Q500 Thermogravimetric Analyzer assessed the carbon mass loss in an alumina sample pan. All experiments used 10 sccm air with 20 sccm nitrogen and a ramp rate of 10 °C/min from RT to 800 °C without a temperature hold.

Low-Angle Powder X-ray Diffraction

Powder diffraction scans were obtained with a Malvern Panalytical Empyrean diffractometer operating in reflection mode using Bragg-Brentano geometry with a Cu X-ray source (40 kV, 40 mA). To maximize detector counts with the small sample volumes, the sample stage was not rotated. Samples were measured on a zero-diffraction Si-111 holder.

Fourier-Transform Infrared Spectroscopy

All Fourier-transform infrared spectroscopy (FTIR) spectra were obtained by attenuated-total-reflectance (ATR) on sample powders over the range 400-4000 cm^{-1} . A total of 50 scans were collected for each sample, with a spectral resolution of 4 cm^{-1} .

Knoevenagel Condensation Catalysis

For the Knoevenagel condensation catalysis, batch reactions were performed. A 30 mg sample was charged into a flask and dried in an oven at 110 °C for 1 h. Next, the vessel was regulated at 40 °C and stirred at 400 rpm. In sequential order, 3 mmol malononitrile (167 μ L), 6.0 mL methanol, and 2 mmol benzaldehyde (204 μ L) were added and left to react for 4 h. The product suspension was transferred to a polypropylene centrifuge tube and spun at 4400 $\times g$ for 10 min. An aliquot of decanted liquid product was diluted 1000 X in methanol for gas chromatography-mass spectrometry (GCMS) analysis.

The initial rate of reaction was also tested for three reaction cycles, where the same reaction conditions were employed as above, but the powder catalyst was thoroughly regenerated between each reaction step by two immersions in methanol, and one rinse step with 0.1M HCl in methanol. Reaction aliquots were taken at $t=0, 1, 2, 3, 4, 5,$ and 10 minutes to determine the initial velocity of the catalyst.

Gas Chromatography-Mass Spectrometry

Liquid products were analyzed on an Agilent 7890B/5977A with GC/MSD with an ALS injector outfitted with an HP-5 GC (95%-5%) column. For every trial: $Temp_{inlet}$: 275 °C; $Temp_{column}$: 75-300 °C; $time_{run}$: 10 min; carrier flow: 1 mL \cdot min⁻¹. Quantification of benzylidenemalononitrile product was achieved by external calibration.

2.5 Results and Discussion

Nitrogen Sorption Isotherms

All OMC samples exhibited a type IV isotherm, embodying H4-type hysteresis according to the International Union of Pure and Applied Chemistry classification (Figure 2.2). These features represent a hierarchical microporous-mesoporous structure. As considered such, we followed recommendations by Rouquerol et al. to report BET surface area for materials exhibiting microporosity.⁴⁹ Pore size distribution plots derived from BJH desorption showed an OMC mesopore diameter centered around 5.3 nm ($d_{FWHM}=0.3$ nm). Attachment of EtNH₂ resulted in a pore diameter reduction to 4.2 nm ($d_{FWHM}=0.2$ nm) and a diminution of pore volume from 1.39 to 0.79 cm³ · g⁻¹, implying the OMC pore surfaces were coated, to some extent, with molecular cargo. Likewise, the surface area of OMC was lowered from 1060 m² · g⁻¹ to 560 m² · g⁻¹ for EtNH₂@OMC (Table 2.1). No determination of micropore volume could be made due to t-plot slope analysis yielding negative pore volume values.

Table 2.1. Nitrogen sorption-derived BET surface area ($0.10 < P/P_0 < 0.22$) and BJH desorption pore volume and pore size distributions.

	BET Surface Area (m ² · g ⁻¹)	Pore Volume (cm ³ · g ⁻¹)	Pore Diameter (nm)
OMC	1060	1.39	5.3 ± 0.3
EtNH ₂ @OMC	560	0.79	4.2 ± 0.2

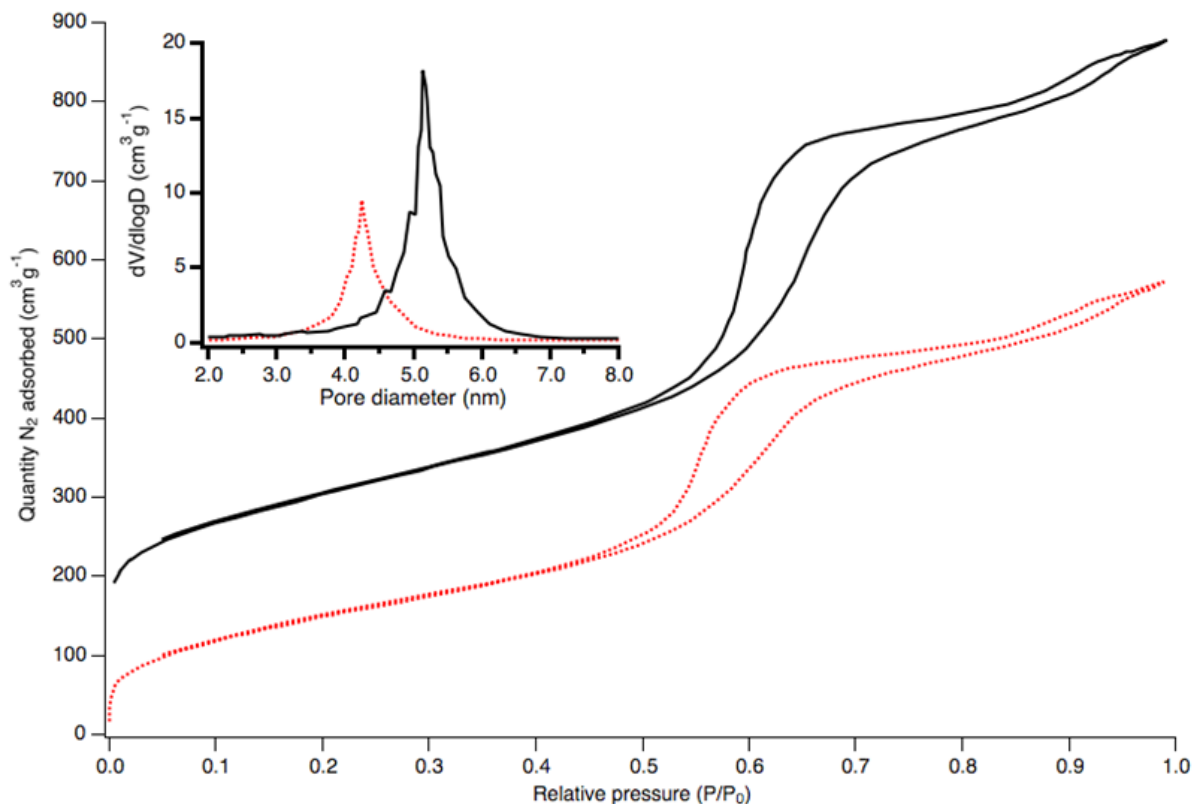


Figure 2.2. Nitrogen sorption isotherms for OMC (solid black trace) and EtNH₂@OMC (dotted red trace) materials with a BJH desorption pore size distribution plot (inset).

Scanning Electron Microscopy

Bulk morphology and particle size dispersity were qualitatively observed by SEM. The displayed micrographs (Figure 2.3) show representative particles that were observed. The MSN-10 silica has similar internal pore structure to SBA-15, but MSN-10 particles are truncated at a nearly spherical aspect ratio whereas SBA-15 is more wormlike and tubular with a higher aspect ratio.⁵² We observed that the OMC morphology is preserved from that of MSN-10 template at a particle-scale, though no conclusions on the mesoporosity for either the template or OMC could be observed by SEM.

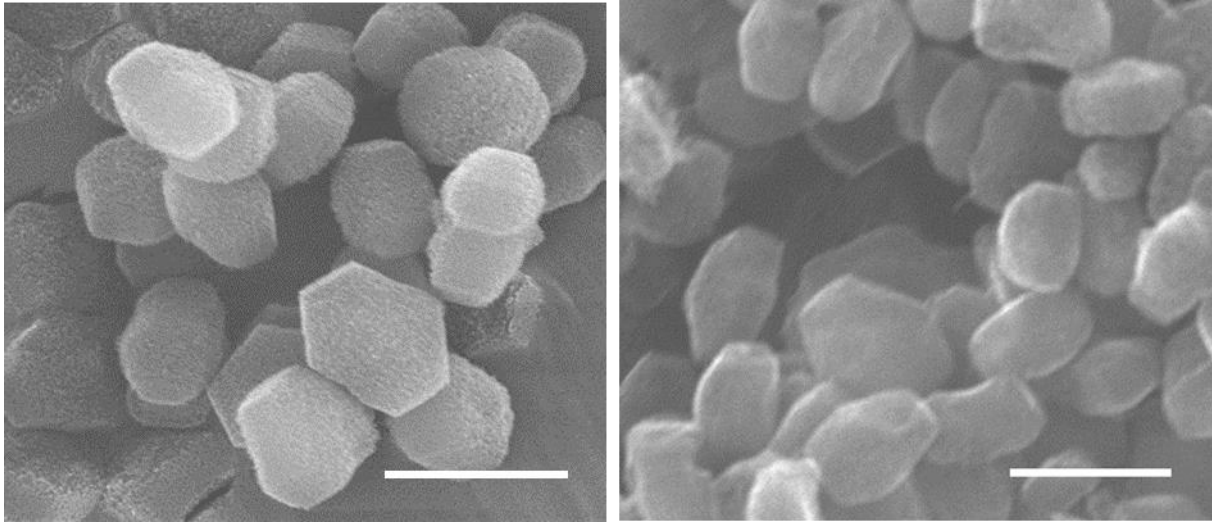


Figure 2.3. Scanning electron micrographs showing particle morphology preservation between the MSN-10 template (left) and OMC (right). Scale bar: 1 μm .

Transmission Electron Microscopy

The lateral spatial resolution of transmission electron microscopy is sufficient to visualize the perpendicularly-aligned carbon nanorod scaffolds comprising the OMC nanoparticles. The hexagonal shaped particles were oriented such that the lamellar orientation of mesoporous channels were clearly visualized (Figure 2.4). Seeing that all particles are sized on the submicron scale, the observed mesoporous features on the collected isotherms confidently pertain to porosity contained within these nanoparticles rather than intra-particle porosity.

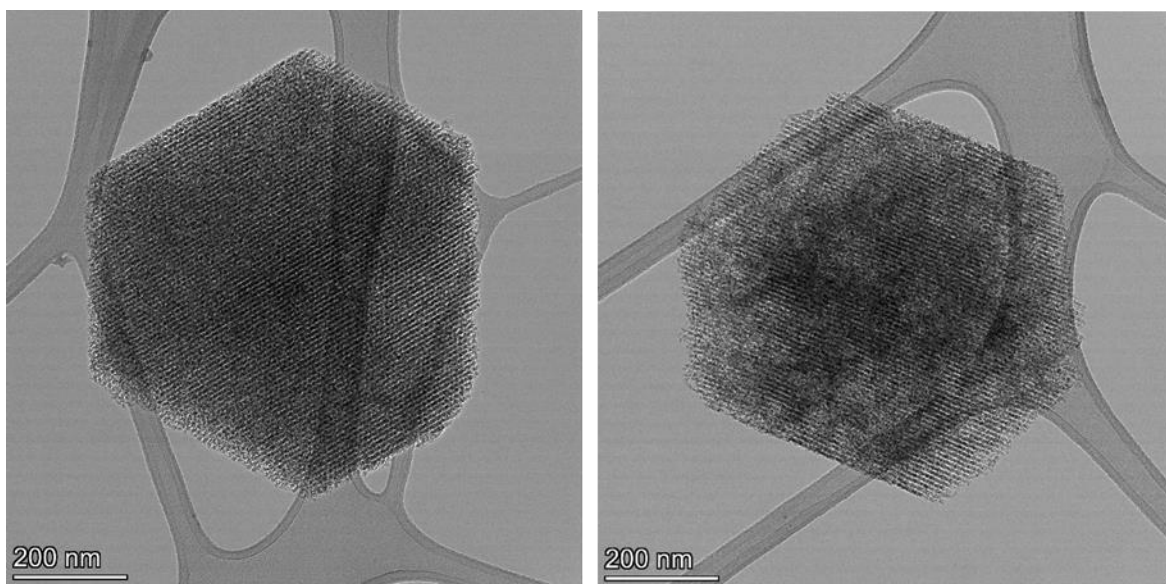


Figure 2.4. Transmission electron micrographs of OMC (left) and EtNH₂@OMC (right).

4-Nitrobenzaldehyde Assay

Both assayed samples were tested in triplicate and a blank sample tube was tested to ensure negligible competitive adsorption occurs onto the plastic tube sidewalls. The amine surface density was calculated by dividing the total amount detected 4-NB in solution and dividing that by the measured BET surface area of each material. The unmodified OMC registered near-zero amounts of surface amine groups, exhibiting less than 0.005 mmol/g. Surface amination imparted a modest 0.100 mmol · g⁻¹ (4.4 mg · g⁻¹) of primary amines, which is in close agreement to the wt. % N detected by elemental analysis (4 mg · g⁻¹).

Low-Angle X-ray Diffraction

The LA-XRD scans were performed on the OMC materials before and after surface functionalization (Figure 2.5) to make a judgement about the presence of mesopore ordering. For

ordered mesoporous materials, diffraction features are observable at 2θ angles well below those utilized to determine crystallographic atomic lattices. Both OMC materials exhibited a peak prominence centered around 1.10° , ascribed to [100] ordering of adjacent carbon nanorods (mesopore walls) corresponding to a d_{100} spacing of 8.03 nm. The lithiation-amination procedure shows no change towards the topological ordering given no difference in peak center between OMC and EtNH₂@OMC. All higher-order diffraction peaks (pertaining to the [110], [200], [210], and [300] indexes) were undetected for the OMC material, and therefore the scan ranges were truncated from $0.5\text{-}5^\circ$ to $0.5\text{-}1.5^\circ$. The identified low-angle powder X-ray diffraction peak feature at 1.1° is analogous to that measured for hard-templated OMCs prepared from a similar mesoporous silica template (SBA-15).^{56,57}

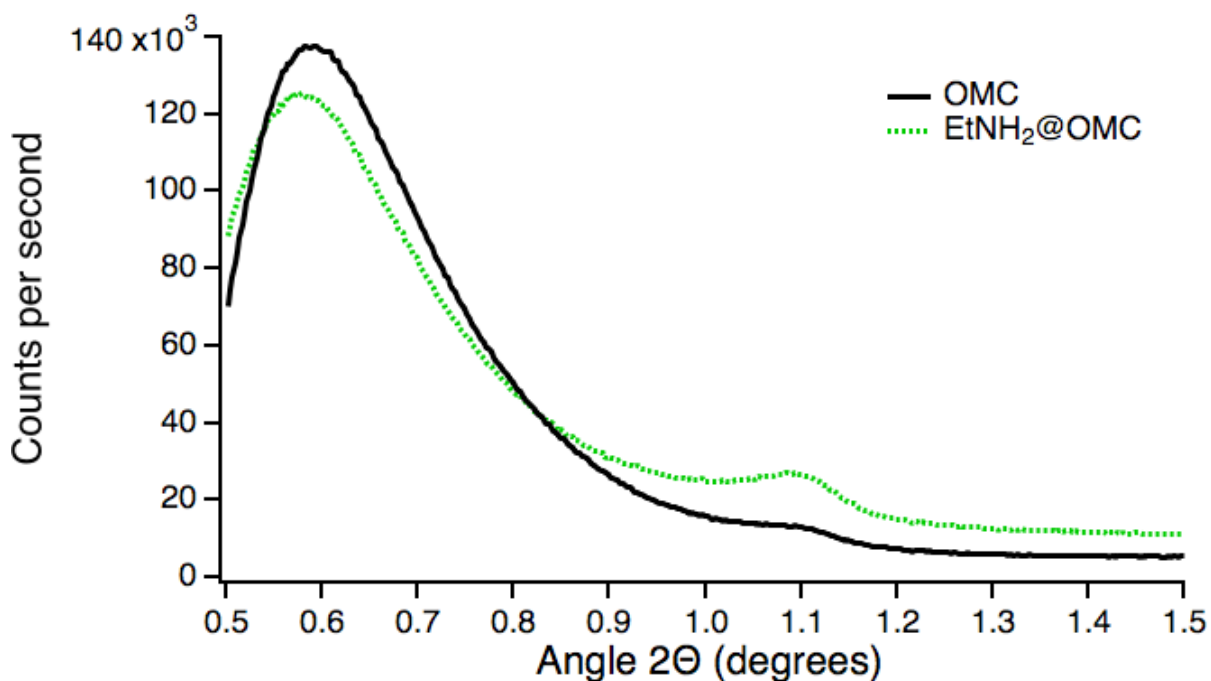


Figure 2.5. Powder XRD patterns of OMC and EtNH₂@OMC. Step size: 0.002° ; scan rate: 0.50 sec/step.

Attenuated Total Reflection FTIR

Attenuated total reflection FTIR spectra from 400 cm^{-1} to 4000 cm^{-1} was assessed for each catalyst to detect signals corresponding to specific functional groups (Figure 2.6).⁵⁰ Unmodified OMC shows three signals at 690 cm^{-1} , 715 cm^{-1} , and 745 cm^{-1} attributed to phenyl C-H stretching. Ligand attachment occurring at deprotonated aryl sites would diminish this signal, observed for the $\text{EtNH}_2\text{@OMC}$ sample. Further, the humplike feature c.a. 1025 cm^{-1} and c.a. 1580 cm^{-1} are signals for a C-N stretch and a primary amine N-H bend, respectively.

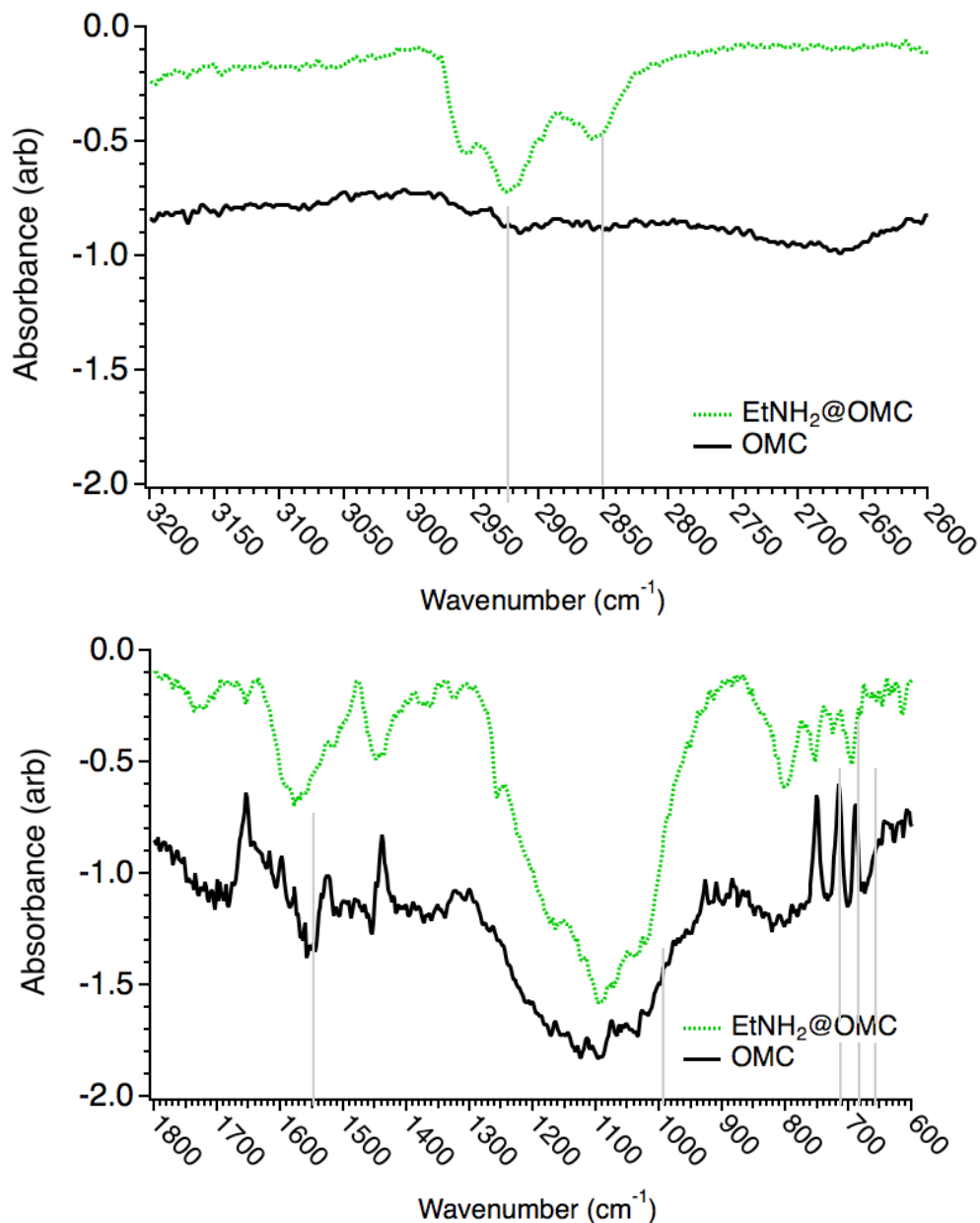


Figure 2.6. FTIR-ATR spectra obtained for unfunctionalized OMC and EtNH₂@OMC highlighting motifs pertaining to the amination.

EtNH₂@OMC presents ridges at 2850 cm⁻¹ and 2925 cm⁻¹ representing symmetric and asymmetric methylene C-H stretches arising from the ethyl chain. The additional peak emerging at 2960 cm⁻¹ is likely a methyl group C-H stretch and may belong to butyl groups appended via

carbometallation. In light of nitrogen sorption measurements, FTIR offers some evidence towards the presence of ethylamine moieties atop or within the OMC scaffold.

It is understood that organolithium reagents “activate” carbon centers by either deprotonation or carbometallation mechanisms.⁵¹ Deprotonation gives rise to one lithiated aryl C-H site, while carbometallation creates a lithiated site adjacent to a carbon that received a butyl addend (from n-butyllithium). In our case, the strongly nucleophilic C-Li bond on the activated OMC reacted with bromoethylamine, added to the synthetic vessel, and oxygen, adsorbed from atmosphere, into the stirred ether during that synthetic step. Thus, three different modifications are anticipated: ethylamine, butane, and phenolic oxygen.

Thermogravimetric Analysis

The TGA curve of OMC showed one mass loss inflection starting at 500 °C, ascribed to the carbonization of the carbon frame (Figure 2.7).

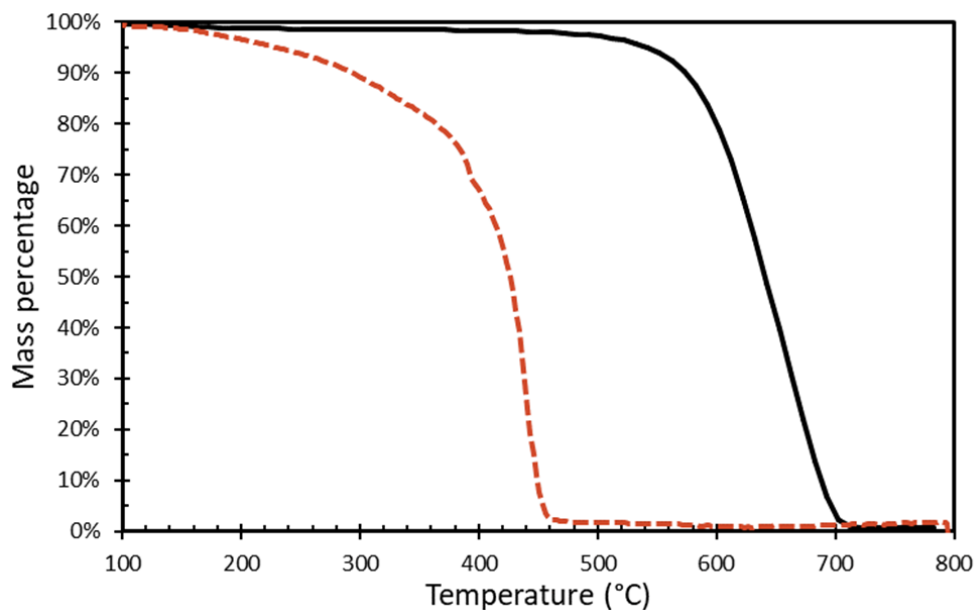


Figure 2.7. Thermogravimetric traces obtained for OMC (black trace) and EtNH₂@OMC (dotted red trace) under 10 °C · min⁻¹ ramp rate.

After the ethylamine functionalization, a new feature was present from 275 °C up to the decomposition temperature of 450 °C, evidencing the presence of combustible functionality before OMC framework decomposition. For EtNH₂@OMC, the mass reduction beginning around 190 °C is believed to arise from thermal decomposition of CO₂ conjugated with the primary amine functional groups or direct surface decarboxylation from carboxylic acids appended during the butyllithium protocol. The derivative of mass loss per temperature for EtNH₂@OMC (Figure 2.8) shows an increase in mass loss from around 150 °C which continues until an abrupt mass loss feature around 390 °C, believed to arise from CO₂ desorption and ethylamine decomposition.

Elemental Analysis

Elemental analysis results (Table 2.2) show the unfunctionalized OMC to mainly comprise carbon, and a small amount of oxygen and hydrogen. EtNH₂@OMC registered an enrichment of nitrogen after ethylamine grafting, accompanied with an increase in detected oxygen and hydrogen wt. %.

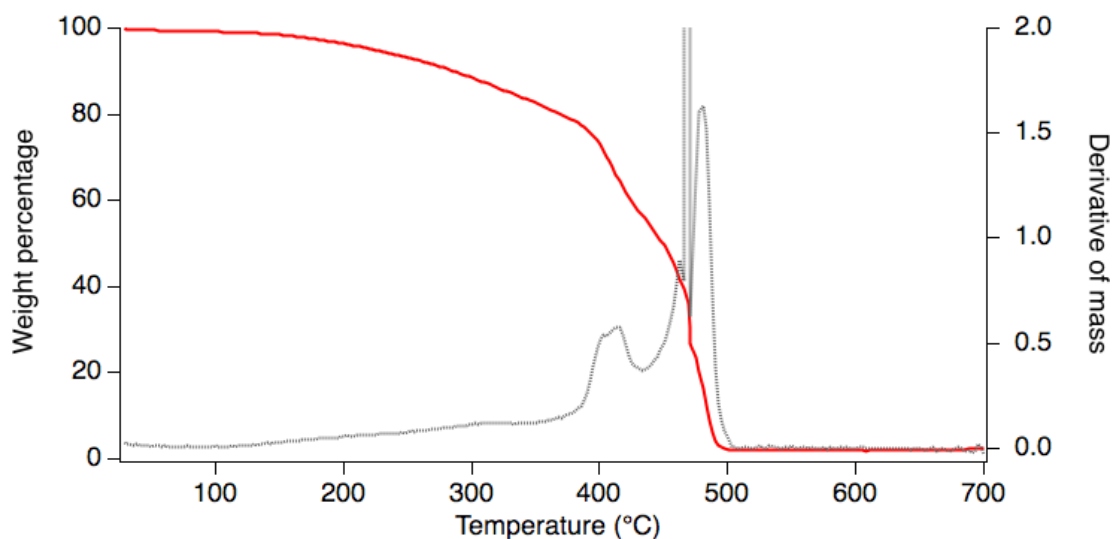


Figure 2.8. TGA and DTG curves for EtNH₂@OMC.

If the grafted ethylamine (C₂H₆N) groups were to substitute one in every four C-H sites, then the resulting surface would see an increase in hydrogen content by a factor of 2.25; We observed a 2.45 difference in hydrogen mass content, justified by the inclusion of butyl groups (C₄H₉) at some C-H sites. The assumption is that the doubling in oxygen content is reminiscent of oxidation from atmospheric carbon dioxide during the amination protocol. The disparity between the summed mass percentages of detected elements and 100.0% wt. % is thought to be due to the prominence of non-detected elements; potentially residual silica and fluorine for the case of OMC (from the MSN template), or fluorine, silica, lithium, or bromine from the butyllithium amination procedure.

Table 2.2. Elemental microanalysis (wt. %) for the analyzed elements. Nitrogen content obtained by the Dumas method.

	Carbon	Hydrogen	Oxygen	Nitrogen
OMC	96.1	0.8	2.0	0.0
EtNH ₂ @OMC	91.5	1.7	4.2	0.4

Knoevenagel Condensation Catalysis

The catalytic results show significant product formation after 4 h of reaction (Figure 2.8). A blank reaction of benzaldehyde and malononitrile *sans* catalyst showed no conversion of reactants and trace amounts of benzoic acid. When OMC was used as a catalyst, the GC chromatogram showed benzoic acid with unreacted benzaldehyde and malononitrile and no benzylidenemalononitrile. The absence of chemical transformation is likely contributed to the OMC surface's trace oxygen content, which was insufficiently acidic to stabilize and activate the carbonyl reactant nor basic enough to abstract an active methylene hydrogen to undergo reaction.

Since the autooxidation of benzaldehyde to benzoic acid occurs under atmospheric conditions, the OMC was likely non-participatory in benzoic acid formation. A microporous ($d_{\text{pore}} < 1 \text{ nm}$) Darco activated carbon (AC) was chosen because its activity gives insight on the participation of surface functional groups and pore size on catalysis. The mixture of phenols, carboxylic acids, and lactones on AC showed some conversion, though benzoic acid was detected too. These two materials however, produced significant amounts of benzoic acid and showed no reactant traces after catalysis.

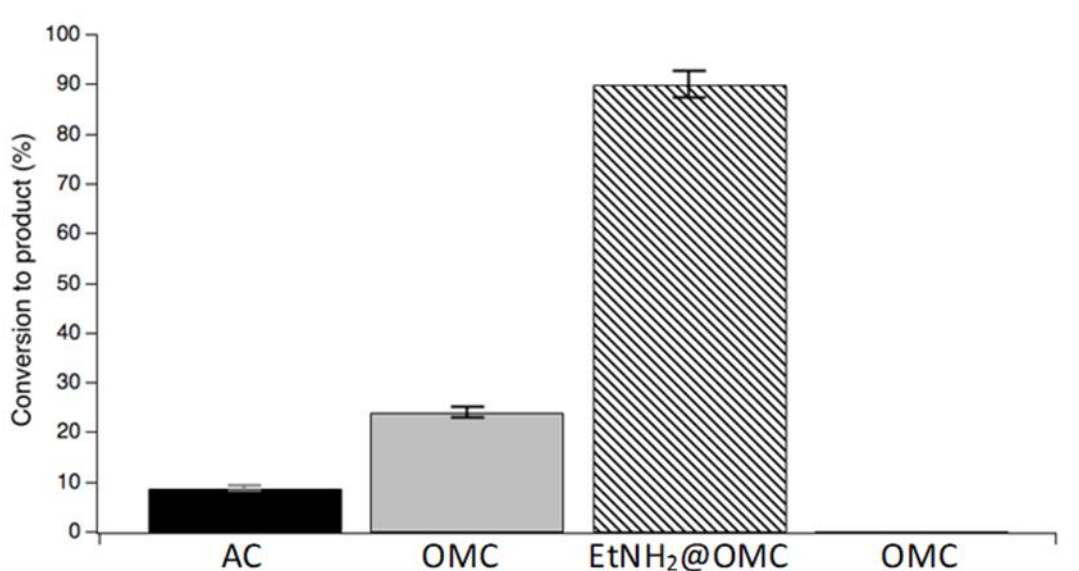


Figure 2.9. Conversion to benzylidenemalononitrile using various solid porous catalysts. Reaction conditions: benzaldehyde (2 mmol), malononitrile (3 mmol), MeOH (6.0 mL), 550 rpm, 40 °C, 4 h.

We believe the surface chemistry of AC was relatively inert towards activating reactants while also being prone to benzoic acid production enabled by water residing nearby hydrophilic oxygen functional group surface sites. An amine-enriched AC, EtNH₂@AC, showed an

improved conversion relative to AC, but to far less of an extent than EtNH₂@OMC and with the production of benzoic acid side-product. When EtNH₂@OMC was employed, only benzylidenemalononitrile was detected by GC with a yield of around 90% of product. These results indicate primary amines on EtNH₂@OMC are responsible for this observed increase in activity. We propose the mechanism where Schiff bases formed between benzaldehyde and surface amine coupling (Figure 2.9) mediate the active methylene abstraction similar to other amine-modified porous materials;⁵² it's the same reaction mechanism which underpins the utility of the 4-nitrobenzaldehyde assay.²¹ Further, the dearth of benzoic acid in the product stream evidences that benzaldehyde is protected from oxidation when reacted into its Schiff base form.

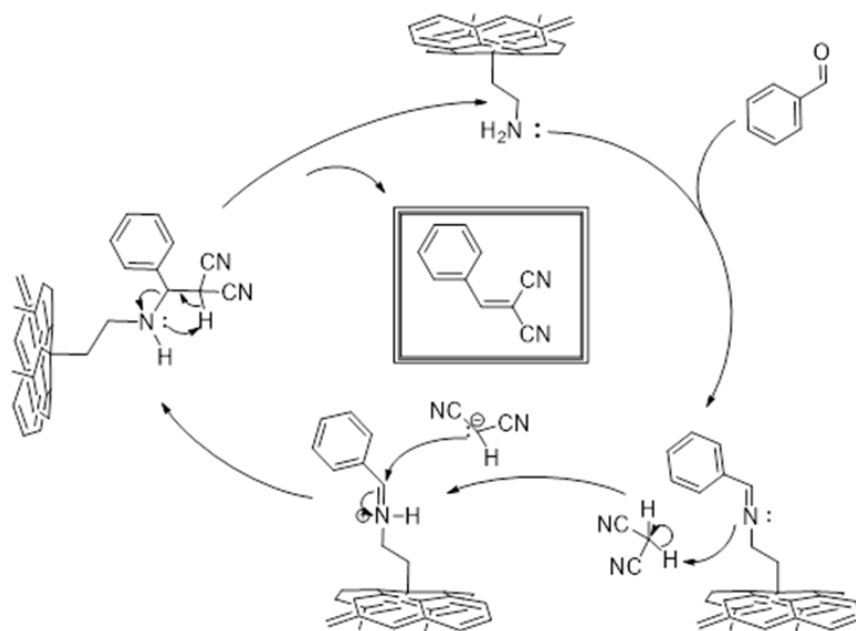


Figure 2.10. Proposed mechanism of the Knoevenagel condensation mediated by surface-bound primary amine groups on OMC involving an imine formation to initiate the abstraction of the acidic malononitrile hydrogen.

Catalytic Recyclability

The catalytic reaction was performed five times, with only one centrifugation after each reaction to collect the product. The conversion to benzylidenemalononitrile by EtNH₂@OMC over 5 reaction cycles (Figure 2.10) is shown below. While 90% conversion was achieved for the first cycle, a decline of conversion over subsequent reactions was observed, likely due to adsorptive blocking of pore apertures.⁵⁴⁻⁵⁵ This is thought to be a prominent factor in the decline in product formation because of the relatively strong interactions between the non-charged OMC surface and the non-charged benzaldehyde and malononitrile (reactants) and benzylidenemalononitrile (product). We believe a more rigorous rinsing protocol using an acid to protonate the amine groups would give rise to a relative electrostatic repulsion between the surface and neutral charged adsorbates (driving desorption of molecules from the pore walls), which would attenuate the declining conversion seen for EtNH₂@OMC if active site blocking was to be the case.

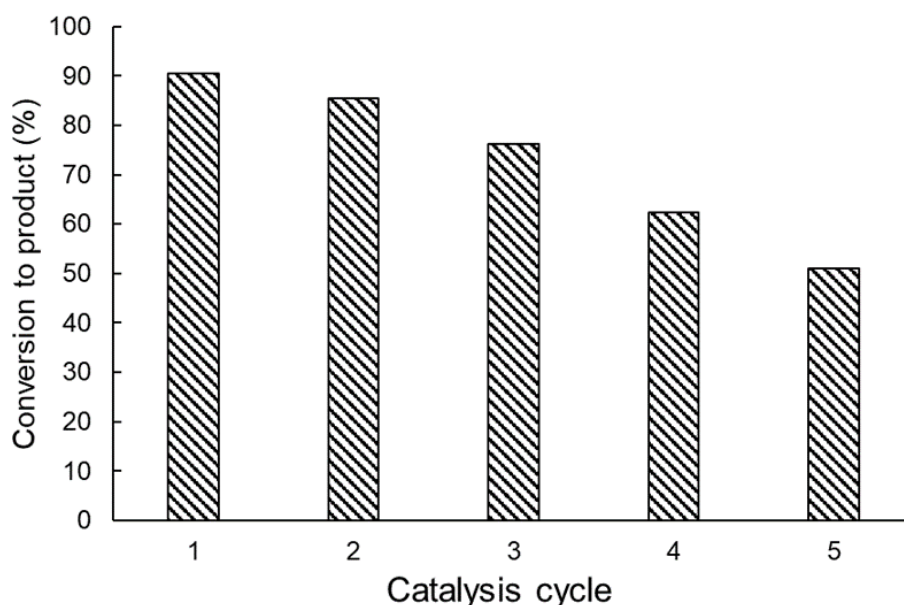


Figure 2.11. Catalyst conversion over five cycles for EtNH₂@OMC.

Following the supposition that the decrease catalytic activity as measured by product conversion is related to insufficient regeneration between reaction cycles, the initial rates of catalyst were assessed for three cycles of reaction cycles including an additional washing step using 0.1 M HCl in methanol to regenerate the EtNH₂@OMC surface. The initial apparent rate constant associated with this catalytic system is nearly identical for the first three reaction trials after the acidic regeneration protocol (Figure 2.11). The apparent rate constant for the first three reaction trials are 110, 112, and 111 $\mu\text{M min}^{-1}$ indicating highly conserved catalytic activity for EtNH₂@OMC.

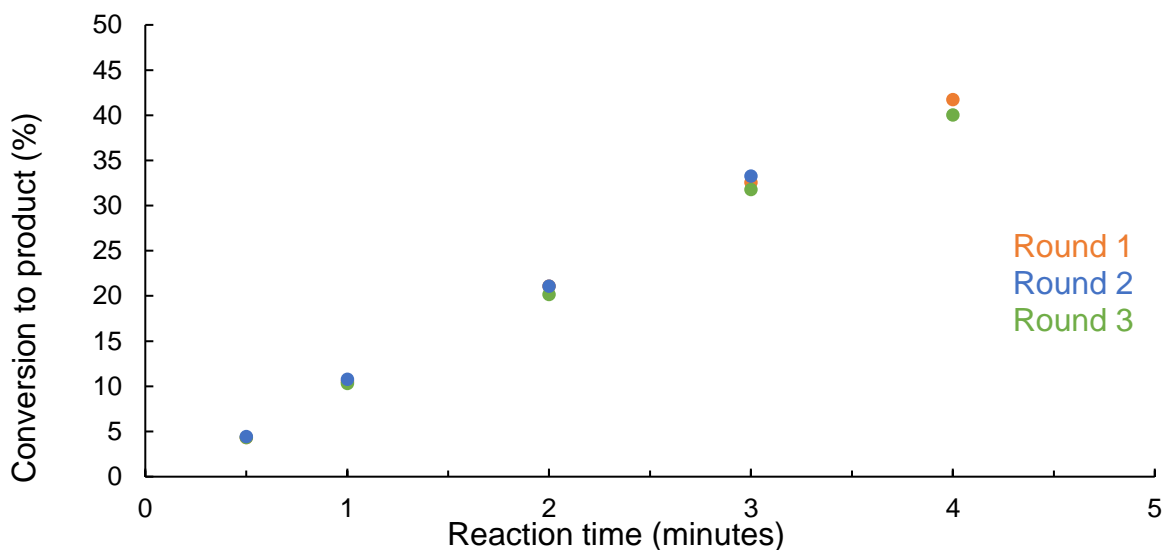


Figure 2.12. Initial rates of product formation for three rounds of catalysis.

2.6 Conclusion

We showed that amination by organolithium-mediated surface activation of a mesoporous carbon modifies the material and instills necessary acidic-basic reactivity that was proven

effective in Knoevenagel condensation between benzaldehyde and malononitrile under mild conditions. The lithiation procedure did not incur measurable changes to the OMC particles, in other words, the ordered mesoporous structure is retained following functionalization. Also, by detecting virtually no benzoic acid, the EtNH₂@OMC catalyst is ideal for converting benzaldehyde and avoiding the oxidation side-reaction.

While this covalently modified ordered mesoporous carbon was proven effective as a heterogeneous base catalyst under mild reaction conditions, the utility for primary amine-based MCs pervade fields which employ highly acidic or highly basic environments. As such, C-C bonded aminated MC surfaces are suitable candidates to withstand a wide range of pH conditions due to the *a priori* recalcitrance of the alkane bond. The following dissertation chapter illustrates this notion by testing the acidic and basic compatibility of the alkane bond on EtNH₂@OMC by a multitude of characterizations ranging from particle-scale down to the surface atomic scale.

2.7 References

1. Carey, J. S.; Laffan, D.; Thomson, C.; Williams, M. T., Analysis of the Reactions used for the Preparation of Drug Candidate Molecules. *Org. Biomol. Chem.* **2006**, 4 (12), 2337-2347.
2. Devendar, P.; Qu, R. Y.; Kang, W. M.; He, B.; Yang, G. F., Palladium-Catalyzed Cross-Coupling Reactions: A Powerful Tool for the Synthesis of Agrochemicals. *J. Agr. Food Chem.* **2018**, 66 (34), 8914-8934.
3. Dinparast, L.; Hemmati, S.; Zengin, G.; Alizadeh, A. A.; Bahadori, M. B.; Kafil, H. S.; Dastmalchi, S., Rapid, Efficient, and Green Synthesis of Coumarin Derivatives via Knoevenagel Condensation and Investigating Their Biological Effects. *ChemistrySelect* **2019**, 4 (31), 9211-9215.
4. Vasquez-Céspedes, S.; Betori, R. C.; Cismesia, M. A.; Kirsch, J. K.; Yang, Q., Heterogeneous Catalysis for Cross-Coupling Reactions: An Underutilized Powerful and Sustainable Tool in the Fine Chemical Industry? *Org. Process Res. Dev.* **2021**, 25 (4), 740-753.
5. Bigi, F.; Quarantelli, C., The Knoevenagel Condensation in Water. *Curr. Org. Synth.* **2012**, 9 (1), 31-39.

6. Appaturi, J. N.; Ratti, R.; Phoon, B. L.; Batagarawa, S. M.; Din, I. U.; Selvaraj, M.; Ramalingam, R. J., A Review of the Recent Progress on Heterogeneous Catalysts for Knoevenagel Condensation. *Dalton Trans.* **2021**, 50 (13), 4445-4469.
7. Acute Exposure Guideline Levels for Selected Airborne Chemicals.
8. Karami, B.; Farahi, M.; Khodabakhshi, S., Rapid Synthesis of Novel and Known Coumarin-3-carboxylic Acids Using Stannous Chloride Dihydrate under Solvent-Free Conditions. *Helv. Chim. Acta.* **2012**, 95 (3), 455-460.
9. Ogiwara, Y.; Takahashi, K.; Kitazawa, T.; Sakai, N., Indium(III)-Catalyzed Knoevenagel Condensation of Aldehydes and Activated Methylenes Using Acetic Anhydride as a Promoter. *J. Org. Chem.* **2015**, 80 (6), 3101-3110.
10. Shaibuna, M.; Hiba, K.; Theresa, L. V.; Sreekumar, K., A new type IV DES: a Competent Green Catalyst and Solvent for the Synthesis of Alpha,Beta-Unsaturated Diketones and Dicyano Compounds by Knoevenagel Condensation Reaction. *New J. Chem.* **2020**, 44 (34), 14723-14732.
11. Yadav, J. S.; Bhunia, D. C.; Singh, V. K.; Srihari, P., Solvent-free NbCl₅ Catalyzed Condensation of 1,3-dicarbonyl Compounds and Aldehydes: a Facile Synthesis of Trisubstituted Alkenes. *Tetrahedron Lett.* **2009**, 50 (21), 2470-2473.
12. Yang, L.; Zhu, J.; Xie, F. K.; Peng, X. S.; Lin, B.; Liu, Y. X.; Cheng, M. S., Solvent-Free FeCl₃-Assisted Electrophilic Fluorine-Catalyzed Knoevenagel Condensation to Yield Alpha,Beta-Unsaturated Dicarbonyl Compounds and Coumarins. *Russ. J. Org. Chem.* **2019**, 55 (7), 1053-1060.
13. Ossowicz, P.; Rozwadowski, Z.; Gano, M.; Janus, E., Efficient Method for Knoevenagel Condensation in Aqueous Solution of Amino Acid Ionic Liquids (AAILs). *Pol. J. Chem. Technol.* **2016**, 18 (4), 90-95.
14. Player, L. C.; Chan, B.; Turner, P.; Masters, A. F.; Maschmeyer, T., Bromozincate Ionic Liquids in the Knoevenagel Condensation Reaction. *Appl. Catal. B-Environ.* **2018**, 223, 228-233.
15. Priede, E.; Brica, S.; Bakis, E.; Udris, N.; Zicmanis, A., Ionic Liquids as Solvents for the Knoevenagel Condensation: Understanding the Role of Solvent-Solute Interactions. *New J. Chem.* **2015**, 39 (12), 9132-9142.
16. Xu, H.; Pan, L. Y.; Fang, X. M.; Liu, B. Y.; Zhang, W. K.; Lu, M. H.; Xu, Y. Q.; Ding, T.; Chang, H. B., Knoevenagel Condensation Catalyzed by Novel Nmm-based Ionic Liquids in Water. *Tetrahedron Lett.* **2017**, 58 (24), 2360-2365.
17. Calvino-Casilda, V.; Martin-Aranda, R. M.; Lopez-Peinado, A. J.; Sobczak, I.; Ziolk, M., Catalytic Properties of Alkali Metal-modified Oxide Supports for the Knoevenagel Condensation: Kinetic Aspects. *Catal. Today* **2009**, 142 (3-4), 278-282.
18. Gao, Z.; Zhou, J. A.; Cui, F. M.; Zhu, Y.; Hua, Z. L.; Shi, J. L., Superparamagnetic Mesoporous Mg-Fe bi-metal Oxides as Efficient Magnetic

- Solid-base Catalysts for Knoevenagel Condensations. *Dalton Trans.* **2010**, 39 (46), 11132-11135.
19. Li, C. X.; Zhong, D. D.; Huang, X. Q.; Shen, G. D.; Li, Q.; Du, J. Y.; Li, Q. L.; Wang, S. N.; Li, J. K.; Dou, J. M., Two Organic-inorganic Hybrid Polyoxovanadates as Reusable Catalysts for Knoevenagel Condensation. *New J. Chem.* **2019**, 43 (15), 5813-5819.
 20. Sharghi, H.; Ebrahimpourmoghaddam, S.; Memarzadeh, R.; Javadpour, S., Tin Oxide Nanoparticles (NP-SnO₂): Preparation, Characterization and their Catalytic Application in the Knoevenagel Condensation. *J. Iran Chem. Soc.* **2013**, 10 (1), 141-149.
 21. Das, A.; Anbu, N.; Gogoi, C.; Dhakshinamoorthy, A.; Biswas, S., Amino Group Functionalized Hf-Based Metal-Organic Framework for Knoevenagel-Doebner Condensation. *Eur. J. Inorg. Chem.* **2021**, **2021** (33), 3396-3403.
 22. Dumbre, D. K.; Mozammel, T.; Selvakannan, P. R.; Hamid, S. B. A.; Choudhary, V. R.; Bhargava, S. K., Thermally Decomposed Mesoporous Nickel Iron Hydroxalate: An Active Solid-base Catalyst for Solvent-free Knoevenagel Condensation. *J. Colloid Interf. Sci.* **2015**, 441, 52-58.
 23. Lolak, N.; Kuyuldar, E.; Burhan, H.; Goksu, H.; Akocak, S.; Sen, F., Composites of Palladium-Nickel Alloy Nanoparticles and Graphene Oxide for the Knoevenagel Condensation of Aldehydes with Malononitrile (vol 4, pg 6848, **2019**). *ACS Omega* **2020**, 5 (41), 26954-26954.
 24. Zhang, T.; Chen, H. T.; Liu, S. R.; Lv, H. X.; Zhang, X. T.; Li, Q. L., Highly Robust {Ln(4)}-Organic Frameworks (Ln = Ho, Yb) for Excellent Catalytic Performance on Cycloaddition Reaction of Epoxides with CO₂ and Knoevenagel Condensation. *ACS Catal.* **2021**, 11 (24), 14916-14925.
 25. Zhang, T.; Zhang, Z. G.; Chen, H. T.; Zhang, X. T.; Li, Q. L., Catalytic Investigation of CO₂ Chemical Fixation and the Knoevenagel Condensation Reaction for a Tm-III-Organic Framework. *Cryst. Growth Des.* **2022**, 22 (1), 304-312.
 26. Zhang, Y.; Wang, Y. X.; Liu, L.; Wei, N.; Gao, M. L.; Zhao, D.; Han, Z. B., Robust Bifunctional Lanthanide Cluster Based Metal-Organic Frameworks (MOFs) for Tandem Deacetalization-Knoevenagel Reaction. *Inorg. Chem.* **2018**, 57 (4), 2193-2198.
 27. Zhao, S. X., A novel 3D MOF with Rich Lewis Basic Sites as a Base Catalysis Toward Knoevenagel Condensation Reaction. *J. Mol. Struct.* **2018**, 1167, 11-15.
 28. Ansari, M. B.; Jin, H. L.; Parvin, M. N.; Park, S. E., Mesoporous Carbon Nitride as a Metal-free Base Catalyst in the Microwave Assisted Knoevenagel Condensation of Ethylcyanoacetate with Aromatic Aldehydes. *Catal. Today* **2012**, 185 (1), 211-216.

29. Zhang, L. N.; Wang, H.; Qin, Z. F.; Wang, J. G.; Fan, W. B., Synthesis of Two-dimensional Mesoporous Carbon Nitride under Different Carbonization Temperatures and Investigation of its Catalytic Properties in Knoevenagel Condensations. *RSC Adv.* **2015**, 5 (29), 22838-22846.
30. Shcherban, N. D.; Maki-Arvela, P.; Aho, A.; Sergiienko, S. A.; Yaremov, P. S.; Eranen, K.; Murzin, D. Y., Melamine-derived Graphitic Carbon Nitride as a new Effective Metal-free catalyst for Knoevenagel Condensation of Benzaldehyde with Ethylcyanoacetate. *Catal. Sci. Technol.* **2018**, 8 (11), 2928-2937.
31. Xu, J.; Wen, L. Z.; Gan, Y. L.; Xue, B., Synthesis of Nitrogen-containing Ordered Mesoporous Carbon Materials with Tunable Nitrogen Distributions and their Application for Metal-free Catalytic Synthesis of Dimethyl Carbonates. *Mol. Catal.* **2020**, 485.
32. Xue, B.; Wen, L. Z.; Ma, D.; Li, M. M.; Xu, J., Knoevenagel Condensation Reactions Catalyzed by Nitrogen-containing Mesoporous Carbon Materials under Mild Reaction Conditions. *Res. Chem. Intermediat.* **2018**, 44 (12), 7641-7655.
33. Xing, R.; Fei, Z. H., Aminated Ordered Mesoporous Carbons: Preparation and Catalytic Performance for Knoevenagel Condensation Reactions. *J. Chin. Chem. Soc.-Taip.* **2014**, 61 (10), 1093-1100.
34. Marciniak, M.; Goscianska, J.; Pietrzak, R., Physicochemical Characterization of Ordered Mesoporous Carbons Functionalized by Wet Oxidation. *J. Mater. Sci.* **2018**, 53 (8), 5997-6007.
35. Sanchez-Sanchez, A.; Suarez-Garcia, F.; Martinez-Alonso, A.; Tascon, J. M. D., Surface Modification of Nanocast Ordered Mesoporous Carbons through a Wet Oxidation Method. *Carbon* **2013**, 62, 193-203.
36. Wu, Z. X.; Webley, P. A.; Zhao, D. Y., Comprehensive Study of Pore Evolution, Mesostructural Stability, and Simultaneous Surface Functionalization of Ordered Mesoporous Carbon (FDU-15) by Wet Oxidation as a Promising Adsorbent. *Langmuir* **2010**, 26 (12), 10277-10286.
37. Cleva, C.; Cachet, C.; CabrolBass, D.; Forrest, T. P., Advantages of a Hierarchical System of Neural-networks for the Interpretation of Infrared spectra in Structure Determination. *Anal. Chim. Acta* **1997**, 348 (1-3), 255-265.
38. Aviles, F.; Sierra-Chi, C. A.; Nistal, A.; May-Pat, A.; Rubio, F.; Rubio, J., Influence of Silane Concentration on the Silanization of Multiwall Carbon Nanotubes. *Carbon* **2013**, 57, 520-529.
39. Parida, K. M.; Mallick, S.; Sahoo, P. C.; Rana, S. K., A Facile Method for Synthesis of Amine-functionalized Mesoporous Zirconia and its Catalytic Evaluation in Knoevenagel Condensation. *Appl. Catal. A-Gen.* **2010**, 381 (1-2), 226-232.

40. Jia, H. H.; Zhao, Y.; Niu, P. P.; Lu, N. Y.; Fan, B. B.; Li, R. F., Amine-functionalized MgAl LDH Nanosheets as Efficient Solid Base Catalysts for Knoevenagel Condensation. *Mol. Catal.* **2018**, 449, 31-37.
41. Vinu, A.; Hossian, K. Z.; Srinivasu, P.; Miyahara, M.; Anandan, S.; Gokulakrishnan, N.; Mori, T.; Ariga, K.; Balasubramanian, V. V., Carboxy-Mesoporous Carbon and its Excellent Adsorption Capability for Proteins. *J. Mater. Chem.* **2007**, 17 (18), 1819-1825.
42. Miller, J. D.; Hoh, K. P.; Ishida, H., Studies of the Simulation of Silane Coupling Agent Structures on Particulate Fillers - the pH Effect. *Polym. Composite* **1984**, 5 (1), 18-28.
43. Samha, H.; Linford, M.; Zhang, F.; Davis, R.; Sautter, K., Chemical Vapor Deposition of Three Aminosilanes on Silicon Dioxide: Surface Characterization, Stability, Effects of Silane Concentration, and Cyanine Dye Adsorption. *Abstr. Pap. Am. Chem. Soc.* **2011**, 241.
44. Joglekar, M.; Pylypenko, S.; Otting, M. M.; Valenstein, J. S.; Trewyn, B. G., Universal and Versatile Route for Selective Covalent Tethering of Single-Site Catalysts and Functional Groups on the Surface of Ordered Mesoporous Carbons. *Chem. Mater.* **2014**, 26 (9), 2873-2882.
45. Joglekar, M.; Nguyen, V.; Pylypenko, S.; Ngo, C.; Li, Q. N.; O'Reilly, M. E.; Gray, T. S.; Hubbard, W. A.; Gunnoe, T. B.; Herring, A. M.; Trewyn, B. G., Organometallic Complexes Anchored to Conductive Carbon for Electrocatalytic Oxidation of Methane at Low Temperature. *J. Am. Chem. Soc.* **2016**, 138 (1), 116-125.
46. Valenstein, J. S.; Kandel, K.; Melcher, F.; Slowing, I. I.; Lin, V. S. Y.; Trewyn, B. G., Functional Mesoporous Silica Nanoparticles for the Selective Sequestration of Free Fatty Acids from Microalgal Oil. *ACS Appl. Mater. Interfaces* **2012**, 4 (2), 1003-1009.
47. Sun, Y.; Kunc, F.; Balhara, V.; Coleman, B.; Kodra, O.; Raza, M.; Chen, M. H.; Brinkmann, A.; Lopinski, G. P.; Johnston, L. J., Quantification of Amine Functional Groups on Silica Nanoparticles: a Multi-method Approach. *Nanoscale Adv.* **2019**, 1 (4), 1598-1607.
48. Leyva, V.; Corral, I.; Schmierer, T.; Gilch, P.; Gonzalez, L., A Comparative Analysis of the UV/Vis Absorption Spectra of Nitrobenzaldehydes. *Phys. Chem. Chem. Phys.* **2011**, 13 (10), 4269-4278.
49. Rouquerol, J.; Llewellyn, P.; Rouquerol, F., Is the BET Equation Applicable to Microporous Adsorbents? *Stud. Surf. Sci. Catal.* **2006**, 160, 49-56.
50. Coates, J., Interpretation of Infrared Spectra, A Practical Approach. John Wiley & Sons Ltd.: **2006**; p 22.

51. Roubeau, O.; Lucas, A.; Penicaud, A.; Derre, A., Covalent Functionalization of Carbon Nanotubes through Organometallic Reduction and Electrophilic Attack. *J. Nanosci. Nanotechnol.* **2007**, 7 (10), 3509-3513.
52. Das, A.; Anbu, N.; Gogoi, C.; Dhakshinamoorthy, A.; Biswas, S., Amino Group Functionalized Hf-Based Metal-Organic Framework for Knoevenagel-Doebner Condensation. *Eur. J. Inorg. Chem.* **2021**, 33, 3396-3403.
53. Che, S. N.; Lund, K.; Tatsumi, T.; Iijima, S.; Joo, S. H.; Ryoo, R.; Terasaki, O., Direct Observation of 3D Mesoporous Structure by Scanning Electron Microscopy (SEM): SBA-15 Silica and CMK-5 Carbon. *Angew. Chem. Int. Ed.* **2003**, 42 (19), 2182-2185.
54. Haas, C. P.; Tallarek, U., Kinetics Studies on a Multicomponent Knoevenagel-Michael Domino Reaction by an Automated Flow Reactor. *ChemistryOpen* **2019**, 8 (5), 606-614.
55. Pandey, R.; Singh, D.; Thakur, N.; Raj, K. K., Catalytic C-H Bond Activation and Knoevenagel Condensation Using Pyridine-2,3-Dicarboxylate-Based Metal-Organic Frameworks. *ACS Omega* **2021**, 6 (20), 13240-13259.
56. Hampsey, J. E.; Hu, Q.; Wu, Z.; Rice, L.; Pang, J.; Lu, Y., Templating Synthesis of Ordered Mesoporous Carbon Particles. *Carbon* **2005**, 43, 2977-2982.
57. Li, Z.; Zhang, J.; Li, Y.; Guan, Y.; Feng, Z.; Li, C., Preparation and Characterization of Ordered Mesoporous Carbons on SBA-15 Template. *J. Mater. Chem.* **2006**, 14, 1350-1354.

CHAPTER 3 ASSESSING THE ACIDIC AND ALKALINE STABILITY OF COVALENTLY BOUND SURFACE AMINES ON ORDERED MESOPOROUS CARBON SCAFFOLDS

Modified from a paper submitted to ACS Langmuir

Nolan C. Kovach^{4,5}, Scott E. Massimi⁴, Jayson Foster⁴, Svitlana Pylypenko^{6,7}, Brian G. Trewyn^{6,7}

3.1 Abstract

While solid carbonaceous materials are known to withstand strongly acidic and strongly basic conditions, there remains a significant amount of uncertainty on the chemical stability of surface bonded functionalities on modified mesoporous carbon. Applied research tends to focus on testing a material in reaction conditions relevant to a specific application which unintentionally ignores the potential for that material to be employed in a different condition and/or field of research. Ordered mesoporous carbon (OMC) scaffolds were covalently modified with primary amine groups by means of oxidation-coupling, yielding C-O-C bonds, or organometallic activation-coupling, yielding C-C bonds. The aminated OMCs were stressed by immersion in either 1M hydrochloric acid or 1M sodium hydroxide solutions at room temperature and characterized by nitrogen sorption, electron microscopy, low-angle X-ray diffraction, thermogravimetric analysis, and amine groups were quantified using 4-nitrobenzaldehyde assay. Results demonstrate aminated surfaces of OMC by butyllithium grafting are stable towards both 1M HCl and 1M NaOH, whereas the oxidation-aminated OMC surfaces can withstand 1M NaOH. We found that OMC with ether-type surface bonding undergo acidic hydrolysis at pH 2 and below. This study illustrates the importance of chemical testing to

⁴ Graduate student, Chemistry Dept., Colorado School of Mines

⁵ Primary researcher and author

⁶ Research Joint Appointment, National Renewable Energy Laboratory (NREL)

⁷ Associate Professor, Chemistry Dept., Colorado School of Mines

supplant chemical intuition when tailoring carbon surfaces for applications where strong acid or base are employed. This is especially emphasized for carbonaceous materials because of the electronic and structural differences exhibited by various carbon allotropes (i.e. metallic CNTs versus insulative CNTs; planar graphene versus porous activated carbon).

3.2 Introduction

Designing porous solid materials to withstand harsh acidic and basic chemical environments is necessary to achieve long-term operability. Heterogeneous catalysts and porous sorbent materials oftentimes use highly acidic or highly basic rinse steps to electrostatically desorb surface-bound compounds in between uses. While porous carbon (pC) materials exhibit inherent stability over pH ranging from 1-14, this is not always the case for functional groups appended to the surfaces of pC. Surface modifications to pC materials are garnering more attention because these change the chemical environment of the carbon surface, which enable new functionality for a wide range of applications.¹ Covalently-modified carbon materials are preferred for many applications due to the relative strength of covalent surface binding against non-covalent (physisorptive) modified surfaces. The latter class of materials suffer from surface adsorbate leaching after multiple applied cycles.

Of course, there many are porous materials which exploit the reactivity of surface-bound chemical functional groups under specific conditions. The most prominent published examples include materials intended for chemotherapeutic drug delivery, where porous materials having bulky structures gating (or covering) the entrance of pore apertures contain S-S bonds which are readily and selectively cleaved in the presence of glutathione, a biomolecule expressed significantly in cancer cells. Similarly, intentional degradation of thermo-, enzymatic-, or pH-responsive moieties are employed to enable release of pore-entrained therapeutics *in vivo*. The

understanding of the conditions in which biologically-labile surface species on porous scaffolds react is relatively thoroughly understood. The temperature and enzymatic conditions within cells are relatively unique to mammalian creatures, being that temperatures tend to reside within 5 degrees C of “body temperature”, and the enzymes present inside cells are almost never encountered anywhere else in the environment. Therefore, temperature-responsive and enzymatically-reactive materials intended for biological applications need only be tested in the ranges relevant to cells. Moreover, the pH conditions within most mammalian cells only range from about 6.8 to 7.4, limiting the design of pH-labile functional groups to this small H^+ concentration window. On one hand, considering the large number of functionalized porous materials for drug delivery and biosensing, it is apparent that these systems are unlikely to find utility in fields which employ temperatures or pHs that reside far outside of biological limits. On the other hand, there is an enormous number of functionalized porous materials intended for adsorptive, catalytic, and electrochemical applications that perform in more extreme temperature and pH conditions.

While carbon allotropes like fullerene, graphene, and carbon nanotubes are structurally understood to the atomic scale, the reactivity for each of these materials are based on the unique structures each of these materials possess.²⁻³ The higher-order dimension (e.g. 3-D) carbons like activated carbon, carbon black, and nuclear graphite are relatively more complex in terms of porous architecture and surface chemical functional groups.⁴⁻⁵ For these commercial carbons, the internal pore structure is randomly tortuous, comprising a heterogeneous distribution of void dimensions, shapes, and connectivity.⁶ Upon inspection of these material surfaces, there exists a wide range of functional groups depending on the carbon material precursor (source) and synthetic conditions.⁷⁻⁸ Perhaps the most utilized surface groups are oxygen species, i.e.,

hydroxyl, carboxyl, lactone, quinone, and ether, since these can become incorporated into the carbon framework depending on the synthetic procedure.⁹⁻¹⁰ Essentially all modifications that target carboxylic acid modification to prepare esters or amides will be susceptible to hydrolysis at much milder pH conditions than O-C linkages in ethers. So, a carbon surface modification originating from hydroxyl groups to create ether functional groups will embody greater acidic/alkaline resistance than carboxylic acid tethered groups. An exception to this surface hydroxyl linkage strength would be surface hydroxyl silanization, where the Si-O-C bond is susceptible to acidic hydrolysis, though this is a popular choice for carbon modification.¹¹ Similarly, the Ti-O-C bond is known to cleave at pH=1 conditions.¹² To date, there is one example in literature describing an etheric covalent functionalization on mesoporous carbon, where Kleitz, et al. in 2017 tethered diglycoamide (DGA) moieties onto oxidized (hydroxylated) MC for rare earth element sequestration. They showed, at pHs 1.9 and 1.2, lanthanum uptake was severely limited and ascribed this to “the functionalities on the surface of the carbon probably tend to be positively charged (H⁺), resulting in electrostatic repulsions between the surface and metal ions”. No efforts were made to assess the MC surface structure following these low pH conditions, and their supposition is called into question as to whether the covalently tethered functional groups are still present, or if the functional groups underwent acidic hydrolysis.

The dearth of information directly investigating the stability of mesoporous carbon surface ether bonds in basic or acidic conditions inspired us to compare the acidic and alkaline durability of etherized OMC and carbon-carbon functionalized OMC surfaces head-to-head since these are the strongest bonds for covalently tethering moieties onto carbon surfaces. Both C-C

and C-O-C bonds are, *a priori*, resistant towards highly basic pHs (~14) and capable of withstanding very low pHs (~0).

Organic chemistry teaches that ether (C-O-C) bonds are resistant to both strong base and strong hydrohalic acid lysis, except for hydrobromic and hydroiodic acid.¹³ The reason that hydrochloric acid cannot cleave the ether bond lies in the fact that Cl^- is a significantly less aggressive nucleophile compared to Br^- and I^- towards a primary carbon, and therefore the $\text{S}_{\text{N}}2$ displacement necessary for the ether to lyse will not occur with Cl^- . Upon this premise, the functionalization of a porous carbon surface with ether bonds was of interest to test their chemical stability when exposed to strongly acidic conditions. Some notable applications of carbons where $\geq 1\text{M}$ HCl is encountered are as electrodes where the working electrolyte is HCl and as heavy metal adsorbents where chemical regeneration conditions employ HCl.¹⁴⁻¹⁵

The selective functionalization of carbon surfaces to install hydroxyl groups can be accomplished in multiple ways (Figure 3.1).¹⁶⁻¹⁸

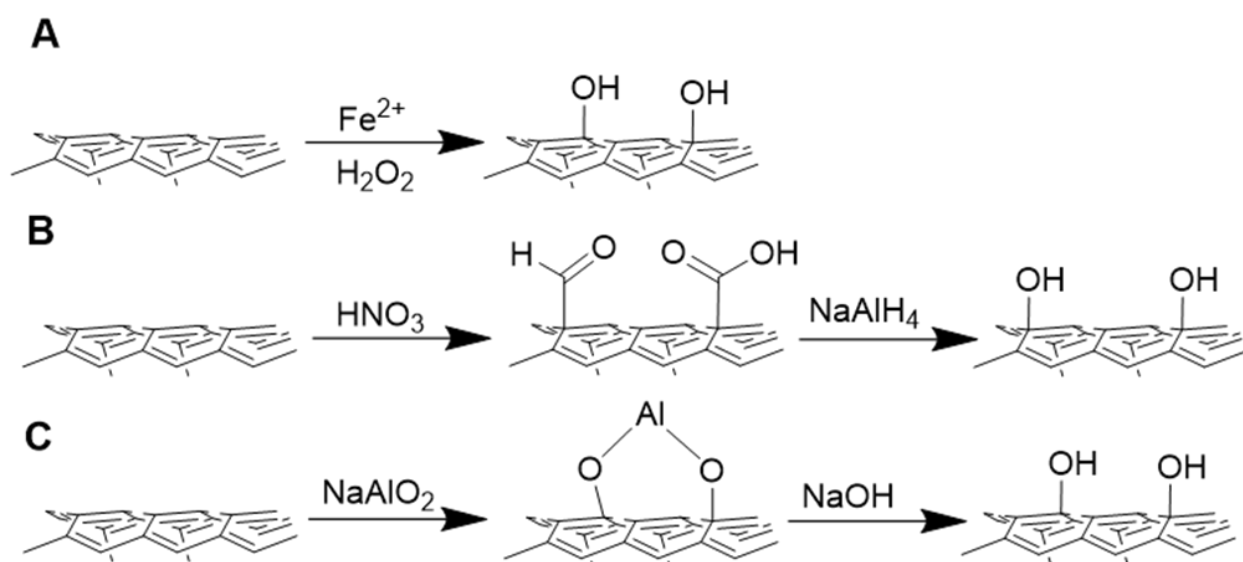


Figure 3.1. Methods for selective hydroxylation of carbon surfaces by means of (A) Fenton reaction using $\text{FeSO}_4 \cdot 7\text{H}_2\text{O}$ and 30% H_2O_2 , (B) Nitric acid oxidation followed by sodium aluminum hydride reduction, and (C) Sodium aluminate surface complexation followed by NaOH hydrolysis.

The availability of all reagents, relative non-toxicity of FeSO₄ to NaAlO₂ and NaAlH₄, and fewer synthetic steps designated path A optimal to utilize. The Fenton reaction is an Fe²⁺-catalyzed decomposition of peroxides into primarily hydroxyl radical species (HO·) which then scavenge electrophilic/aromatic regions on carbon surfaces, thereby appending the hydroxyl moiety. The surface groups then underwent a Williamson ether synthesis-style conversion, where the surface alcohol was deprotonated to which a solution of haloalkylamines was added.¹⁸⁻¹⁹

The organolithium activation method was chosen for installing ethylamine onto OMC because of the synthetic method's proven utility on OMC, with examples demonstrating covalent surface modification with 2,2-bipyridine, 1,10-phenanthroline, and triethylamine.²⁰⁻²² Illustrated in Scheme 2, "activation" refers to the deprotonation of surface sp³ (C-H) defect sites by an organolithium base, like *n*-butyllithium. The resulting anionic C-Li locations on the OMC surface then completes an S_N2 reaction at an electrophilic carbon species to yield C-C linkages between surface and adsorbate.

3.3 Experimental Section

OMC Fabrication

The method for OMC synthesis described in Chapter 3 was also used for this experiment.

Organolithium OMC Amination

The lithiation-coupling protocol in Chapter 3 describes this process.

OMC Oxidation-Amination

The OMC was oxidized by means of the Fenton reaction to selectively install surface hydroxyl moieties. About 300 mg OMC was suspended in 300 mL water, to which 297 mg

FeSO₄·7H₂O was added and stirred for 30 minutes. Then, 45 mL 30% H₂O₂ was added over the course of 2 min and left to stir for 6 h at RT. The solid was then centrifuged at 4400 ×g for 3 min and liquid decanted. The oxidized OMC (oxOMC) was then rinsed with 30 mL MeOH containing 1.0 mL of 3M HCl then finally washed with MeOH and dried overnight at 75 °C. The amination protocol was slightly modified from Gray, et. al. to install ethylamine groups at base-activated surface hydroxyl groups.¹⁹ First, 150 mg oxOMC was suspended in 1.0 M NaOH in MeOH for 6 h and then decanted by centrifugation at 4400 ×g to obtain a surface hydroxyl Na-exchanged oxOMC. Next, 150 mL of a methanolic solution containing chloroethylamine hydrochloride was added and stirred overnight at room temperature. The final product, EtNH₂@oxOMC was then washed with methanol three times and dried at 75 °C.

Acid-base Immersion Testing

Between 20-50 mg of sample was contacted with either NaOH (pH 14) or HCl (pH 0, 1, 2 and 3). The NaOH exposed samples are denoted with the prefix B-, where the HCl treated materials show the prefixes A0-, A1-, A2-, and A3- for pH 0, 1, 2, and 3, respectively. The EtNH₂@oxOMC materials were tested at pH 0, 1, 2, and 3, while EtNH₂@OMC was only tested at pH 0.

3.4 Material Characterization

Boehm Titration

For the oxidation-amination synthetic route, surface hydroxyl groups are required as nucleophilic sites to attack and couple with a haloalkylamine analogous to the Williamson ether synthesis reaction. To better understand the chemical groups appended to OMC following the Fenton oxidation procedure, the Boehm titration was chosen as it can quantitate accessible

surface carboxyl, lactone, and phenol groups.²⁶ The titration begins with immersion of a solid sample in a standardized 0.01M reaction base solution of either NaHCO₃, Na₂CO₃, or NaOH. These bases are intended to selectively deprotonate surface carboxylic acids, carboxylic acids and lactones, or carboxylic acids, lactones, and hydroxyls. Following, the solutions are acidified with a quantitative amount of 0.01M HCl, from which these solutions are back-titrated with 0.01M Na₂CO₃. A blank vessel *sans* material is prepared concurrently and also titrated. The difference in amount of titrant added to reach pH equivalence between the sample and blank is used to calculate the amount of surface functional groups (3.1).

$$n_{FG} = \frac{eq_{samp} - eq_{blank}}{m_{samp}} \quad (3.1)$$

Where n_{FG} , measured in $\mu\text{mol} \cdot \text{g}^{-1}$, representing the amount of surface functional groups determined from the difference in volumes to reach equivalence for the sample, eq_{samp} , and titration blank, eq_{blank} . The quantification of functional groups is simply determined for carboxylic acids (3.2), lactones (3.3), and hydroxyls (3.4)

$$n_c = n_{FG,NaHCO_3} \quad (3.2)$$

$$n_l = n_{FG,NaOH} - n_{FG,NaHCO_3} \quad (3.3)$$

$$n_h = n_{FG,NaOH} - n_{FG,Na_2CO_3} \quad (3.4)$$

Where the amount of carboxylic acids, n_c , is directly measured by the NaHCO₃ trial. The amount of lactones, n_l , and hydroxyls, n_h , are made possible by comparison of results from various titrations.

Point-of-zero-charge measurement

All materials were subjected to point-of-zero-charge (pzc) measurements to corroborate the presence of basic functional groups identified in the 4-nitrobenzaldehyde assay.²⁴ Assessing the net surface charge of a material at a given pH is made possible by a point-of-zero-charge (pzc) pH drift experiment.²⁵ Briefly, 20 mL 0.05 M NaCl solutions were prepared and adjusted to pH values 2-11. Then, about 4 mg of sample was added to each container and sonicated until sufficiently dispersed into solution. After 24 h of immersion, the pH of liquid from each vessel was measured and the ΔpH was determined ($\text{pH}_f - \text{pH}_i$) and plotted against pH_i . The point where the trace for a given material crosses $\Delta\text{pH} = 0$ (x-axis) is the ascribed pzc for a measured sample.

3.5 Results and Discussion

Point-of-zero-charge determination

The surface of carbohydrate-based OMC materials can contain acidic oxygen groups, typically on the order of one percent (at. %) or less when fabricated above 800 °C.³² For these carbons, the average pKa—or pzc—of all surface groups on OMC are less than 7 (Figure 3.2). Compared to OMC, a carbon surface appended with amines will embody an increased surface basicity, or a higher pzc value. Our OMC exhibits a slightly acidic pzc of 5.5, likely due to the presence of surface carboxylic acid or phenolic groups in light of the Boehm titration and elemental analysis results. The substantial increase in pzc to pH 8 indicates a successful surface grafting of base functionality from the ethylamine groups. For aqueous applications, the pzc is useful to elucidate electrostatic adsorbate-adsorbent interactions at a given solution pH.

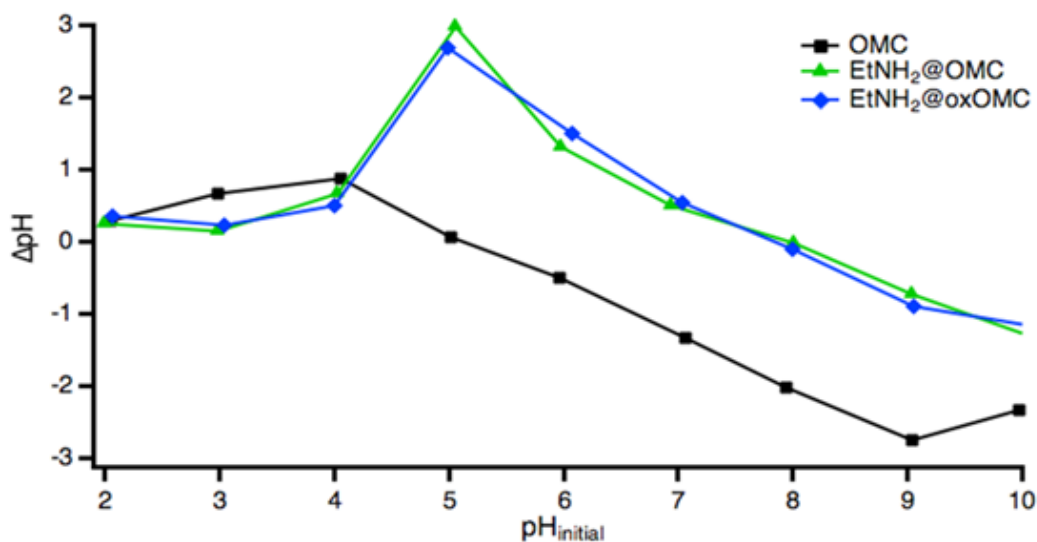


Figure 3.2. Point of zero charge assessment by the pH drift method.

Boehm Titration

Both the identity and the quantity of surface oxygenation is important for many carbon surface modifications. Conveniently, the Boehm titration is effective in assessing three main types of oxygen groups: phenols, carboxylic acids, and lactones/anhydrides. The titration was performed on oxOMC for the purpose of quantifying hydroxyl groups that were subsequently converted into etherized ethylamine moieties. The results for the NaOH trial (Figure 3.3) identified a surface density of hydroxyls of $130 \mu\text{mol} \cdot \text{g}^{-1}$. The Na_2CO_3 and NaHCO_3 trials are seen in Figure 4.S1, where the amount of surface lactone and carboxylic acid concentrations are less than $15 \mu\text{mol} \cdot \text{g}^{-1}$ and $5 \mu\text{mol} \cdot \text{g}^{-1}$, respectively.

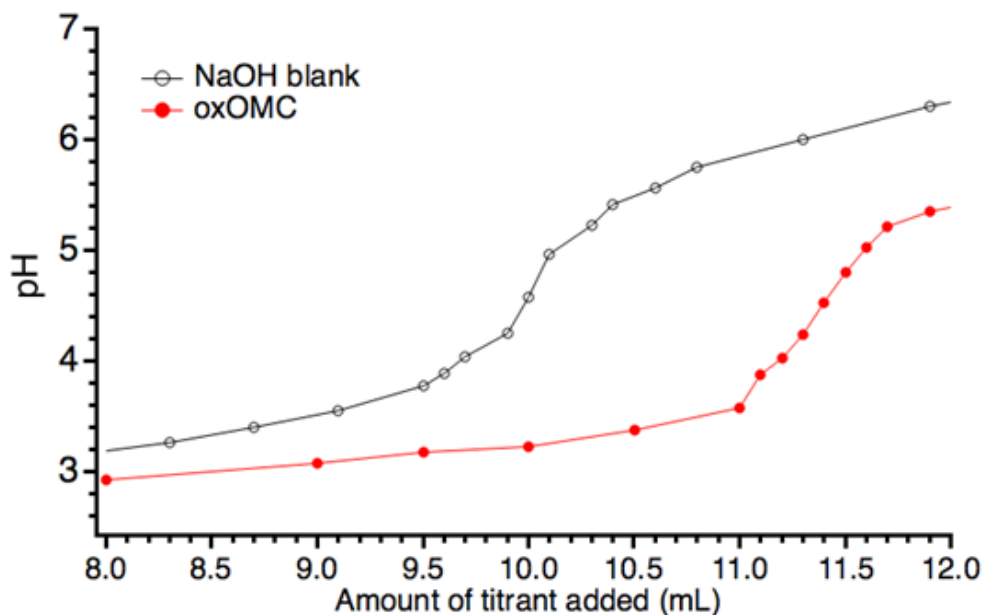


Figure 3.3. Boehm titration results for NaOH treated oxOMC using 0.01N Na₂CO₃ as the titrant solution.

Nitrogen Adsorption Isotherms

From nitrogen sorption, it is apparent that the amine functionalized OMC materials underwent mesopore surface modification based on the significant reduction in BET specific surface area, pore volume, and average pore diameter compared to the unmodified samples. The isotherms and BJH desorption pore size distributions (Figure 3.4) and the computed BET surface area, BJH desorption pore volume, and BJH desorption pore size distributions from the isotherms provide initial evidence towards aminated OMC surface reactivity (Table 3.1). Before amination protocols, OMC and oxOMC displayed BET surface areas which then by 42% and 29%, respectively after amination. To a similar extent for both OMC and oxOMC, the BJH desorption pore volume lowered by 48% and 24%, respectively. The BJH desorption branch yielded an average pore diameter constriction of approximately 1 nm which is interpreted as the ethylamine

moiety residing on the OMC and oxOMC surfaces. Given the low partial pressure limitation of N₂ isotherms (with the available sorption instrument), the extent of micropore modification could not be quantitatively ascertained. However, an indication of micropore functionalization was inferred by the reduction in low P/P₀ uptake (adsorption) observed for the aminated OMC materials when compared to that of the parent materials. The acid and base immersions did not incur a measurable change towards EtNH₂@OMC based on isotherm shape and pore size distributions. For EtNH₂@oxOMC, the acid conditions effected a large change in surface area, pore volume, and average pore diameter. This provides preliminary evidence towards the scission of etherized ethylamine groups by acid hydrolysis.

Table 3.1. Nitrogen sorption derived porosity metrics for all materials, before and after testing. The BET SA was calculated between 0.02 and 0.18 P/P₀. *BJH desorption branch derived values.

	BET Surface Area (m ² · g ⁻¹)	BJH Pore Volume (cm ³ · g ⁻¹)*	Pore Size (nm)*
OMC	1050	1.40	5.5
EtNH ₂ @OMC	605	0.73	4.5
A0-EtNH ₂ @OMC	605	0.73	4.5
B-EtNH ₂ @OMC	595	0.69	4.5
oxOMC	770	1.10	5.9
EtNH ₂ @oxOMC	550	0.84	4.8
A0-EtNH ₂ @oxOMC	750	1.11	5.2
B-EtNH ₂ @oxOMC	590	0.91	4.8

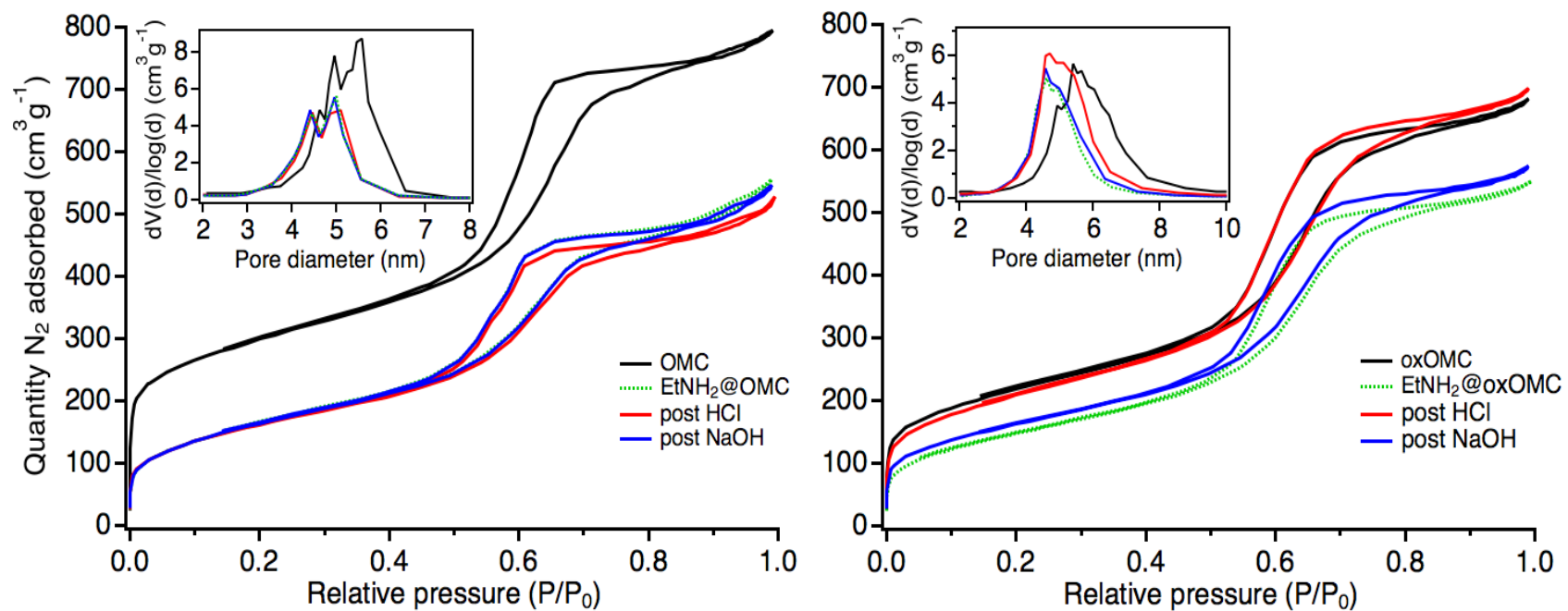


Figure 3.4. Nitrogen adsorption isotherms for OMC (A) and oxOMC (B) materials before and after functionalization, and after acid and base exposure.

The sorption results from the preliminary strong acid (pH 0) and strong base (pH 14) conditions reveal a clear susceptibility of ethylamine tethered by surface ether functionality. Given the sole reactivity exhibited by EtNH₂@oxOMC, this material was subsequently tested at three more pH conditions to ascertain a more precise threshold of reactivity. The nitrogen sorption isotherms and pore size distributions for EtNH₂@oxOMC exposed to pH 1, 2, and 3 (Figure 3.5) reveal similar changes for the etherized OMC at pH 1 as observed for the pH 0 condition. A bimodal pore size distribution is observed for OMC and EtNH₂@OMC, likely reminiscent of the MSN template pore walls having a slight prominence of 4.9 and 5.6 nm. The OMC pore size distribution appearance is considered a normal variation of expected OMC structure, where other MSN templated OMC batches could exhibit a more or less symmetric BJH desorption distribution of measured pore widths.

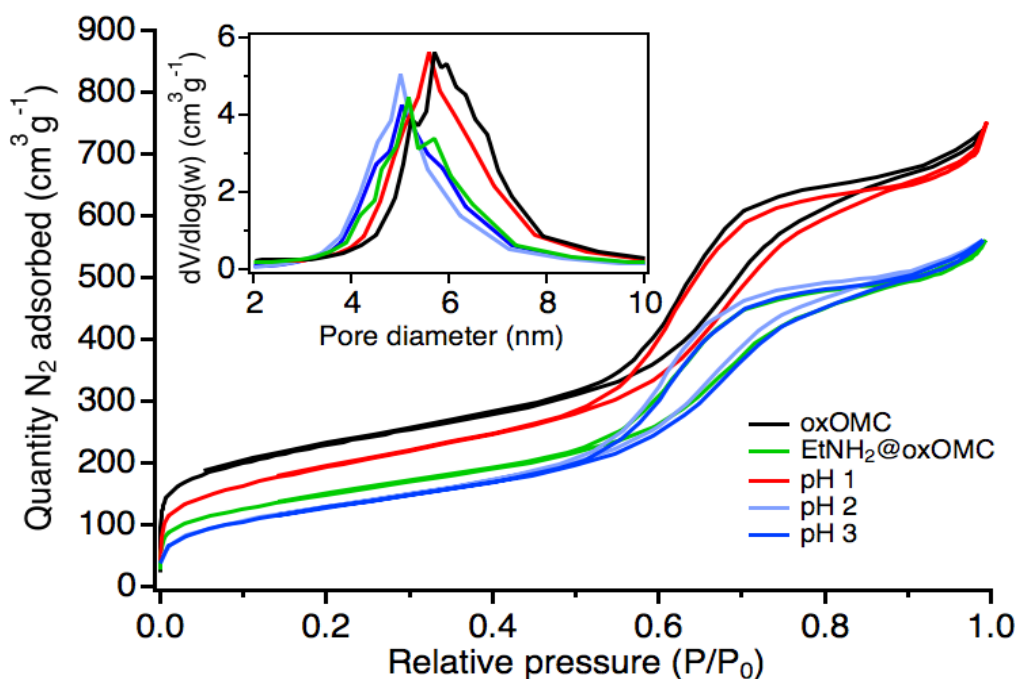


Figure 3.5. Nitrogen sorption isotherms with BJH desorption pore size distribution inset for EtNH₂@oxOMC tested at pH 1, 2, and 3.

The tabulated BET surface areas, pore volumes, and average pore diameters (Table 3.2) similarly corroborate the pore surface changes to the etherized OMC as seen in the above isotherm. The sorption data shows preliminary indication that the surface ethylamine groups are undergoing changes at pH 1.

Table 3.2. Porosity metrics for EtNH₂@oxOMC exposed to pH 1, 2, and 3.

	BET Surface Area (m ² · g ⁻¹)	BJH Pore Volume (cm ³ · g ⁻¹)*	Pore Size (nm)*
oxOMC	807	1.16	5.5
EtNH ₂ @oxOMC	540	0.87	4.5
A1-EtNH ₂ @oxOMC	702	1.12	5.4
A2-EtNH ₂ @oxOMC	482	0.88	4.5
A3-EtNH ₂ @oxOMC	472	0.88	4.5

Low-Angle X-ray Diffraction

The topological ordering (Figure 3.6) for both OMC and oxOMC is made apparent with the diffraction feature c.a. 1.10 °2θ, corresponding to the [100] plane. Given the congruency of the [100] feature between OMC and oxOMC, the Fenton oxidation protocol seems to have no effect on the carbon mesopore wall spacing. Furthermore, both EtNH₂@OMC and EtNH₂@oxOMC exhibited a similar peak prominence which was interpreted as ordering topology being preserved after both amination protocols. There is also no difference in the peak position for A-EtNH₂@OMC, B-EtNH₂@OMC indicating that the OMC pore ordering was recalcitrant towards both 1M HCl and 1M NaOH conditions. The same can be said for B-EtNH₂@oxOMC. For A-

EtNH₂@oxOMC, the 1M eliminated the [100] diffraction feature, indicating topological destruction of the OMC surface. This destruction may be resultant of the hydroxylation towards the nanotubules connecting the larger carbon rod domains together. Another possibility is that the protonated hydroxyl groups in 1M HCl underwent condensation-like surface cleavage at the surface followed by a disintegrating rearrangement of carbon bonds.

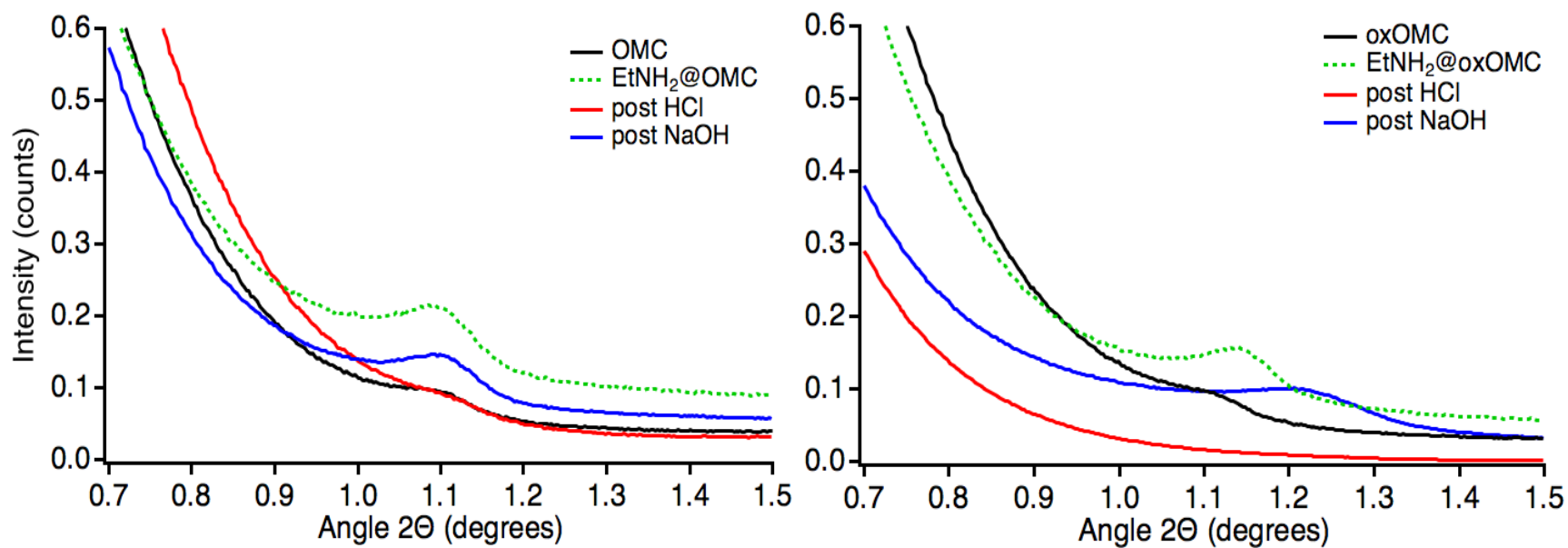


Figure 3.6. Low-angle X-ray diffractograms for the tested OMC materials before and after acid and base testing.

Transmission Electron Microscopy

The transmission electron microscopy results (Figure 3.7) indicate that the aminated OMC materials retained the particle structures, sizes, and morphologies that were observed for OMC and oxOMC. Representative particles imaged along a side-on view were selected to observe any potential changes to the pore spacing. While both oxidative and organolithium functionalization protocols incurred negligible changes to the spacing between adjacent carbon rods (which form the walls of the mesopores) for both OMC and oxOMC, the TEM and LA-XRD data show clearly that the oxOMC materials undergo a framework shrinkage following exposure to 1M HCl, and more notably after 1M NaOH immersion. The LA-XRD scans for A-EtNH₂@OMC and A-EtNH₂@oxOMC showed attenuated [110] diffraction features while both B-EtNH₂@OMC and B-EtNH₂@oxOMC diffraction peaks were easily discernible. For the acid immersed materials, despite the decrease in measured diffraction ordering on the front-face of the OMC pore system, the particles remained wholly in-tact with directly observable corrugated mesopores (Figure 3.8). While no attempts were taken to discern the degree of pore entrance degradation by TEM, the images show that the OMC particles were resilient towards the tested acid and base conditions.

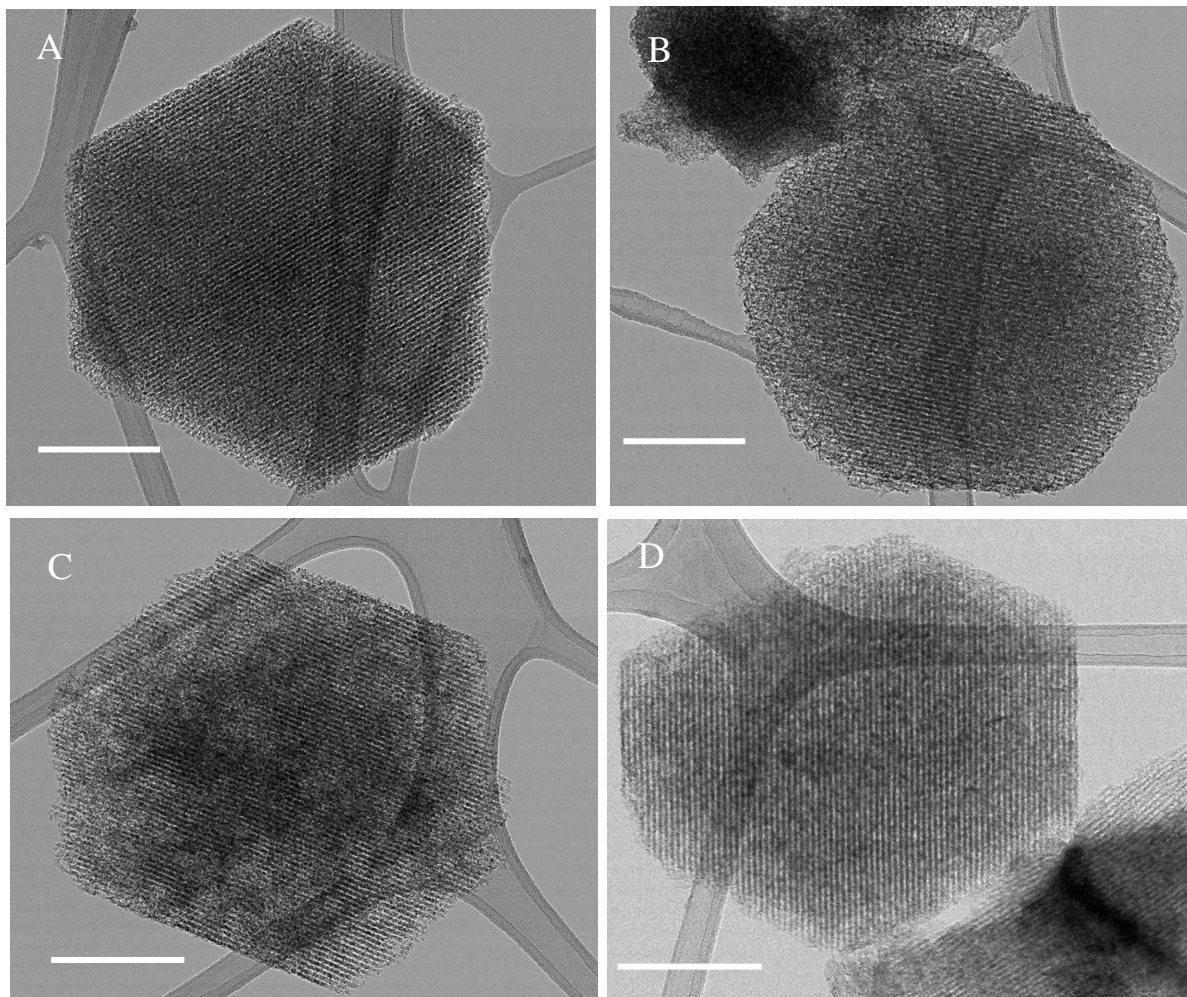


Figure 3.7. Bright field transmission electron micrographs showing particle size and shape similarity for OMC (A) and oxOMC (B), as well as the aminated versions, EtNH₂@OMC (C) and EtNH₂@oxOMC (D). Scale bar = 100 nm.

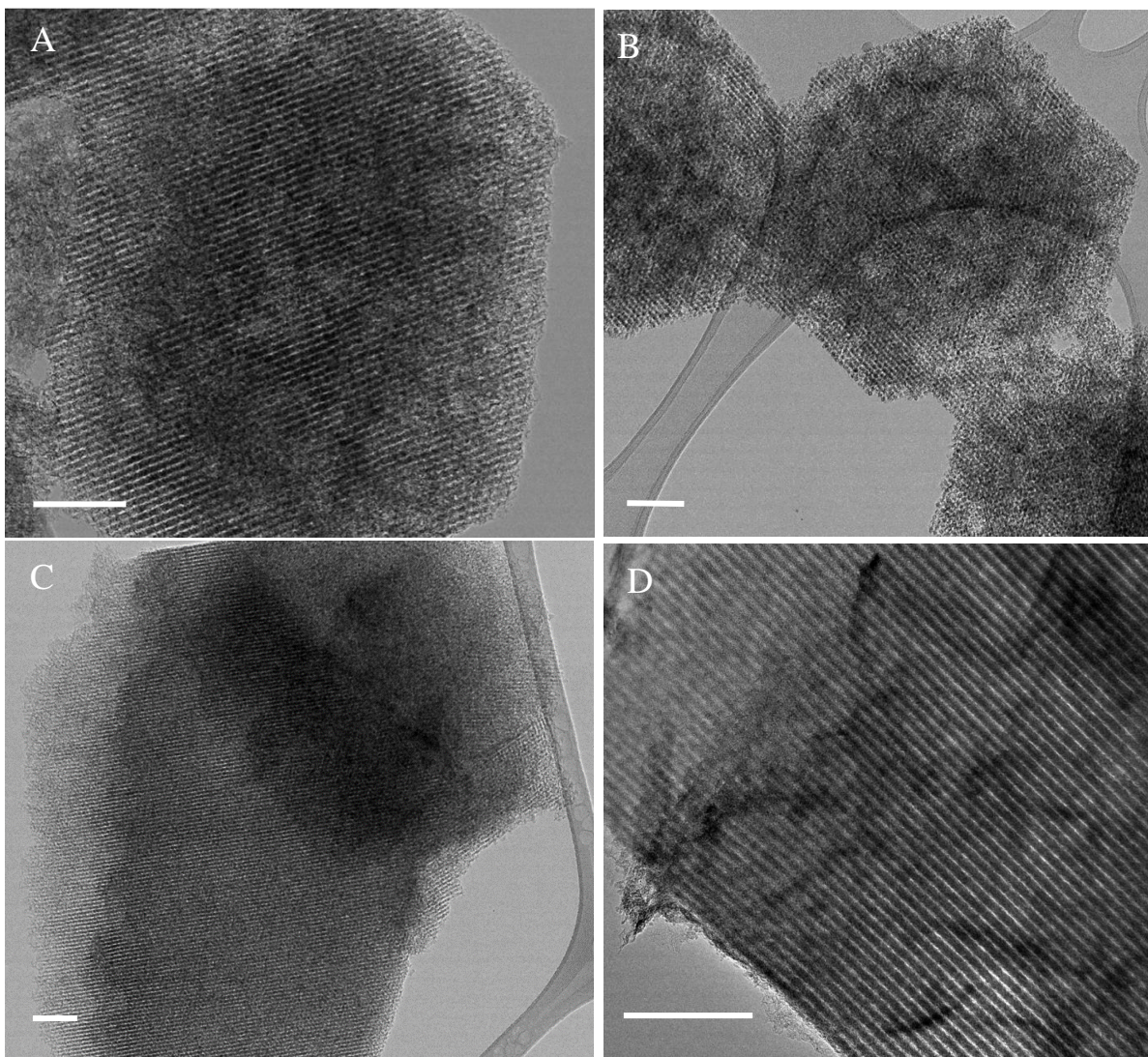


Figure 3.8. Transmission electron microscope images showing preservation of parallel mesopores after acid exposure (left) and base exposure (right) for EtNH₂@OMC (top) and EtNH₂@oxOMC (bottom). Scale bar = 100 nm.

4-Nitrobenzaldehyde Assay

This colorimetric assay is a quantitative measure for primary amines including those tethered to a solid material surface. The assay benefits from excellent reactivity between the nontoxic 4-NB molecule and primary amines to generate Schiff base complexes at mild conditions. The main drawback for it is the inability for the 4-NB probe to react with primary

amines sites buried in sterically non-accessible microporous cavity. Thus, the 4-NB assay is a measure of chemically accessible primary amines on the surface for both EtNH₂@OMC and EtNH₂@oxOMC show functionalization with values of 100 μmol · g⁻¹ and 101 μmol · g⁻¹, respectively (Table 3.3). Similarly to the LA-XRD and physisorption data, the 4-NB assay for A-EtNH₂@OMC and B-EtNH₂@OMC resulted in a negligible reduction in surface-reactive primary amine content. The expectation that C-C bonds were resistant to strong acid and base conditions held true. The same was observed for B-EtNH₂@oxOMC, registering a minor reduction in surface accessible primary amines, but this loss was negligible compared to the original measured amount for EtNH₂@oxOMC. Interestingly, A0-EtNH₂@oxOMC experienced a near complete loss in primary amine content. Based on organic chemistry principles, ether bonds should be resilient towards HCl cleavage—there exists 2M HCl in diethyl ether. The O-C linkage on the surface of EtNH₂@oxOMC is apparently susceptible to acidic hydrolysis in HCl acidified environments of pH 0 and pH 1, where the measured primary amine content is very close to that of unfunctionalized oxOMC. This observation suggests that the chemical reactivity of carbon surface groups cannot be predicted with so-called chemical intuition, and we suggest that all covalently modified carbon materials undergo chemical tests to ensure the recalcitrance of grafted functionalities. A scarcity of available material for pH 1, 2, and 3 tests caused for single sample values; the error values associated with the triplicate measurements are expected to be similar for the singular measurements, allowing for a relatively definitive conclusion for the amounts of accessible -NH₂ to be made.

Table 3.3. Results from the 4-Nitrobenzaldehyde colorimetric assay for materials at all stages.

	Unfunctionalized	Aminated	Amount of detected -NH ₂ (μmol · g ⁻¹)				
			pH 0	pH 1	pH 2	pH 3	pH 14
OMC	3 ± 1	100 ± 10	98 ± 5	--	--	--	98 ± 8
oxOMC	10 ± 1	101 ± 2	19 ± 6	17	98	95	92 ± 9

Thermogravimetric Analysis

Comparing both OMC to EtNH₂@OMC and oxOMC to EtNH₂@oxOMC (Figure 3.9), the aminated TGA profiles include a new, lower mass loss region ascribed to the combustion of the ethylamine surface groups.

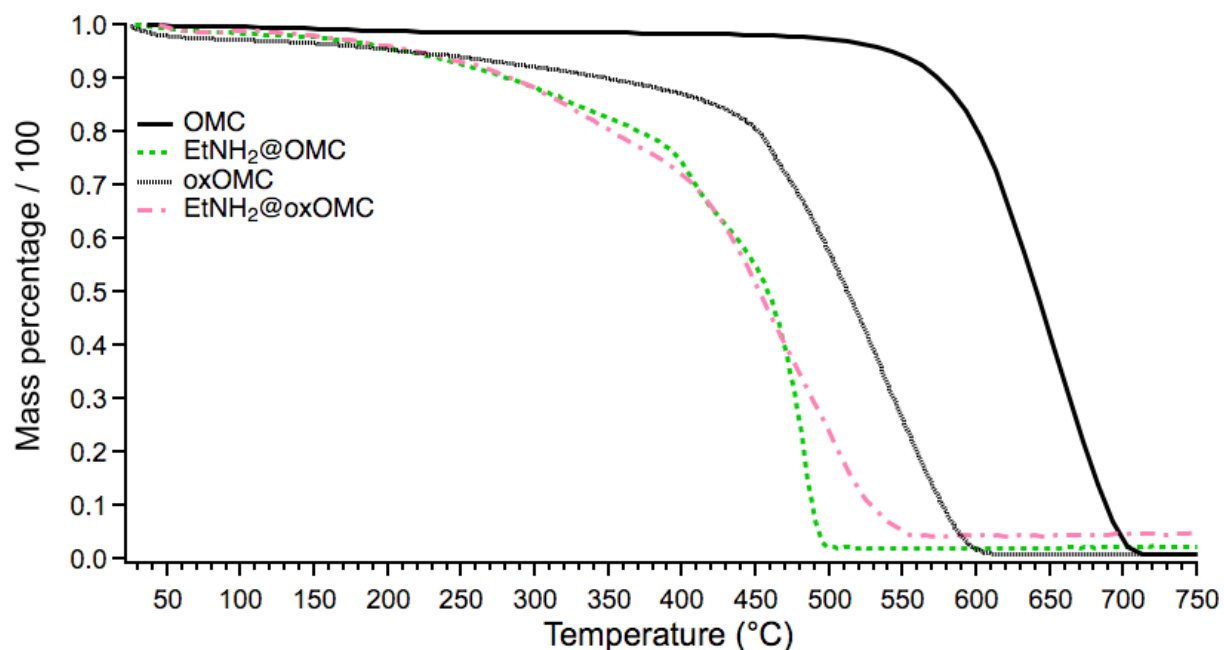


Figure 3.9. Thermogravimetric decomposition for OMC, oxOMC, EtNH₂@OMC, and EtNH₂@oxOMC performed under air flow.

Also, the Fenton oxidation altered the decomposition behavior of OMC, rendering the scaffold less thermally stable due to the presence of surface oxygen groups responsible for combustion. For both EtNH₂@OMC and EtNH₂@oxOMC, the onset of thermal degradation was lesser than that of the OMC and oxOMC, respectively. If the amount of surface ethylamine groups is assumed to be 100 μmol · g⁻¹, then the mass loss associated with this decomposition, between 250 °C to 350 °C, would be about 0.4 wt.%. The thermal scission of surface ethylamine groups may be immediately followed by further combustion of the OMC surface, reflected by a greater than 0.4 wt. % loss observed. For EtNH₂@OMC, there could have been an enrichment of surface carboxylic acid groups following the lithiation procedure, since the reaction vessel was not protected under inert gas for that portion of surface modification. Carbon surface -COOH moieties often decompose (decarboxylate) above 200 °C, which may be responsible for the observed mass loss deviation for EtNH₂@OMC versus OMC.

Fourier-transform infrared spectroscopy

Attenuated total reflection FTIR spectra from 400 cm⁻¹ to 4000 cm⁻¹ was analyzed to detect various functional group signals (Figure 3.10). Unmodified OMC shows three signals at 690 cm⁻¹, 710 cm⁻¹, and 730 cm⁻¹ attributed to phenyl C-H stretching. Ligand attachment at these aryl C-H sites diminishes this signal, observed for the EtNH₂@OMC sample. Further, broad humplike features c.a. 1020 cm⁻¹ and 1585 cm⁻¹ represent C-N stretch and primary amine N-H bends, respectively. EtNH₂@OMC present features at 2850 cm⁻¹ and 2925 cm⁻¹ evidencing symmetric and asymmetric methylene C-H stretches in the grafted ethyl chains, signals which are absent in OMC. The additional peak emerging at 2960 cm⁻¹ could be a methyl C-H stretch belonging to some butyl groups appended via carbometallation in EtNH₂@OMC. Taken together with sorption

results, the 4-NB assay, and TGA analysis, FTIR corroborates the presence of ethylamine groups associated with the OMC scaffold.

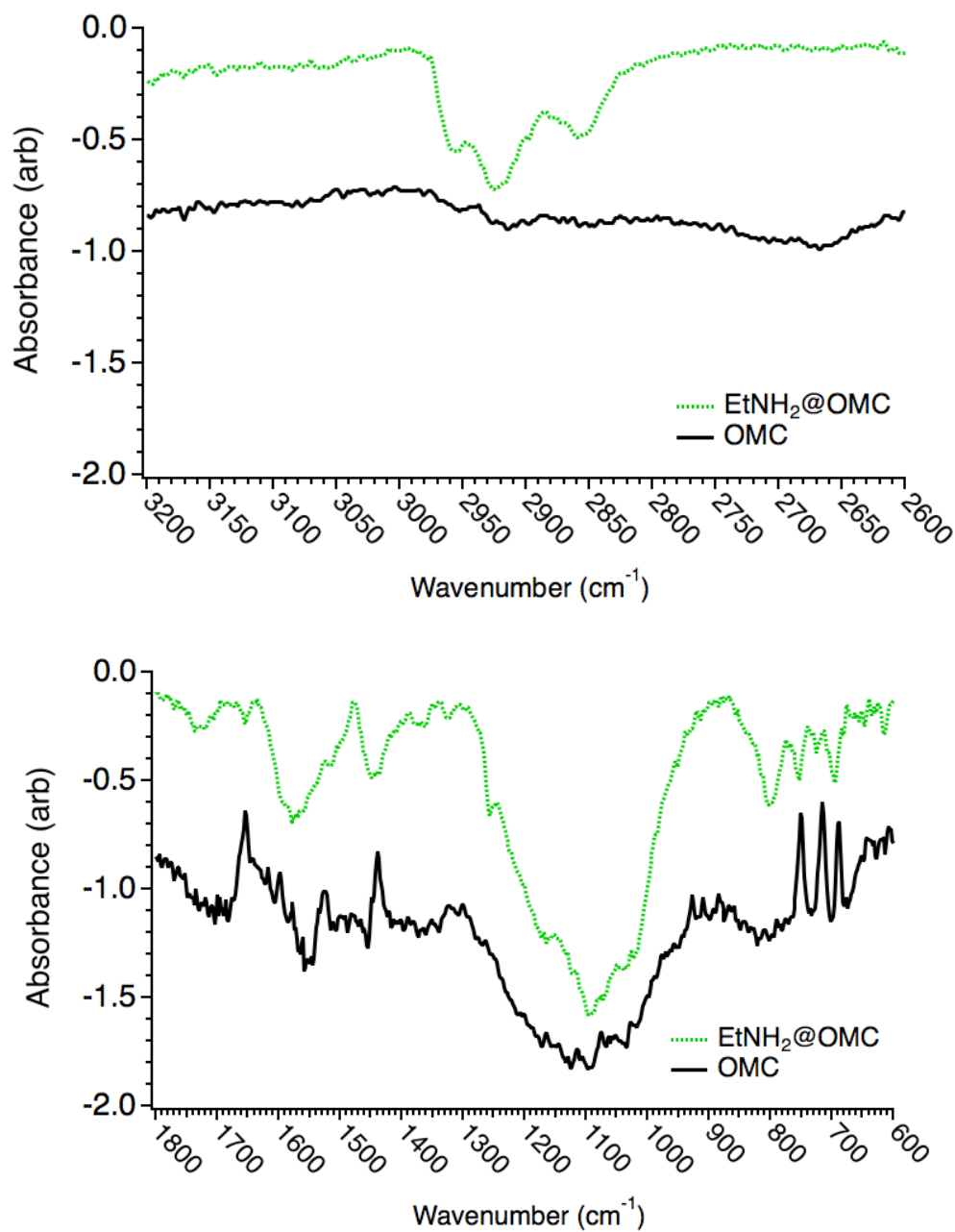


Figure 3.10. FTIR spectra exhibiting signals for methylene-CH motions (top) and N-H bending and aryl C-H motions (bottom) for OMC and EtNH₂@OMC.

X-ray Photoelectron Spectroscopy

XPS characterization of the surface was performed for its high surface sensitivity (~3-10nm) of chemical speciation. The overlaid C 1s and O 1s spectra in Figure 9 of EtNH₂@oxOMC and EtNH₂@OMC show an increase in surface oxidation primarily ~286-287 eV and ~530-532 eV. Curve-fitting analysis of the C 1s (Figure 3.11) was performed using well established C 1s fitting protocol.⁴³ The C 1s spectra in Figure 9 and respective components in Table 3 reveal subtle differences due to post HCl and post NaOH treatments in carbonaceous species at the surface. Notably, sp³ type C-C bonding is significantly higher in EtNH₂@OMC indicative of more ethyl ligands present. C-O, C=O, and O-C=O functionalities are also reportedly an increased surface presence for EtNH₂@oxOMC than EtNH₂@OMC. The N 1s spectra (Figure 4.S2) shows a lack of amination at the surface. However, this is to be expected that the majority of the ethylamine groups with the OMC scaffold are within the pore and outside of the information depth for lab-based spectrometers.

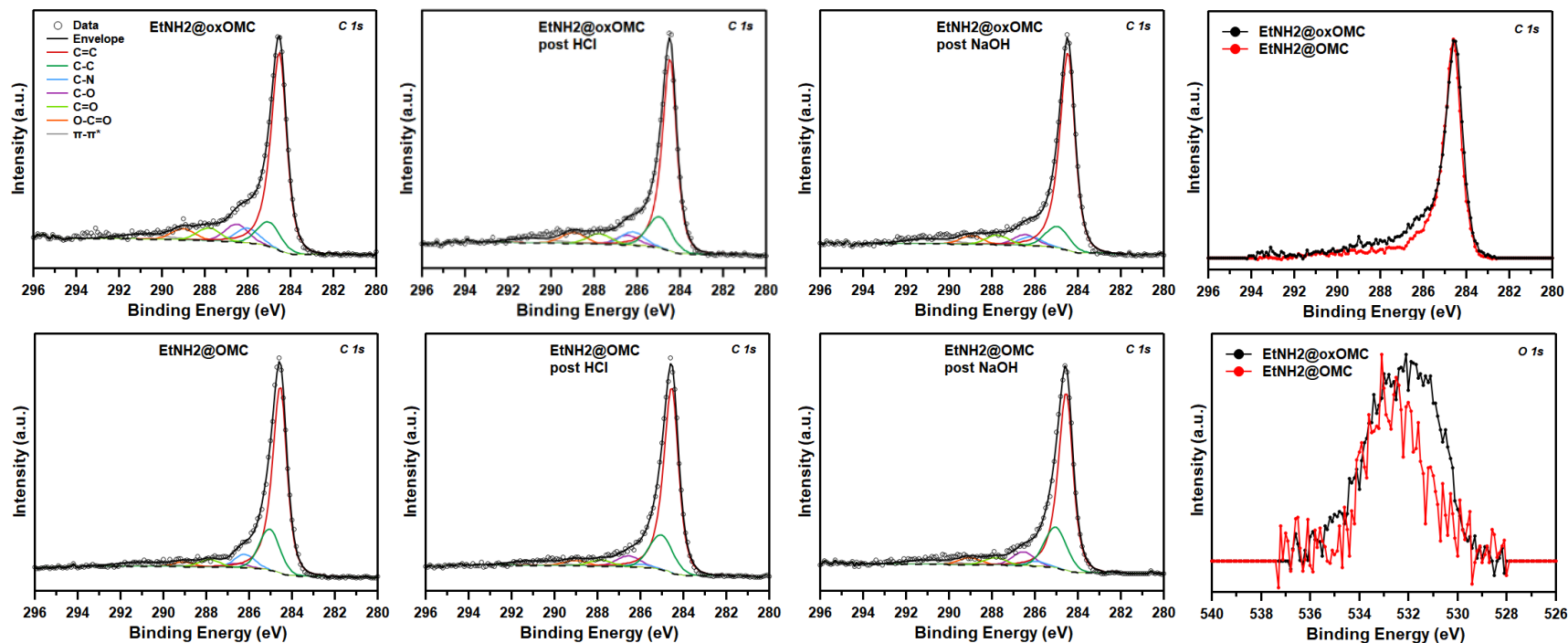


Figure 3.11. Curve-fitted XPS spectra of the C 1s core level for EtNH₂@oxOMC and EtNH₂@OMC, post HCl and post NaOH treatment. On the right, overlaid C 1s and O 1s of EtNH₂@oxOMC and EtNH₂@OMC spectra that has been background subtracted and normalized at peak maximum to emphasize differences due to treatment.

Elemental Analysis

The primary indicator of amination from the elemental analysis (Table 3.4) for the samples is the detection of nitrogen. Prior to functionalization, the amount of nitrogen detected was very small for OMC and oxOMC. Following amination, the nitrogen content for both EtNH₂@OMC and EtNH₂@oxOMC was significantly enriched, which alludes the presence of amines in these materials. The differences in nitrogen detected for the EtNH₂@oxOMC materials following acid and base exposure corroborate well with the 4-NB assay results. The nitrogen amount for EtNH₂@oxOMC-A was the same as oxOMC, and the nitrogen detected for EtNH₂@oxOMC-B was very similar to that of EtNH₂@oxOMC, and, indicating surface amine scission following acid exposure, but not base. While the nitrogen content EtNH₂@OMC-A and EtNH₂@OMC-B were still elevated from that of OMC, there is a slight decrease in nitrogen amount for these two samples relative to EtNH₂@OMC. The diminished nitrogen detected for these samples may be due to the limitations of the measurement only analyzing analyzing C, H, and N. The possibility of undetected residual elements, like Cl from HCl and Na from NaOH, may have affected the mass balance obtained for EtNH₂@OMC-A and EtNH₂@OMC-B.

Table 3.4. Detected wt. % of selected elements by elemental combustion microanalysis.

	Carbon	Hydrogen	Nitrogen
OMC	96.1	0.8	0.0
EtNH ₂ @OMC	91.5	1.7	0.4
EtNH ₂ @OMC-A	92.8	1.3	0.3
EtNH ₂ @OMC-B	91.9	1.2	0.2
oxOMC	92.6	2.7	0.1
EtNH ₂ @oxOMC	85.6	3.0	0.7
EtNH ₂ @oxOMC-A	92.6	0.6	0.1
EtNH ₂ @oxOMC-B	83.0	1.1	0.6

3.6 Conclusion

Covalently modified OMC surfaces were investigated for their robustness towards varying HCl concentrations and 1M NaOH. From a nitrogen sorption porosity and LA-XRD topological ordering standpoint, both etherized and organolithium-modified OMCs were able to withstand 1M NaOH, which incurred negligible changes to the material by these measurements. The 4-NB assay quantitatively proved the retention (>90% starting amount) of surface amines for all of the base-exposed aminated OMC materials. The same can be claimed for the organolithium-modified OMC under acid conditions, from both physicochemical characterizations and the 4-NB assay, which was expected. The etherized OMC was lysed in hydrochloric acid conditions at pH 0 and pH 1, contrary to solution-based organic chemistry ether stability, showing the importance of chemical testing on covalently-modified porous carbon materials. Since the electronic environment on a given carbon material is unique, the reactivity for a given functional group (i.e., ether) cannot be predicted by organic chemistry knowledge alone, and therefore researchers utilizing a given type of covalently functionalized carbonaceous material should

systematically experimentally determine for which pH condition the surface functional groups are labile in.

3.7 References

1. Kovach, N. C.; Russell-Parks, G. A.; Trewyn, B. G., Strategies for Post-synthetic Functionalization of Mesoporous Carbon Nanomaterial Surfaces. *Microporous Mesoporous Mater.* **2022**, 329.
2. Ismar, E.; Sarac, A. S., Carbon Nanomaterials: Carbon Nanotubes, Graphene, and Carbon Nanofibers. In Research Anthology on Synthesis, Characterization, and Applications of Nanomaterials, Management Association, I. R., Ed. IGI Global: Hershey, PA, USA, **2021**; pp 784-809.
3. Zhang, P. F.; Zhu, H. Y.; Dai, S., Porous Carbon Supports: Recent Advances with Various Morphologies and Compositions. *ChemCatChem* **2015**, 7 (18), 2788-2805.
4. Bradley, R. H.; Pendleton, P., Structure, Chemistry and Energy of Carbon Surfaces. *Adsorpt. Sci. Technol.* **2013**, 31 (2-3), 113-133.
5. Falcao, E. H. L.; Wudl, F., Carbon Allotropes: Beyond Graphite and Diamond. *J. Chem. Technol. Biot.* **2007**, 82 (6), 524-531.
6. Rodriguez-Reinoso, F., The Role of Carbon Materials in Heterogeneous Catalysis. *Carbon* **1998**, 36 (3), 159-175.
7. Rondeau-Gagné, S.; Morin, J. F., Preparation of Carbon Nanomaterials from Molecular Precursors. *Chem. Soc. Rev.* **2014**, 43 (1), 85-98.
8. Pérez-Mayoral, E.; Matos, I.; Bernardo, M.; Fonseca, I. M., New and Advanced Porous Carbon Materials in Fine Chemical Synthesis. Emerging Precursors of Porous Carbons. *Catalysts* **2019**, 9 (2).
9. Figueiredo, J. L.; Pereira, M. F. R.; Freitas, M. M. A.; Orfao, J. J. M., Modification of the Surface Chemistry of Activated Carbons. *Carbon* **1999**, 37 (9), 1379-1389.
10. Moreno-Castilla, C.; López-Ramón, M. V.; Carrasco-Marín, F., Changes in Surface Chemistry of Activated Carbons by Wet Oxidation. *Carbon* **2000**, 38 (14), 1995-2001.
11. Yellampalli, S., Carbon Nanotubes: Polymer Nanocomposites. *IntechOpen* **2011**.
12. Paoprasert, P.; Kandala, S.; Sweat, D. P.; Ruther, R.; Gopalan, P., Versatile Grafting Chemistry For Creation of Stable Molecular Layers on Oxides. *J. Mater. Chem.* **2012**, 22 (3), 1046-1053.
13. Vollhardt, K. P. C.; Schore, N. E., Organic Chemistry. W. H. Freeman: **2010**.

14. Zhang, X.; Liu, R. J.; Wang, H.; Liu, L. C.; Yue, C. T., Fabrication of Phosphate-Containing Mesoporous Carbon for Fast and Efficient Uranium (VI) Extraction. *Colloid Surface A* **2023**, 662.
15. Liu, X.; Wang, X.; Jiang, W.; Zhang, C. R.; Zhang, L.; Liang, R. P.; Qiu, J. D., Covalent Organic Framework Modified Carbon Nanotubes for Removal of Uranium (VI) from Mining Wastewater. *Chem. Eng. J.* **2022**, 450.
16. Ling, X. L.; Wei, Y. Z.; Zou, L. M.; Xu, S., Preparation and Characterization of Hydroxylated Multi-walled Carbon Nanotubes. *Colloid Surface A* **2013**, 421, 9-15.
17. Bradley, R. H.; Cassity, K.; Andrews, R.; Meier, M.; Osbeck, S.; Andreu, A.; Johnston, C.; Crossley, A., Surface Studies of Hydroxylated Multi-wall Carbon Nanotubes. *Appl. Surf. Sci.* **2012**, 258 (11), 4835-4843.
18. Herold, F.; Leubner, O.; Pfeifer, P.; Zakgeym, D.; Drochner, A.; Qi, W.; Etzold, B. J. M., Synthesis Strategies Towards Amorphous Porous Carbons with Selective Oxygen Functionalization for the Application as Reference Material. *Carbon* **2021**, 171, 658-670.
19. Gray, M. L.; Soong, Y.; Champagne, K. J.; Baltrus, J.; Stevens, R. W.; Toochinda, P.; Chuang, S. S. C., CO₂ Capture by Amine-enriched Fly Ash Carbon Sorbents. *Sep. Purif. Technol.* **2004**, 35 (1), 31-36.
20. Savameri, A. H.; Izadbakhsh, A.; Zarenezhad, B., Study of the Performance of Amino-Functionalized Ordered Mesoporous Carbon in the Transesterification of Soybean Oil. *React. Kinet. Mech. Cat.* **2018**, 124 (1), 247-264.
21. Joglekar, M.; Pylypenko, S.; Otting, M. M.; Valenstein, J. S.; Trewyn, B. G., Universal and Versatile Route for Selective Covalent Tethering of Single-Site Catalysts and Functional Groups on the Surface of Ordered Mesoporous Carbons. *Chem. Mater.* **2014**, 26 (9), 2873-2882.
22. Joglekar, M.; Nguyen, V.; Pylypenko, S.; Ngo, C.; Li, Q. N.; O'Reilly, M. E.; Gray, T. S.; Hubbard, W. A.; Gunnoe, T. B.; Herring, A. M.; Trewyn, B. G., Organometallic Complexes Anchored to Conductive Carbon for Electrocatalytic Oxidation of Methane at Low Temperature. *J. Am. Chem. Soc.* **2016**, 138 (1), 116-125.
23. Kim, T. W.; Slowing, I. I.; Chung, P. W.; Lin, V. S. Y., Ordered Mesoporous Polymer-Silica Hybrid Nanoparticles as Vehicles for the Intracellular Controlled Release of Macromolecules. *ACS Nano* **2011**, 5 (1), 360-366.
24. Yang, Y. N.; Chun, Y.; Sheng, G. Y.; Huang, M. S., pH-dependence of Pesticide Adsorption by Wheat-residue-derived Black Carbon. *Langmuir* **2004**, 20 (16), 6736-6741.
25. Veerakumar, P.; Jeyapragasam, T.; Surabhi; Salamalai, K.; Maiyalagan, T.; Lin, K. C., Functionalized Mesoporous Carbon Nanostructures for Efficient Removal

- of Eriochrome Black-T from Aqueous Solution. *J. Chem. Eng. Data* **2019**, 64 (4), 1305-1321.
26. Schönherr, J.; Buchheim, J. R.; Scholz, P.; Adelhelm, P., Boehm Titration Revisited (Part I): Practical Aspects for Achieving a High Precision in Quantifying Oxygen-Containing Surface Groups on Carbon Materials. *C* **2018**, 4 (2), 21.
 27. Rouquerol, J.; Llewellyn, P.; Rouquerol, F., Is the BET Equation Applicable to Microporous Adsorbents? *Stud. Surf. Sci. Catal.* **2006**, 160, 49-56.
 28. Bardestani, R.; Patience, G. S.; Kaliaguine, S., Experimental Methods in Chemical Engineering: Specific Surface Area and Pore Size Distribution Measurements-BET, BJH, and DFT. *Can. J. Chem. Eng.* **2019**, 97 (11), 2781-2791.
 29. Kunc, F.; Nirmalanathan-Budau, N.; Rühle, B.; Sun, Y.; Johnston, L. J.; Resch-Genger, U., Interlaboratory Comparison on the Quantification of Total and Accessible Amine Groups on Silica Nanoparticles with qNMR and Optical Assays. *Anal. Chem.* **2021**, 93 (46), 15271-15278.
 30. Sun, Y.; Kunc, F.; Balhara, V.; Coleman, B.; Kodra, O.; Raza, M.; Chen, M. H.; Brinkmann, A.; Lopinski, G. P.; Johnston, L. J., Quantification of Amine Functional groups on Silica Nanoparticles: a Multi-method Approach. *Nanoscale Adv.* **2019**, 1 (4), 1598-1607.
 31. Leyva, V.; Corral, I.; Schmierer, T.; Gilch, P.; González, L., A Comparative Analysis of the UV/Vis Absorption Spectra of Nitrobenzaldehydes. *Phys. Chem. Chem. Phys.* **2011**, 13 (10), 4269-4278.
 32. Chen, S. G.; Yang, R. T.; Kapteijn, F.; Moulijn, J. A., A New Surface Oxygen Complex on Carbon - toward a Unified Mechanism for Carbon Gasification Reactions. *Ind. Eng. Chem. Res.* 1993, 32 (11), 2835-2840.

Supporting Information

The following figure (Figure 3.S1) shows the Boehm titrations showing a miniscule difference between the oxOMC sample and titration blank titrant volumes to reach pH equivalence for the NaHCO₃ trial, and approximately 0.13 mL difference for the Na₂CO₃ trial. For the Na₂CO₃ titration, the amount of detected surface lactones is 13 μmol g⁻¹. This value allows for the amount of surface hydroxyl groups to be computed.

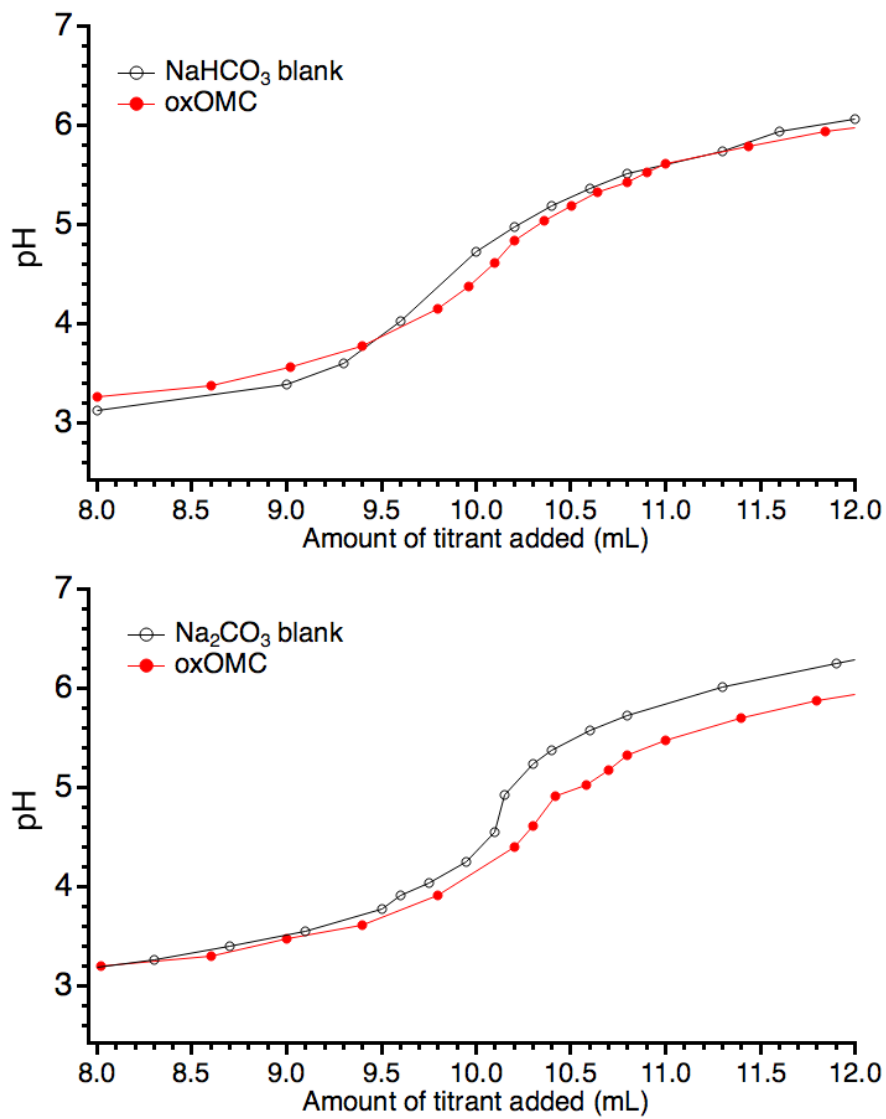


Figure 3.12. Boehm titration NaHCO₃ and Na₂CO₃ trial results for oxOMC.

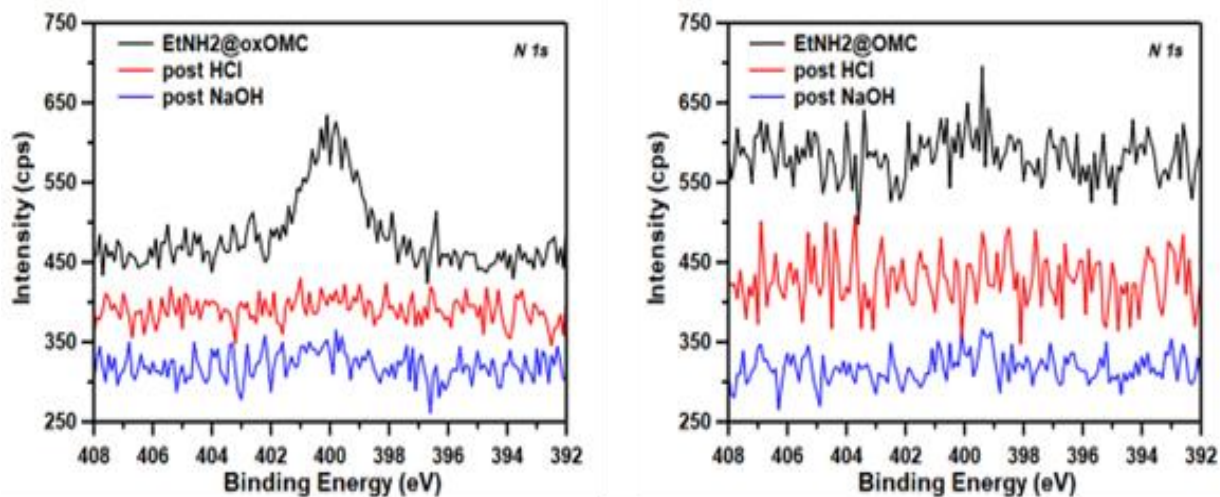


Figure 3.13. N 1s spectra of EtNH₂@oxOMC and EtNH₂@OMC, both post HCl and post NaOH.

CHAPTER 4 EXPOUNDING THE APPLIED SCOPE OF THE ORGANOLITHIUM AND HYDROXYLATION-ETHERIZATION METHODS

4.1 Abstract

The documented dissertation research comprises the significant finding regarding the acidic reactivity of etherized ethylamine groups on OMC surfaces. These findings will inform the future use of etherized OMC and OMC-like porous carbon materials. This dissertation's research scope was designed to elucidate the pH stability of a primary ethylamine functionalization and static (room temperature) exposure to pH 0-3 (HCl), and pH 14 (NaOH) on hard-templated OMC. Attempts to alter the degree of organolithium C-C functionalization was conducted by means of changing OMC carbonization temperatures and varying the pore dimensions of mesoporous silica template; These synthetic attempts were unsuccessful in that the preliminary data showed no differences in material properties (by N₂ sorption and TGA analysis) for the aminated OMCs. However, a variety of other techniques for controlling C-H defect density could be assessed. Also, the hydroxylation method by Fenton reaction was comparable in terms of degree of ethylamine functionalization relative to the organolithium method for this research, so no changes or optimization to the Fenton protocol was pursued. Despite this, many synthetic alterations could be studied in order to control the amount of surface hydroxyl groups installed to OMC surfaces.

4.2 Improvements to the Organolithium Method

The organolithium-mediated functionalization for carbonaceous materials beyond fullerene, CNTs, and graphene since 2010 has only been published upon a handful of times. In 2014, Joglekar, et. al, showed OMC treated with *n*-butyllithium covalently grafted 2.5 mmol · g⁻¹ bpy ligands, from which bound Cu²⁺.¹ Two years later, the same procedure was utilized to screen

metal chelating ligands to bind Pt^{2+} on OMC for use as a direct-methane fuel cell anode.² Researchers in 2018 used the same method to install approximately 0.7 mmol g^{-1} triethylamine groups onto OMC as a transesterification base catalyst.³ The reliability of the data's interpretation is called into question when the rationale for reduced catalytic activity over four cycles could be due to "evaporation of amine functional groups by sequential drying at the temperature of $80 \text{ }^\circ\text{C}$ ", where such temperature is insufficient to decompose a covalently bonded triethylamine and also far below the boiling point of the amine precursor, 2-(diethylamino)ethyl bromide hydrobromide ($208 \text{ }^\circ\text{C}$). Further, the researcher's rinsing protocol would have been sufficient to remove any non-reacted precursor, so the boiling phenomenon is unlikely. The triethylamine-functionalized research was synthetically novel in that the amine precursor was a salt, whereas the previous OMC publications used bromo-2,2-bipyridine. The bromo-2,2-bipyridine is fully soluble in diethyl ether, while organic salts do not solubilize well in ether; it's believed that the miniscule solubility into ether could be sufficient to contact with the highly reactive C-Li sites over 6 hours of contact.

OMC surfaces comprise a significant degree of planar sp^2 carbon bonding with varying amounts of oxygenated functional groups and some number of sp^3 defect sites embodying surface-terminated C-H moieties. The abundance of each of these features rely on the synthetic conditions applied to create the OMC. It has been experimentally observed that an increase in carbonization temperature results in an enrichment of sp^2 bonding and a diminution of surface oxygen groups.⁴ However, there remains a challenge in controlling the density of sp^3 defects when fabricating carbonaceous solids. Some successful procedures for intentionally installing sp^3 defects utilize nitrogen-doped carbons, as in the transformation of N-doped highly oriented pyrolytic graphite (HOPG) to a highly sp^3 "defective" D-HOPG⁵ or salt vaporization of ZIF-8

MOFs to create a sp^3 -enriched N-doped carbon.⁶ The identification of sp^3 sites on carbon surfaces is largely evidenced from computational support and are possible for materials with very well-defined architectures, like HOPG and ZIF-8.

Identifying sp^3 defects in larger carbonaceous structures, like OMC, has not been realized computationally. However, one significant step was made in 2022 when F. L. Sebastian, et. al. demonstrated for the first time a positive relationship between the measured Raman disordered to graphitic (D/G) ratio of and the defect density on fluorescently labeled CNTs.⁷ This breakthrough research is the first to establish this relationship for a non-planar carbon material, and this information is an a priori proxy for anticipating sp^3 defect densities on curved OMC surfaces. It is understood that during the carbonization step of synthesis, a higher temperature drives graphitization, resulting in a lower Raman D/G ratio for most carbons.⁸ A 2019 study clearly show the Raman D/G ratio evolution for 3.3 nm pore sized OMC carbonized at 500, 600, 700, and 800 °C.⁹ With this established notion, it was predicted that 5 nm pore sized OMC fabricated at increasing temperatures would embody a decreasing amount of surface-accessible C-H defect sites suitable for organolithium activation. From this notion, OMC produced at 700, 800, and 900 °C were aminated by the organolithium method followed by addition of bromoethylamine hydrobromide. Nitrogen sorption isotherms indicated that the reduction in surface area, pore volume, and pore diameter reduction for every aminated OMC were identical across the synthetic temperature range. Also, by TGA, the amount of weight loss measured for all aminated OMCs prior to structural degradation were much alike. These first two characterizations suggest the carbonization temperatures between 700-900 °C do not significantly affect the amount of derivatizable sp^3 defects on the material surface by means of organolithium modification.

4.3 Improvements to Hydroxylation-Etherization

Since the hydroxylation protocol was adopted from CNT research, there is an opportunity for the Fenton reaction to be studied with respect to hydroxylating MC structures. Investigating the rate of hydroxyl group formation as a function of temperature and reactant concentration on MC surfaces would provide researchers with a synthetic handle on hydroxylation extent. While a longer reaction time should yield greater -OH functionalization, determining a maximum amount of grafted hydroxyl groups by this method would be useful to know for applications which utilize surface hydroxyl groups directly.

The high temperature fabricated ($> 800\text{ }^{\circ}\text{C}$) OMC surfaces is predominantly aromatic in nature with a small ($< 2\text{ at. }%$) amount of C-H defects and oxygenation. Generally, a carbon surface's chemical makeup is relatively unreactive towards forming new chemical bonds. Since covalent carbon modification requires surface reactive functional groups, researchers have discovered how to enrich carbon surfaces with oxygen-containing moieties by oxidation. The lion's share of oxidations are chemically derived, where concentrated oxyacids (HNO_3 , H_2SO_4), oxidants (H_2O_2 , $\text{Na}_2\text{S}_2\text{O}_8$), bases (NaOH , KOH), and combinations of thereof are shown to install a plurality of functional groups like carboxylic acids, phenols, lactones, ketones, and ethers.¹⁰⁻¹⁴ Physical activation, primarily through high temperatures and a reactive gas (CO_2 , H_2O , CO , steam) can generate similar surfaces at the expense of an energy consumptive heating process.¹⁵⁻¹⁶ For OMC, oxidations inherently constrict the dimensions of pores and can physically degrade the OMC superstructure.^{11, 17} Oxidized carbons represent a large amount of functional carbons in fields like water filtration, aqueous electrochemistry, and heterogeneous catalysis. For aqueous applications, oxygen groups introduce carbon surface polarity, and thereby enables water contact as opposed to a carbon surface devoid of such oxygenation.¹⁸

Additionally, in catalysis, the acidity of carboxylic acids and phenols can act as acidic active sites and can also affect the sorption of molecular substrates/products. Hydrophilicity imparted by oxygenation also facilitates contact with aquated metal cations, which improves metal sorption for remediation as well as improves metal ion dispersion during metal nanoparticle synthesis.¹⁹⁻²⁰

One notable utility of oxidized carbons is to covalently react certain oxygen surface groups with an adsorbate to introduce new functionality. Of the known oxygen groups to occupy carbon surfaces, only a handful are regarded as covalent attachment sites. Researchers have converged to convert carboxylic acids into esters and amides, and phenols into ethers. In these cases, every other surface oxygen not participating in the targeted reaction will be unreactive and fill surface space which could otherwise be occupied by a reactive oxygen group. To this end, methods to imbue carbons selectively with carboxylic acids or phenols have been developed.

Two recent studies used carboxylated OMC materials to covalently tether oligonucleotides for rare earth element (REE) sequestration. Predicated by success in adsorbing REEs with phosphate-modified OMC, the researchers wanted to study the sorptive effects of tethering amine-terminated a 20 thymine unit oligo, a 100 thymine unit oligo, and a 2000 base pair long ssDNA.²¹ Carboxylic acids on carboxylated OMC underwent amidation with the N-terminus of the oligos and then utilized as Nd³⁺ sorbents. While the unfunctionalized OMC could adsorb 3.4 mg · g⁻¹ Nd³⁺, all of the oligo-grafted OMC exhibited >9 mg · g⁻¹ Nd³⁺.¹³ XPS analysis measured shortened Nd-O and Nd-P distances, indicating these features of the oligonucleotides as adsorption sites. Another group similarly tethered a 100 thymine unit oligo strand onto OMC and showed by XPS that oxygen is primary binding functionality in oligo-grafted OMC for Dy³⁺ and La³⁺.¹⁴

State-of-the-art selective hydroxylation methods are available for CNT and graphene, where fewer have been proven for mesoporous carbon.²²⁻³¹ Albeit so, one notable example of covalent tethering onto OMC surface hydroxyls came from F. Kleitz, et. al. in 2017; while the functionalization targeted the hydroxyl functionality, the group utilized an oxidation which installed a plurality of oxygen groups onto the OMC.³² They showed the covalent grafting of chlorinated diglycoamide molecules, reacting at nucleophilic -OH sites, forming metal chelating sites for aqueous REE extraction. More recently, a mesoporous carbon templated by spherical CaCO₃ nanoparticles exhibited both surface carbonyl and hydroxyl groups³³. While this procedure gave rise to two functional groups, both hydroxyls and ketones are suspected active sites for forming surface hydroxy-negative anions to improve contact with alkaline electrolytes as a supercapacitor electrode. While the effect The dearth of OMC research to install surface hydroxyls can be rationalized by the burgeoning variety of surface modifications which researchers can choose from. Further, the size of the OMC community is relatively smaller than the research population studying other carbon allotropes. There is clearly an unfilled gap in OMC research regarding surface hydroxylation and using hydroxyl groups as sites for grafting functional molecules.

Historically, functionalizations of OMC have drawn upon the knowledge procured by researching surface reactions on other carbon allotropes. After surveying the reaction scope of surface hydroxylation for graphene, nanodiamonds, and CNTs, there emerged three protocols which were synthetically feasible by means of chemical activation. A majority of these publications feature the Fenton reaction (Fe²⁺, H₂O₂) to confer hydroxyl groups by means of radical addition with unsaturated surface C=C sites. The reactions which the Fenton-generated

radicals undergo on nanodiamond, graphene, and CNT are precedent to the Fenton reaction's applicability for OMC surfaces.

This reaction has been proven on fly-ash derived activated carbon, which inherently contain hydroxyls and carboxylic acids.³⁴ The authors claimed the creation of both ethers and esters (Figure 4.1). However, the reported basic (NaOH) reaction conditions are inappropriate to esterify a carboxylic acid, so it's believed that only etherized groups were created. This research was seminal in showing that etherization by means of substitution between nucleophilic porous carbon hydroxylates and an electrophilic primary carbon-halogenated functional group.

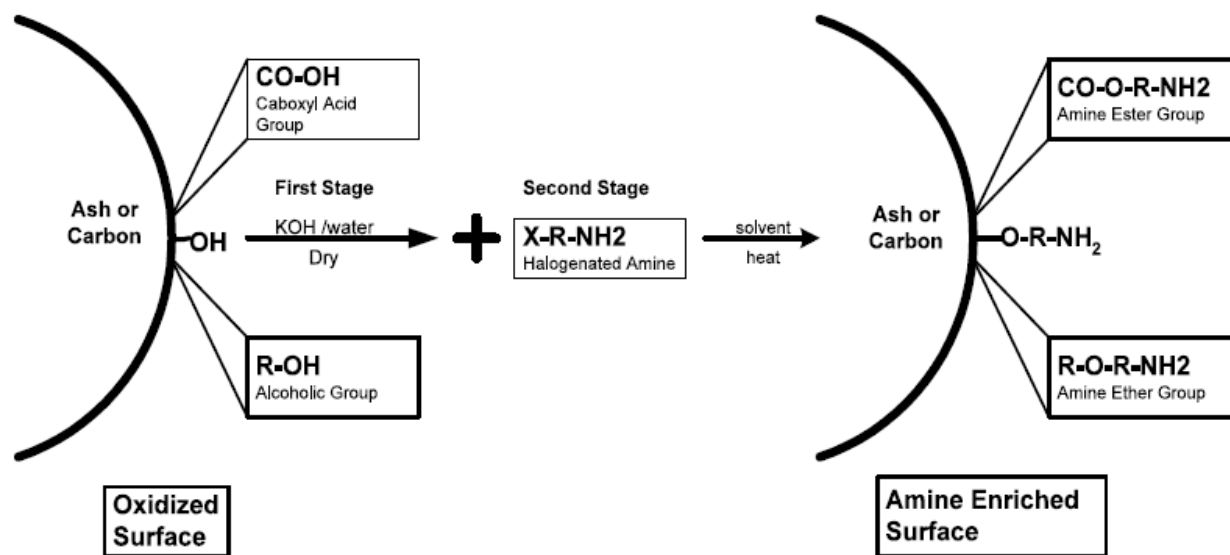


Figure 4.1. Proposed reactions for preparation of the amine-enriched fly ash sorbent.

Greater comprehension of hydroxyl derivatization came from a 2021 study by F. Herold, et. al. who synthesized hydroxylated amorphous, mesoporous polymer-derived carbon (PDC) and performed etherizations and esterifications.³⁵ The hydroxylation was achieved by an initial bulk oxidation with HNO₃ followed by a chemical reduction by LiAlH₄ to reduce surface ketones and carboxylic acids to hydroxyl groups. Notably, this research was performed on amorphous

carbon, which bears surface chemical resemblance to OMC. The surface reactions they performed targeted specific functional groups to derivatize and subsequently quantify (Figure 4.2). Only O-PDC-LiAlH₄-COOH registered near-quantitative functionalization, where the hydroxyls in O-PDC-LiAlH₄-BzCl and O-PDC-LiAlH₄-Me only partially reacted to form esters and ethers, respectively. They found the thermal stability of the etherized functionality on O-PDC-LiAlH₄-COOH was greater than that of carboxylic acid moieties alone on carbon surfaces. On the other hand, the thermal decomposition temperature for both phenyl and methyl esters were lesser than that of reported surface lactones and ethers. This observation was attributed to the thermal reactions which occur during TPD including: Carboxylic acid condensation to anhydrides, formation of lactones between carboxylic and hydroxyl groups, and the Boudouard equilibrium process.³⁶

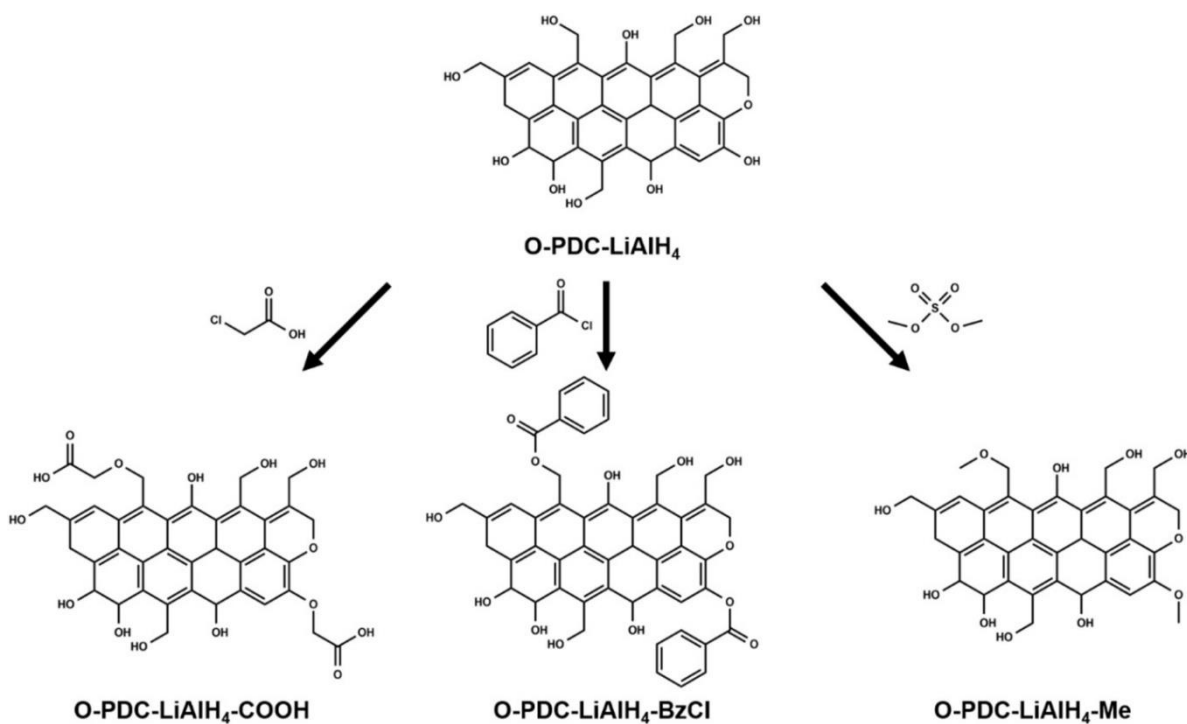


Figure 4.2. Introduction of phenyl esters, carboxylic acids or methyl ethers by utilizing hydroxyl surface groups of a reduced carbon as nucleophiles.

Amines have emerged as versatile functional groups, being applied across a range of fields. A few notable uses of primary amines include: Active sites for base catalysis, coordinating metal cations for water purification and to improve metal loading for nanoparticle formation, chemisorbing CO₂ for gas purification, electrostatic binding sites for pollutants or pharmaceuticals, conjugating with acyl-chloride amino acid C-termini to install proteins or enzymes, and coupling with fluorophores for medical imaging applications.

From our study comparing the reactivity of covalently-grafted ethylamine OMC materials, it is apparent that pHs 0 and 1 at room temperature under static conditions deaminates etherized surfaces. It is hypothesized that under the excess acidic environment, both the amine and etheric oxygen are protonated. The protonated ether allows for nucleophilic displacement to occur at the adjacent 1 carbon, rendering the hydroxylated OMC as the reaction's leaving group along with a chloroethylamine molecule (Figure 4.3).

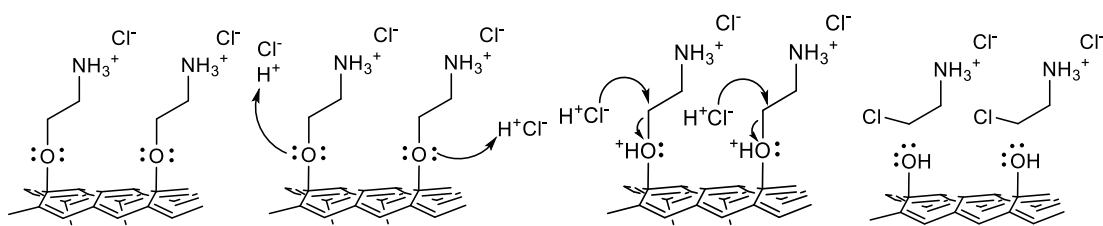


Figure 4.3. Mechanism of ethylamine surface cleavage occurring at the etheric oxygen.

Alternatively, the sterics of the ethylamine moiety allow for amine back-bending, where the etheric oxygen lone pair interacts with the hybridized σ^* C-N bond located on the 1° carbon

to the protonated amine, allowing for a nucleophilic displacement to occur giving rise to a strained oxirane ring on the OMC surface and an ammonia leaving group (Figure 4.4).

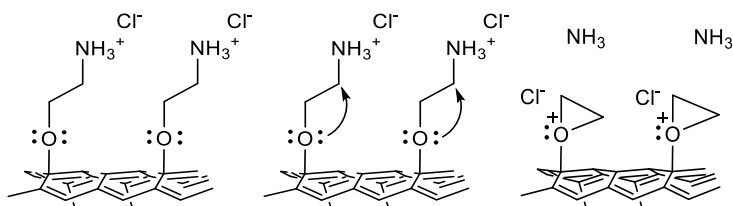


Figure 4.4. Mechanism for amine liberation by means of S_N2 attack by the etheric oxygen.

One other considered case, involving an S_N2 displacement of ammonia by the chloride anion in concentrated HCl solution, was envisaged but deemed unlikely since C-C bonded amine groups remained after acid exposure (Figure 4.5). Computational chemistry would provide energetic and mechanistic insight into the reactivity of etherized ethylamine groups on OMC, indicating which decomposition route is most likely to occur.

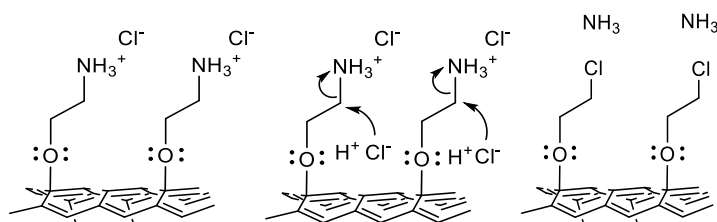


Figure 4.5. Mechanism of deamination from chloride S_N2 attack on the amine α carbon.

To understand the mechanism by which the material reacts would require more extensive surface analysis to probe the connectivity of the surface groups present after the acidic exposure, but surface-sensitive characterizations such as XPS, SAXS, and WAXS cannot unambiguously

identify functionality, which many solution-based analyses do routinely. Alternatively, the liquid retentate following acidic exposure could be assessed by GCMS, mass spectrometry, liquid FTIR, or $^1\text{H}/^{13}\text{C}$ NMR to elucidate whether ethylamine or ammonia is produced. In the case of ammonia being a reaction product, the supernatant could be titrated against a weak base to quantify the amount of liberated ammonia. The surface chemistry of the reacted OMC could be characterized by means of carbon and nitrogen XPS, only if the surface concentration of analyzable elemental groups provides sufficient count statistics to provide meaningful curve-fits. The Boehm titration would be able to identify hydroxyl presence, cluing acidic cleavage at the etheric oxygen. Chemically probing whether the aminated OMC decomposes by path B would be possible by either an acid or base mediated ring-opening of the epoxide to generate an ether bond with a new chemical signature. This selective functionalization can be followed by thermogravimetric analysis, to quantify the degradation of newly appended functionality, and FTIR to fingerprint the new etheric chemical signature. Under either basic or acidic ring-opening conditions on an oxirane-terminated OMC surface, there would be no such reaction on a hydroxylated OMC surface. In order to maximize the TGA detectability of the reaction product, a long-chain alkoxide, like sodium hexoxide, would be selected for reacting with the oxirane OMC surface—this way, the surface product would be a heavy hexyl ether, where a surface with $100\ \mu\text{mol} \cdot \text{g}^{-1}$ hexyl functionalization would exhibit a well-resolvable 1.5 wt.% mass loss prior to framework fragmentation. Furthermore, the FTIR signals for C-H stretching would be easily differentiable for a hexyl-appended OMC versus a non-functionalized (hydroxylated) OMC surface.

Just as important as elucidating the reaction mechanism for etherized OMC surfaces would be finding the minimum concentration of acid required to cleave surface groups. If this

condition could be determined, it too could be informative towards determining which mechanism proceeds. It would also be interesting to see if the surface ether bond can be decomposed by human biologically-relevant acid conditions like the stomach (approximate HCl concentration: 150 μ M). If so, an OMC could be fabricated such that the pore apertures are gated by means of bulky molecular complexes tethered by ether bonds that react only when in the stomach's environment. In this embodiment, the pH-responsive gated OMC would act as a protective carrier for pharmaceuticals with a high risk of insufflation abuse.

4.4 Final Remarks

While a majority of this dissertation's concern is with observing the acidic reactivity of etherized OMC material surfaces, a reasonable outset to this research includes determining whether covalently etherized OMC materials possess superior applied capabilities compared to OMC with C-C covalently tethered surface groups. Surface ether oxygens can improve wettability, and thereby contact with dissolved aqueous compounds. For both catalysis and aqueous adsorption, material hydrophilicity plays a large role in facilitating adsorptive-surface attraction. Thus, a comparison of C-C and etherized OMC in either of these broad applications would be beneficial to understand how near-surface OMC polarity influences its applied functions.

The rationale for studying primary amine surface functionalization was previously introduced, as was the application (Knoevenagel condensation catalysis) for the studied OMC materials. There are other functions permitted by a primary amine however, like transition metal cation coordination, C-terminus amino acid coupling, and conversion to azides (N=N). The attraction of primary amines towards divalent metal cations means that aminated OMC materials would act as chelation sites for dissolved metals in aqueous solution. While this has direct

implications towards aqueous metal sequestration, the surface metal affinity can be utilized for attracting metal precursors to the OMC surface for nanoparticle formation. There is plenty of literature precedence showing how porous aminated materials are superior to non-functionalized materials for dispersing and covalently tethering metal nanoparticles. Lastly, converting amines to azides would open up a much greater collection of surface reactions to occur, namely azide-alkyne “click” chemistry which is proven applicable to CNTs and other porous carbons.³⁷⁻⁴⁰ The click chemistry reaction scope opens numerous pathways to covalently link compounds to OMC scaffolds as opposed to reactions off of primary amines alone.

Lastly, this research illustrated the effectiveness of both the organolithium and hydroxylation-etherization protocols to install ethylamine groups onto OMC. It was serendipitous in that both types of aminated OMCs embodied similar amounts of assay-detected primary amine groups. Because of this, the modified materials could be compared directly (gravimetrically) with one another without mass correction. However, the levels of amine enrichment fall about an order of magnitude below what other publications claim for surface amine density. For the organolithium method, finding out how to tune the amount of surface derivatizable sp^3 defects by synthetic or post-synthetic means would be helpful to increase the degree of functionalization. Being the case, the knowledge emerging from the CNT and graphene communities will be instrumental in guiding the development of surface defect engineering with OMC materials.

4.5 References

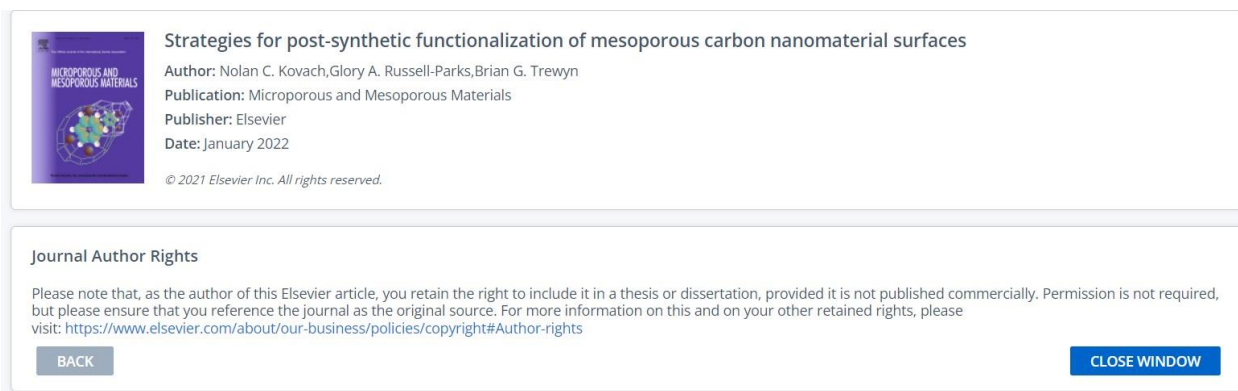
1. Joglekar, M.; Pylypenko, S.; Otting, M. M.; Valenstein, J. S.; Trewyn, B. G., Universal and Versatile Route for Selective Covalent Tethering of Single-Site Catalysts and Functional Groups on the Surface of Ordered Mesoporous Carbons. *Chem. Mater.* **2014**, *26* (9), 2873-2882.

2. Joglekar, M.; Nguyen, V.; Pylypenko, S.; Ngo, C.; Li, Q. N.; O'Reilly, M. E.; Gray, T. S.; Hubbard, W. A.; Gunnoe, T. B.; Herring, A. M.; Trewyn, B. G., Organometallic Complexes Anchored to Conductive Carbon for Electrocatalytic Oxidation of Methane at Low Temperature. *J. Am. Chem. Soc.* **2016**, *138* (1), 116-125.
3. Savameri, A. H.; Izadbakhsh, A.; Zarenezhad, B., Study of the performance of amino-functionalized ordered mesoporous carbon in the transesterification of soybean oil. *React Kinet. Mech. Cat.* **2018**, *124* (1), 247-264.
4. Sevilla, M.; Fuertes, A. B., Catalytic graphitization of templated mesoporous carbons. *Carbon* **2006**, *44* (3), 468-474.
5. Jia, Y.; Zhang, L. Z.; Zhuang, L. Z.; Liu, H. L.; Yan, X. C.; Wang, X.; Liu, J. D.; Wang, J. C.; Zheng, Y. R.; Xiao, Z. H.; Taran, E.; Chen, J.; Yang, D. J.; Zhu, Z. H.; Wang, S. Y.; Dai, L. M.; Yao, X. D., Identification of active sites for acidic oxygen reduction on carbon catalysts with and without nitrogen doping. *Nat. Catal.* **2019**, *2* (8), 688-695.
6. Cao, Y. J.; Liu, Z.; Tang, Y. T.; Huang, C. J.; Wang, Z. L.; Liu, F.; Wen, Y. W.; Shan, B.; Chen, R., Vaporized-salt-induced sp²-hybridized defects on nitrogen-doped carbon surface towards oxygen reduction reaction. *Carbon* **2021**, *180*, 1-9.
7. Sebastian, F. L.; Zorn, N. F.; Settele, S.; Lindenthal, S.; Berger, F. J.; Bendel, C.; Li, H.; Flavel, B. S.; Zaumseil, J., Absolute Quantification of sp³ Defects in Semiconducting Single-Wall Carbon Nanotubes by Raman Spectroscopy. *The Journal of Physical Chemistry Letters* **2022**, *13* (16), 3542-3548.
8. Ko, T. H.; Kuo, W. S.; Chang, Y. H., Raman study of the microstructure changes of phenolic resin during pyrolysis. *Polym. Composite* **2000**, *21* (5), 745-750.
9. Ma, X. H.; Yuan, H.; Hu, M. Q., A simple method for synthesis of ordered mesoporous carbon. *Diam. Relat. Mater.* **2019**, *98*.
10. Bazula, P. A.; Lu, A. H.; Nitz, J. J.; Schüth, F., Surface and pore structure modification of ordered mesoporous carbons via a chemical oxidation approach. *Microporous Mesoporous Mat.* **2008**, *108* (1-3), 266-275.
11. Wu, Z. X.; Webley, P. A.; Zhao, D. Y., Comprehensive Study of Pore Evolution, Mesostructural Stability, and Simultaneous Surface Functionalization of Ordered Mesoporous Carbon (FDU-15) by Wet Oxidation as a Promising Adsorbent. *Langmuir* **2010**, *26* (12), 10277-10286.
12. Hadoun, H.; Sadaoui, Z.; Souami, N.; Sahel, D.; Toumert, I., Characterization of mesoporous carbon prepared from date stems by H₃PO₄ chemical activation. *Appl. Surf. Sci.* **2013**, *280*, 1-7.
13. Choi, M.; Ryoo, R., Mesoporous carbons with KOH activated framework and their hydrogen adsorption. *J. Mater. Chem.* **2007**, *17* (39), 4204-4209.

14. Enterría, M.; Suárez-García, F.; Martínez-Alonso, A.; Tascón, J. M. D., Synthesis of ordered micro-mesoporous carbons by activation of SBA-15 carbon replicas. *Microporous Mesoporous Mat.* **2012**, *151*, 390-396.
15. Xia, K. S.; Gao, Q. M.; Wu, C. D.; Song, S. Q.; Ruan, M. L., Activation, characterization and hydrogen storage properties of the mesoporous carbon CMK-3. *Carbon* **2007**, *45* (10), 1989-1996.
16. Girgis, B. S.; Soliman, A. M.; Fathy, N. A., Development of micro-mesoporous carbons from several seed hulls under varying conditions of activation. *Microporous Mesoporous Mat.* **2011**, *142* (2-3), 518-525.
17. Martinhopkins, M. B.; Gilpin, R. K.; Jaroniec, M., Studies of the Surface Heterogeneity of Chemically Modified Porous Carbons by Gas Solid Chromatography. *J Chromatogr Sci* **1991**, *29* (4), 147-152.
18. Li, Z. J.; Yan, W. F.; Dai, S., Surface functionalization of ordered mesoporous carbons - A comparative study. *Langmuir* **2005**, *21* (25), 11999-12006.
19. Li, Y. L.; Gui, F. S.; Wang, F. H.; Liu, J. J.; Zhu, H., Synthesis of modified, ordered mesoporous carbon-supported Pt3Cu catalyst for enhancing the oxygen reduction activity and durability. *Int. J. Hydrogen Energ.* **2021**, *46* (76), 37802-37813.
20. Calvillo, L.; Lázaro, M. J.; García-Bordejé, E.; Moliner, R.; Cabot, P. L.; Esparbé, I.; Pastor, E.; Quintana, J. J., Platinum supported on functionalized ordered mesoporous carbon as electrocatalyst for direct methanol fuel cells. *J. Power Sources* **2007**, *169* (1), 59-64.
21. Unsworth, C. E.; Kuo, C. C.; Kuzmin, A.; Khalid, S.; Saha, D., Adsorption of Rare Earth Elements onto DNA-Functionalized Mesoporous Carbon. *ACS Appl. Mater. Interf.* **2020**, *12* (38), 43180-43190.
22. Bradley, R. H.; Cassity, K.; Andrews, R.; Meier, M.; Osbeck, S.; Andreu, A.; Johnston, C.; Crossley, A., Surface studies of hydroxylated multi-wall carbon nanotubes. *Appl. Surf. Sci.* **2012**, *258* (11), 4835-4843.
23. Ling, X. L.; Wei, Y. Z.; Zou, L. M.; Xu, S., Preparation and characterization of hydroxylated multi-walled carbon nanotubes. *Colloid Surface A* **2013**, *421*, 9-15.
24. Vacchi, I. A.; Raya, J.; Bianco, A.; Ménard-Moyon, C., Controlled derivatization of hydroxyl groups of graphene oxide in mild conditions. *2D Mater.* **2018**, *5* (3).
25. Çakir, U.; Kestel, F.; Kizilduman, B. K.; Bicil, Z.; Dogan, M., Multi walled carbon nanotubes functionalized by hydroxyl and Schiff base and their hydrogen storage properties. *Diam. Relat. Mater.* **2021**, *120*.
26. Huang, C. Y.; Lin, J.; Tang, H. Q.; Wang, Q.; Majima, T.; Wang, N.; Luo, Z. H.; Zhu, L. H., Mechanochemical Preparation of Edge-Selectively justify Hydroxylated Graphene Nanosheets Using Persulfate via a Sulfate Radical-Mediated Process. *ChemSusChem* **2023**, *16* (3).

27. Sun, J.; Deng, Y.; Li, J. P.; Wang, G.; He, P.; Tian, S. Y.; Bu, X. M.; Di, Z. F.; Yang, S. W.; Ding, G. Q.; Xie, X. M., A New Graphene Derivative: Hydroxylated Graphene with Excellent Biocompatibility. *ACS Appl. Mater. Interf.* **2016**, *8* (16), 10226-10233.
28. Deng, H. H.; Huang, J.; Qin, C. Q.; Xu, T. H.; Ni, H. G.; Ye, P., Preparation of high-performance nanocomposite membranes with hydroxylated graphene and graphene oxide. *J. Water Process Eng.* **2021**, *40*.
29. Kasahara, S.; Ogose, T.; Ikemiya, N.; Yamamoto, T.; Natsui, K.; Yokota, Y.; Wong, R. A.; Iizuka, S.; Hoshi, N.; Tateyama, Y.; Kim, Y.; Nakamura, M.; Einaga, Y., In Situ Spectroscopic Study on the Surface Hydroxylation of Diamond Electrodes. *Anal. Chem.* **2019**, *91* (8), 4980-4986.
30. Wang, F.; Li, Q. Q.; Chu, X. Z.; Zhu, F. X.; Zhao, P. S.; Wu, F. Y.; Xiao, G. M., The Synergistic Effect of Hydroxylated Carbon Nanotubes and Ultrasound Treatment on Hierarchical HZSM-5 in the Selective Catalytic Upgrading of Biomass Derived Glycerol to Aromatics. *Catal. Lett.* **2022**, *152* (8), 2421-2433.
31. Li, W. K.; Chen, J.; Zhang, H. X.; Shi, Y. P., Selective determination of aromatic acids by new magnetic hydroxylated MWCNTs and MOFs based composite. *Talanta* **2017**, *168*, 136-145.
32. Perreault, L. L.; Giret, S.; Gagnon, M.; Florek, J.; Larivière, D.; Kleitz, F., Functionalization of Mesoporous Carbon Materials for Selective Separation of Lanthanides under Acidic Conditions. *ACS Appl. Mater. Interf.* **2017**, *9* (13), 12003-12012.
33. Xie, M. J.; Xiao, R.; Yu, Y.; Zhang, Y.; Du, C.; Wan, L.; Chen, J., Superhydrophilicity and ultrahigh-rate supercapacitor performances enabled by mesoporous carbon doped with conjugated hydroxyl. *J. Energy Storage* **2021**, *43*.
34. Gray, M. L.; Soong, Y.; Champagne, K. J.; Baltrus, J.; Stevens, R. W.; Toochinda, P.; Chuang, S. S. C., CO₂ capture by amine-enriched fly ash carbon sorbents. *Sep. Purif. Technol.* **2004**, *35* (1), 31-36.
35. Herold, F.; Leubner, O.; Pfeifer, P.; Zakgeym, D.; Drochner, A.; Qi, W.; Etzold, B. J. M., Synthesis strategies towards amorphous porous carbons with selective oxygen functionalization for the application as reference material. *Carbon* **2021**, *171*, 658-670.
36. Düngen, P.; Schlögl, R.; Heumann, S., Non-linear thermogravimetric mass spectrometry of carbon materials providing direct speciation separation of oxygen functional groups. *Carbon* **2018**, *130*, 614-622.
37. Devadoss, A.; Chidsey, C. E. D., Azide-modified graphitic surfaces for covalent attachment of alkyne-terminated molecules by "click" chemistry. *J. Am. Chem. Soc.* **2007**, *129* (17), 5370-+.
38. Han, J.; Gao, C., Functionalization of carbon nanotubes and other nanocarbons by azide chemistry. *Nano-Micro Lett.* **2010**, *2* (3), 213-226.

39. Stenehjem, E. D.; Ziatdinov, V. R.; Stack, T. D. P.; Chidsey, C. E. D., Gas-Phase Azide Functionalization of Carbon. *J. Am. Chem. Soc.* **2013**, *135* (3), 1110-1116.
40. Coates, M.; Griveau, S.; Bedioui, F.; Nyokong, T., Layer by Layer Electrode Surface Functionalisation Using Carbon Nanotubes, Electrochemical Grafting of Azide-Alkyne Functions and Click Chemistry. *Electroanal.* **2012**, *24* (9), 1833-1838.



Strategies for post-synthetic functionalization of mesoporous carbon nanomaterial surfaces
 Author: Nolan C. Kovach, Glory A. Russell-Parks, Brian G. Trewyn
 Publication: Microporous and Mesoporous Materials
 Publisher: Elsevier
 Date: January 2022
 © 2021 Elsevier Inc. All rights reserved.

Journal Author Rights
 Please note that, as the author of this Elsevier article, you retain the right to include it in a thesis or dissertation, provided it is not published commercially. Permission is not required, but please ensure that you reference the journal as the original source. For more information on this and on your other retained rights, please visit: <https://www.elsevier.com/about/our-business/policies/copyright#Author-rights>

BACK CLOSE WINDOW

Figure A.1. Copyright permission obtained for “Strategies for post-synthetic functionalization of mesoporous carbon nanomaterial surfaces”, modified for Chapter 1.

Multiscale investigations of europium(III) complexation with tetra-*n*-octyl diglycolamide confined in porous solid supports

E. R. Bertelsen, N. C. Kovach, B. J. Reinhart, B. G. Trewyn, M. R. Antonio and J. C. Shafer, *CrystEngComm*, 2020, **22**, 6886 DOI: 10.1039/D0CE00956C

To request permission to reproduce material from this article, please go to the [Copyright Clearance Center request page](#).

If you are **an author contributing to an RSC publication, you do not need to request permission** provided correct acknowledgement is given.

If you are **the author of this article, you do not need to request permission to reproduce figures and diagrams** provided correct acknowledgement is given. If you want to reproduce the whole article in a third-party publication (excluding your thesis/dissertation for which permission is not required) please go to the [Copyright Clearance Center request page](#).

Read more about [how to correctly acknowledge RSC content](#).

Figure A.2. Copyright permission given for the manuscript in which SAXS data was discussed in Chapter 2.

This Agreement between Colorado School of Mines -- Nolan Kovach ("You") and Elsevier ("Elsevier") consists of your license details and the terms and conditions provided by Elsevier and Copyright Clearance Center.

License Number	5681571136970
License date	Dec 03, 2023
Licensed Content Publisher	Elsevier
Licensed Content Publication	Separation and Purification Technology
Licensed Content Title	CO2 capture by amine-enriched fly ash carbon sorbents
Licensed Content Author	M.L Gray, Y Soong, K.J Champagne, John Baltrus, R.W Stevens, P Toochinda, S.S.C Chuang
Licensed Content Date	Feb 1, 2004
Licensed Content Volume	35
Licensed Content Issue	1
Licensed Content Pages	6
Start Page	31
End Page	36

Figure A.3. Copyright permission granted for reuse of the manuscript for Figure 5.1.

This Agreement between Colorado School of Mines -- Nolan Kovach ("You") and Elsevier ("Elsevier") consists of your license details and the terms and conditions provided by Elsevier and Copyright Clearance Center.

License Number	5681571264326
License date	Dec 03, 2023
Licensed Content Publisher	Elsevier
Licensed Content Publication	Carbon
Licensed Content Title	Synthesis strategies towards amorphous porous carbons with selective oxygen functionalization for the application as reference material
Licensed Content Author	Felix Herold, Oliver Leubner, Philipp Pfeifer, Dina Zakgeym, Alfons Drochner, Wei Qi, Bastian J.M. Etzold
Licensed Content Date	Jan 1, 2021
Licensed Content Volume	171
Licensed Content Issue	n/a
Licensed Content Pages	13
Start Page	658
End Page	670

Figure A.4. Copyright permission received for reuse of Figure 5.2.

B.1 Introduction

This project was funded by the United States Department of Defense, Defense Threat Reduction Agency for preliminary research pertaining to microscale separations of transuranic elements present in nuclear fission products. The interest in creating a solid-liquid extraction extraction system comprising a porous solid to heterogenize organic molecule extractants small-scale separations arose from the infeasibility of miniaturizing liquid-liquid separation systems.

The high surface area of molecularly-accessible pore apertures renders OMC as a candidate for supporting *f*-element extractants because of three physiochemical characteristics inherent to OMC: 1) Carbon materials are inherently stable in strongly acidic (Molar) chemical environments,¹ 2) The hydrophobicity of carbon surfaces enable noncovalent interactions with lipophilic groups² (which constitute some classes of *f*-element chelator molecules), and 3) The OMC structure can attenuate the degradative effects of γ -radiolysis present in all “hot” nuclear material.³

Inherently hydrophobic OMC was selected for this aqueous extraction because of van Der Waal forces and London dispersion forces which arise between the OMC surface and the lipophilic portion of a metal extractant molecule (adsorbate). When immersed in water, the relative strength between the OMC and hydrophobic adsorbate can be greater than that between water (reaction medium) and the adsorbate. In 2019, E. R. Bertelsen, *et. al.* used OMC physically impregnated with bis(2-ethylhexyl) phosphate extractant as a microcolumn and demonstrated separation of Eu^{3+} and Nd^{3+} , proving the utility of metal chelator surface-functionalized OMC for chromatographic, intra-group lanthanide extractions.⁴ To gain a more fundamental

understanding on the binding of metals with *f*-element extractants physically adsorbed on OMC, a different thoroughly investigated liquid-liquid phase chelator was selected.

The dynamics of N,N,N,N-tetraoctyldiglycoamide (TODGA) as a trivalent lanthanide and actinide chelator is well known, as it is used extensively in nuclear fuel reprocessing in ALSEP (Actinide Lanthanide SEparation),⁵ EURO-GANEX,⁶ and innovative-SANEX processes.⁷

Apart from liquid-liquid extractions, TODGA heterogenized by physical adsorption onto a polymeric ester-based resin (Amberchrom GC71) is a commercially available *f*-element adsorbent. Similarly, TODGA can be adsorbed onto OMC and used to sequester actinides. This is made possible by the abundant hydrophobic-hydrophobic interactions between the TODGA octyl chain and OMC surface. Since OMC is lipophilic, utilizing it as an acidic aqueous adsorbent brings about wettability issues, making it prohibitive to initial water contact for many hours. Thus, the addition of a wettability agent is necessary to improve the OMC hydrophilicity and promote water contact. The molecule 2-octanol, in liquid-liquid extractions, acts as a wettability agent for TODGA, by introducing a secondary hydroxyl juxtaposed with the TODGA octyl tails. Concomitantly, alcoholic diluents prevent aggregation of TODGA molecules. In the TODGA OMC system, 2-octanol improves wettability throughout the material and also acts as a TODGA dispersant.⁸

B.2 Probing Eu³⁺ Uptake on TODGA Modified OMC

To understand the impact of pore confinement and phase modifier on heterogeneous actinide sequestration, a series of OMC materials with 5 nm pore diameters loaded with varying wt. % of TODGA and 2-octanol were fabricated. Also, a commercial resin impregnated with TODGA and TODGA/2-octanol supplied by Eichrom Technologies (Amberchrom GC71) was assessed because the resin material possesses large, 25 nm pores, where pore confinement effects are

assumed negligible. To probe the sub-nanometer scale of molecular interactions of Eu^{3+} , TODGA, and material surfaces, synchrotron beamline measurements were conducted at beamline 12-ID-B (small-angle X-ray scattering, SAXS, and wide-angle X-ray scattering, WAXS) of the Advanced Photon Source at Argonne National Laboratory. The X-ray analyses were performed on the adsorbent materials before and after contact with different amounts Eu^{3+} . The SAXS and WAXS data both displayed notable differences between OMC and resin materials, irrespective of 2-octanol addition. The SAXS profile of TODGA and TODGA/2-octanol modified OMC, at highest Eu^{3+} uptake, exhibited diffraction peaks (0.31 \AA^{-1} , 0.289 \AA^{-1}) indicating a non-crystalline to crystalline phase transformation of Eu within the OMC pores (Figure 2.1). The diffraction profile originating for the high Eu^{3+} loading, indicated by the dark traces, is only present for the confined TODGA OMC system, whereas no such peak pattern is observed for the TODGA GC71 resin material. Another SAXS study showed similar behavior of polyoxoanion complexes in mesoporous carbon scaffolds.⁹ The scattering profiles of Eu-loaded TODGA resins were devoid of diffraction features, with only a correlation peak identified for the resin with highest Eu^{3+} uptake.

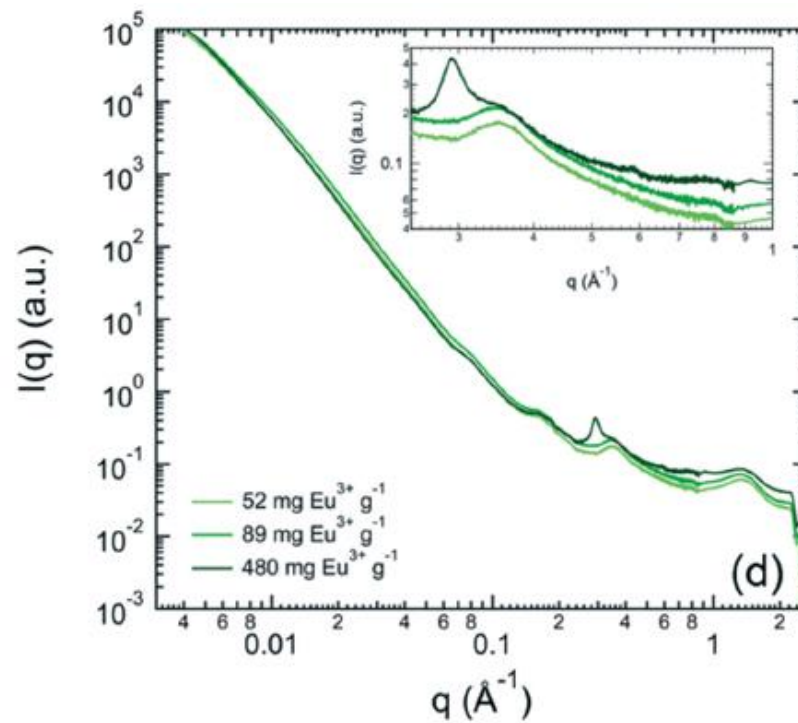
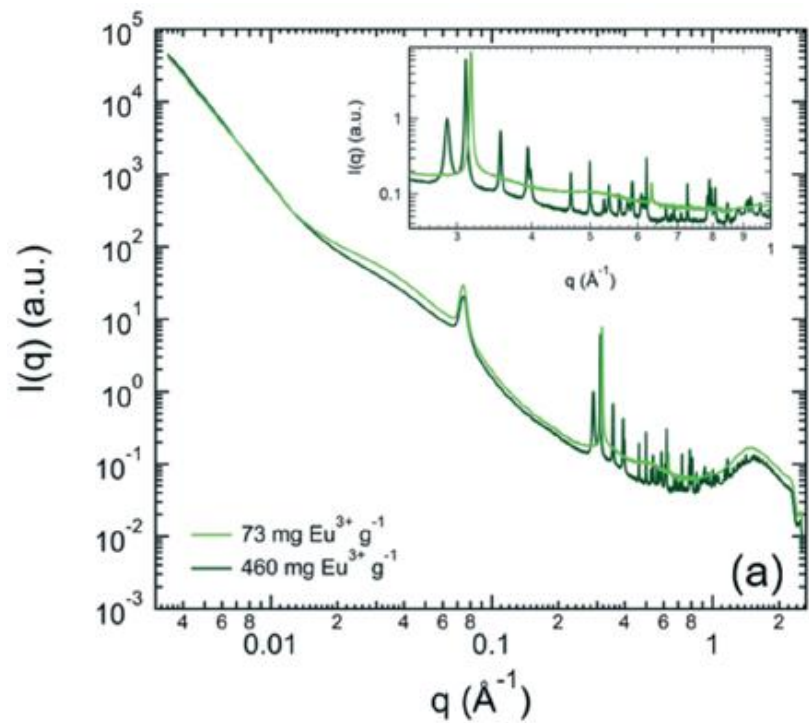


Figure B.1. SAXS profiles for 34 wt.% TODGA OMC (left) and 40 wt.% TODGA GC71 commercial resin (right).

The microcrystalline-like Eu^{3+} domains observed for functionalized OMC materials are confidently ascribed to the confinement imparted by the mesoporous structure, whereas the functionalized resins comprised pores which were too large to induce crystal formation. This exciting observation is a first step towards improving solid-liquid extraction technologies, where pore size-tuned materials could be developed to selectively crystallize a select cation from a mixed solution.

It would be useful to understand the minimum pore dimension which results in the microcrystallization-like phenomena observed for 5 nm pore OMC. Another interesting comparison could be made between mesoporous materials with similar pore dimensions, but different surface chemistries. There are examples of OMC-polymer composites, where OMC scaffolds are enshrouded by a polymer coating, covering both pore surfaces and particle exterior. However, not all polymers are suited for mesopore infiltration. If the conditions for infiltrating OMC pores with a monomer and initiator for a given polymer allow for the polymerization to proceed such that a surface coating is obtained; otherwise, aggregations of polymers can occlude pore entrances and exclude internal surface area. So, if the synthetic conditions permit, the polyester of Amberchrom GC71 could conformally coat OMC to create a resin-like material with ordered mesoporous structure. Furthermore, it is not clear whether the linearly aligned OMC pore structure promoted the SAXS observed crystal-like domains or if the pore dimensions alone facilitated the crystallization. Since other, less costly mesoporous carbons exist, it could be useful to understand the differences between Eu^{3+} crystallization in OMC and disordered mesoporous carbon solids. Lastly, given the time limitations in collecting synchrotron beamline data, the study of TODGA/2-octanol on OMC and Amberchrom CG71 resin was only possible for Eu^{3+} complexation. An obvious future direction could determine whether the pore

confinement crystallization effect is reflected with other f-element extractant molecules, such as P,P'-di(2-ethylhexyl)methanediphosphonic acid (DIPEX) or octylphenyl-N,N-diisobutyl carbamoylphosphine oxide (CMPO) commercially employed on resins similar to Amberchrom GC71.10, 11 The 2-ethylhexyl moiety on DIPEX and octyl chain on CMPO are the same functionality found on HDEHP and TODGA, respectively, so these extractants are likely to physisorb strongly onto OMC.

B.3 Towards the Covalent Grafting of f-Element Extractants

While the physical adsorption of extractants onto porous supports is the state-of-the-art for solid-liquid extractions, the long-term recyclability of these adsorbents is predicted to be lesser than that of materials with covalently-bonded extractants due to leaching. The funding for research on TODGA/2-octanol functionalized OMC materials with Dr. Erin Bertelsen terminated following the SAXS publication. A low hanging fruit for developing covalently-modified OMC surfaces with an extractant such as *N*-(2-hydroxyethyl)ethylenediamine-*N,N,N'*-triacetic acid (HEDTA).¹² Utilizing the organolithium mediated functionalization, there are two viable synthetic pathways to achieve covalent linkages between HEDTA and OMC. One possible synthesis starts with lithiated OMC (Figure 2.2), is relatively simple compared to the numerous transformations/purifications required in the HEDTA bromination synthetic pathway (Figure 2.3). Synthetic hurdles for steps beyond ethylamine functionalization could include: 1) Uncontrolled reaction propagation between the haloethylamine and EtNH₂@OMC, resulting in polymeric ethyleneamine chains rather than ethylenediamine@OMC, 2) Incompletely reacting all available amine groups with chloroacetic acid in the final step, and 3) unambiguously characterizing the surface functionality of the material after each synthetic step.

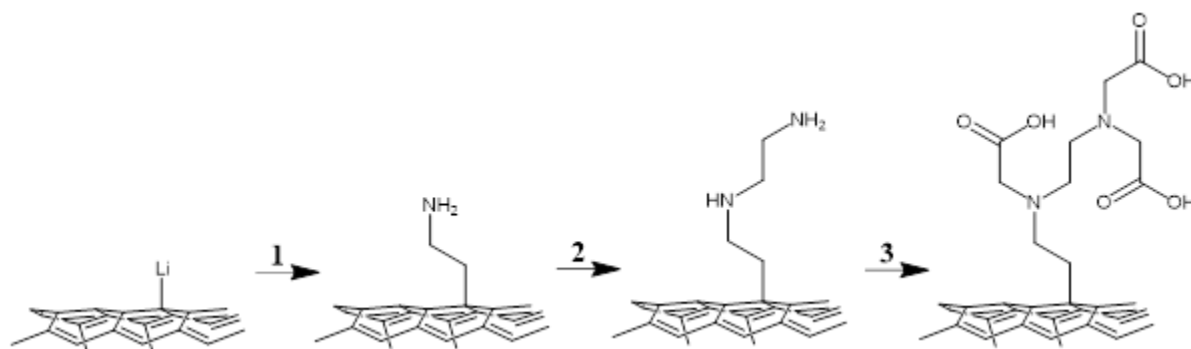


Figure B.2. Covalent attachment synthetic route for covalently tethering HEDTA onto OMC starting with lithiated OMC. (1) Attachment of bromoethylamine, (2) Reaction with bromoethylamine, and (3) reaction with chloroacetic acid.

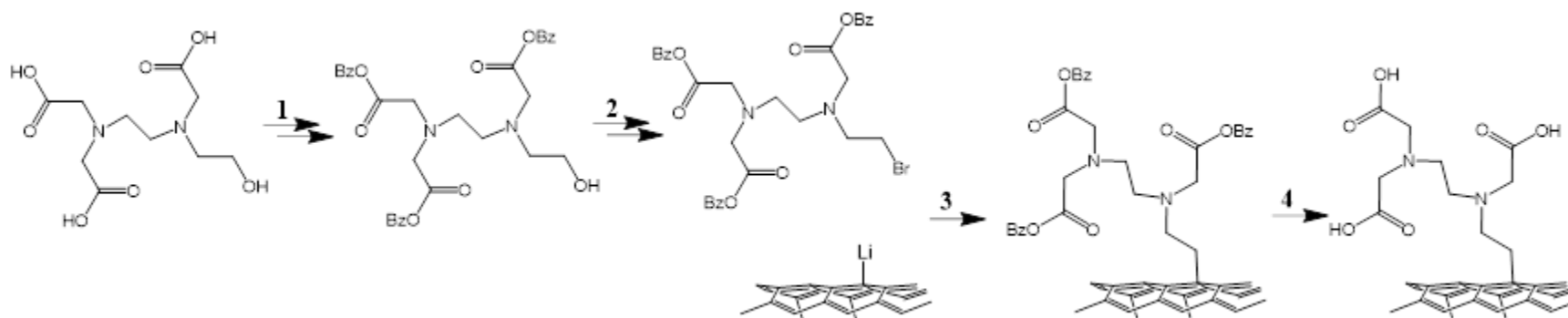


Figure B.3. Covalent attachment of HEDTA by means of brominated and carboxyl-protected HEDTA with lithiated OMC. (1) Protection of carboxylic acids with benzyl (Bz) functional group and purification, (2) bromination of Bz-protected HEDTA and purification, (3) reaction with lithiated OMC, and (4) chemical deprotection of Bz group.

The bottom synthetic route is rather tedious compared to the top pathway, primarily due to the need to add protecting groups to the acetate pendants on HEDTA in order for the bromination conditions to only transform the primary hydroxyl group and not brominate the carboxyl species too. Benzyl-protected carboxylic acids are recalcitrant towards strong base nucleophilic attack and should allow for the brominated, Bz-protected HEDTA to only react at the electrophilic primary carbon on the bromoethyl group.¹³ The protection and bromination steps would also require small molecule purification (i.e. column chromatography), but would benefit by the ability to ascertain the product structure by solution state ¹H/¹³CNMR. Also, if the brominated, protected HEDTA is sufficiently soluble in diethyl ether, then the organolithium grafting onto OMC will be viable.

Going forward with the pursuit of covalently enriching OMC materials underwent a change in scope with respect to the material's final application, going from *f*-element separation to heterogeneous catalysis, with the ultimate manifestation of developing surface reactivity fundamentals under a range of pH conditions.

B.4 References

1. Ryoo, R.; Joo, S. H.; Jun, S.; Tsubakiyama, T.; Terasaki, O., 07-O-01 - Ordered Mesoporous Carbon Molecular Sieves by Templated Synthesis: the Structural Varieties. In *Studies in Surface Science and Catalysis*, Galarneau, A.; Fajula, F.; Di Renzo, F.; Viedrine, J., Eds. Elsevier: **2001**; Vol. 135, p 150.
2. Huang, R. X.; Li, X.; Wu, Y. X.; Huang, Z. S.; Ye, H. Y.; Niu, Y. L.; Li, L. S.; Wang, J., A Study on the Adsorption Behaviors of Three Hydrophobic Quinolones by Ordered Mesoporous CMK-3. *Chemosphere* **2022**, 294.
3. Jones, K. L.; Matthews, G. P.; Laudone, G. M., The Effect of Irradiation and Radiolytic Oxidation on the Porous Space of Gilsocarbon Nuclear Graphite Measured with Mercury Porosimetry and Helium Pycnometry. *Carbon* **2020**, 158, 256-266.
4. Bertelsen, E. R.; Deodhar, G.; Kluherz, K. T.; Davidson, M.; Adams, M. L.; Trewyn, B. G.; Shafer, J. C., Microcolumn Lanthanide Separation using Bis-(2-ethylhexyl) Phosphoric Acid Functionalized Ordered Mesoporous Carbon Materials. *J Chromatogr A* **2019**, 1595, 248-256.

5. Gelis, A. V.; Lumetta, G. J., Actinide Lanthanide Separation Process-ALSEP. *Ind. Eng. Chem. Res.* **2014**, *53* (4), 1624-1631.
6. Taylor, R.; Carrott, M.; Galan, H.; Geist, A.; Hères, X.; Maher, C.; Mason, C.; Malmbeck, R.; Miguiritchian, M.; Modolo, G.; Rhodes, C.; Sarsfield, M.; Wilden, A., The EURO-GANEX Process: Current Status of Flowsheet Development and Process Safety Studies. *Procedia. Chem.* **2016**, *21*, 524-529.
7. Magnusson, D.; Geist, A.; Malmbeck, R.; Modolo, G.; Wilden, A., Flow-sheet Design for an Innovative SANEX Process using TODGA and SO-Ph-BTP. *Atalante 2012 International Conference on Nuclear Chemistry for Sustainable Fuel Cycles* **2012**, *7*, 245-250.
8. Bertelsen, E. R.; Kovach, N. C.; Trewyn, B. G.; Antonio, M. R.; Shafer, J. C., Electrochemical Reduction of Europium(III) using Tetra-octyl Diglycolamide Functionalized Ordered Mesoporous Carbon Microelectrodes. *J. Mater. Chem. C* **2020**, *8* (20), 6689-6700.
9. Juan-Alcañiz, J.; Goesten, M.; Martinez-Joaristi, A.; Stavitski, E.; Petukhov, A. V.; Gascon, J.; Kapteijn, F., Live Encapsulation of a Keggin Polyanion in NH-MIL-101(Al) Observed by Time Resolved X-ray Scattering. *Chem. Commun.* **2011**, *47* (30), 8578-8580.
10. Horwitz, E. P.; Chiarizia, R.; Dietz, M. L.; Diamond, H., Separation and Preconcentration of Actinides from Acidic Media by Extraction Chromatography. *Anal. Chim. Acta* **1993**, *281* (2), 361-372.
11. Horwitz, E. P.; Chiarizia, R.; Dietz, M. L., DIPEX: A New Extraction Chromatographic Material for the Separation and Preconcentration of Actinides from Aqueous Solution. *React. Funct. Polym.* **1997**, *33* (1), 25-36.
12. Eddy, M. A.; Picayo, G. A.; Jensen, M. P., Characterization of a Ternary Neodymium-HEDTA-Citrate Complex in the Actinide Lanthanide Separation Process. *ACS Omega* **2022**, *7* (17), 15005-15015.
13. Protection for the Carboxyl Group. In *Greene's Protective Groups in Organic Synthesis*, **2014**; pp 686-836.

APPENDIX C RAW DATA FOR PREVIOUS CHAPTER MEASUREMENTS

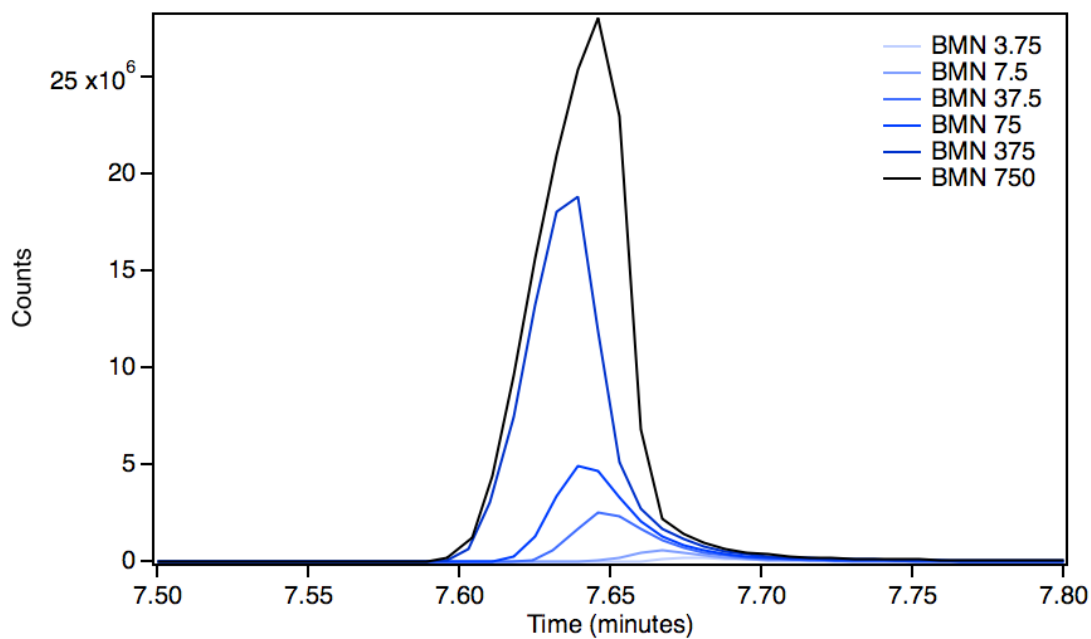


Figure C.1. Gas chromatography traces used for the calibration curve of benzylidenemalononitrile (BMN).

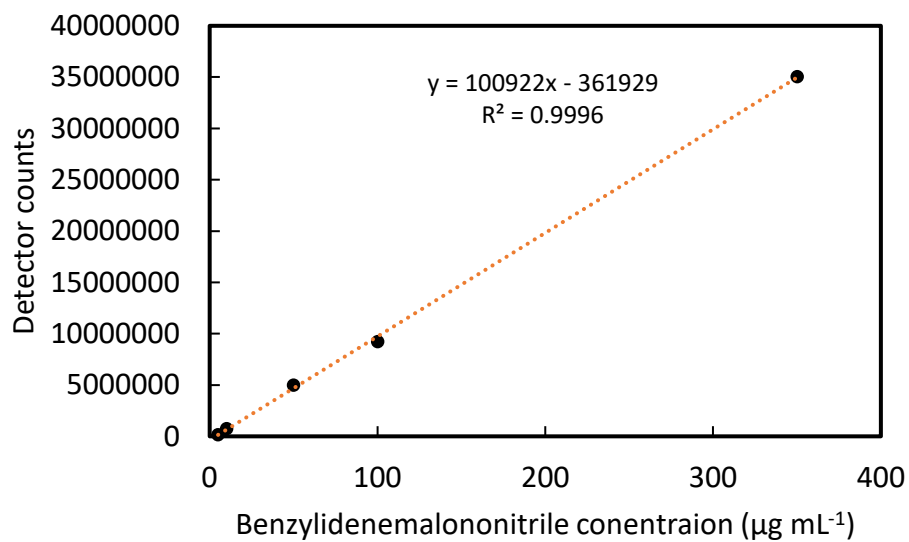


Figure C.2. Calibration curve for BMN by gas chromatography.

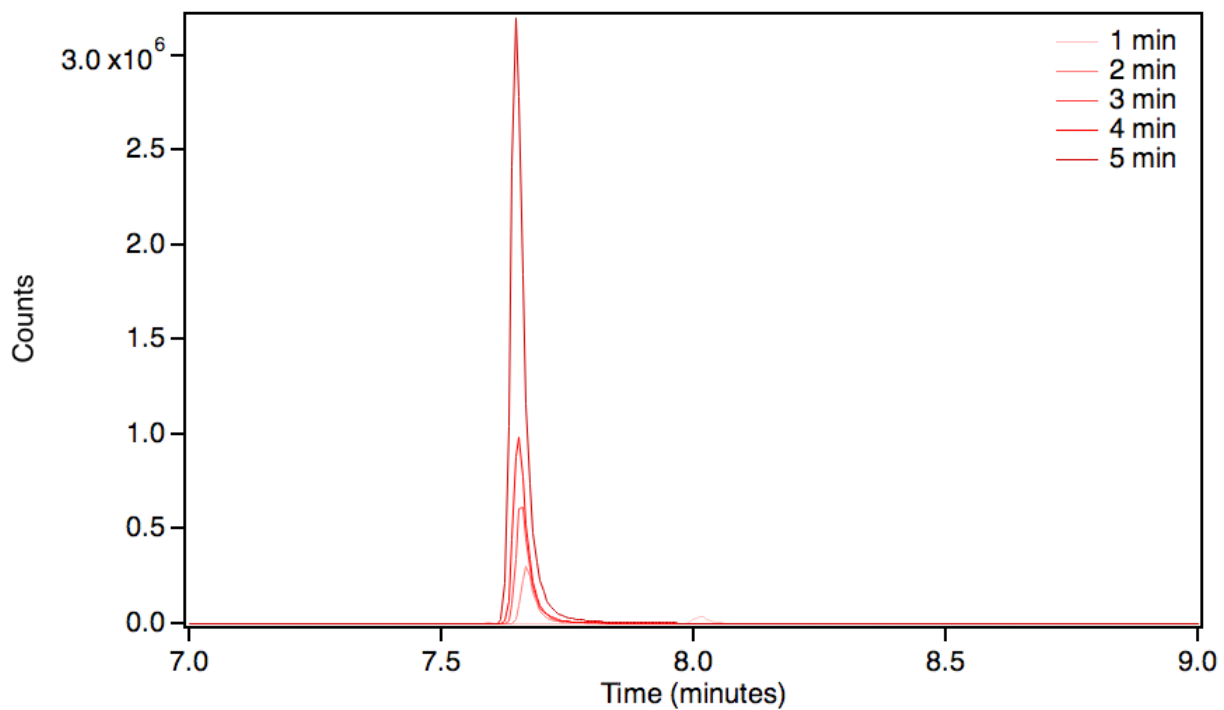


Figure C.1. First round of BMN product formation for the Knoevenagel condensation (associated with Figure 2.11).

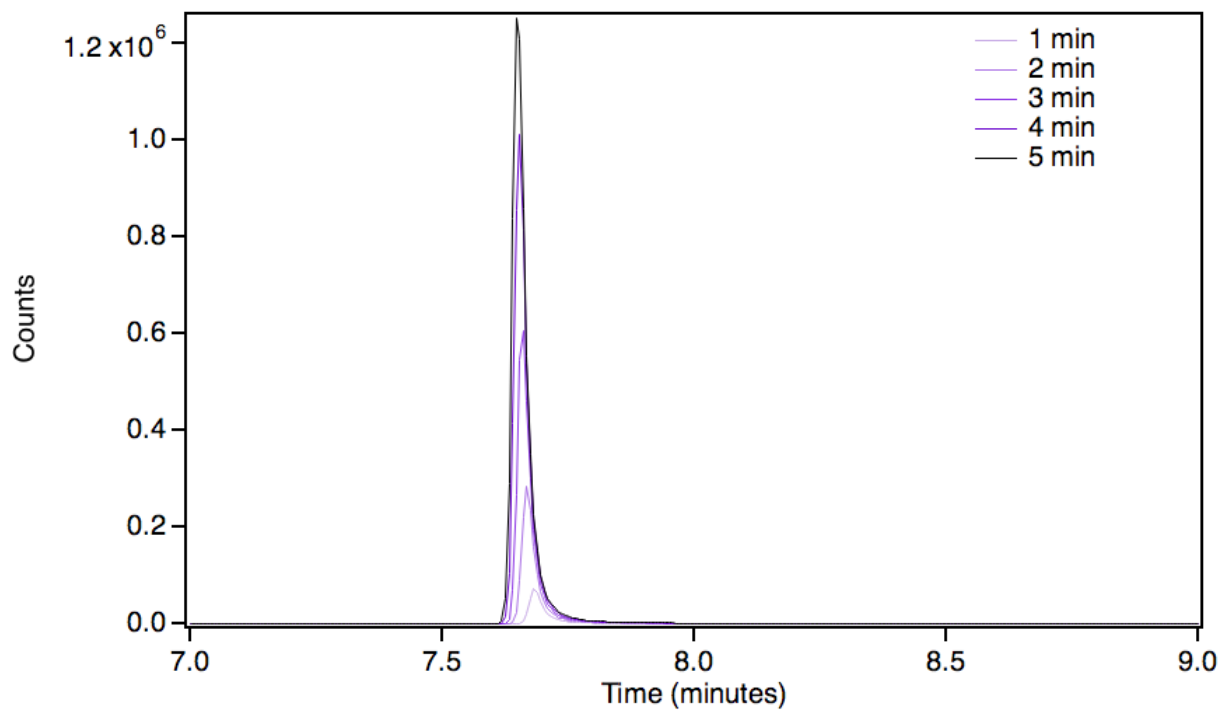


Figure C.2. Second round of catalyst use for the Knoevenagel condensation reaction (associated with Figure 2.11).

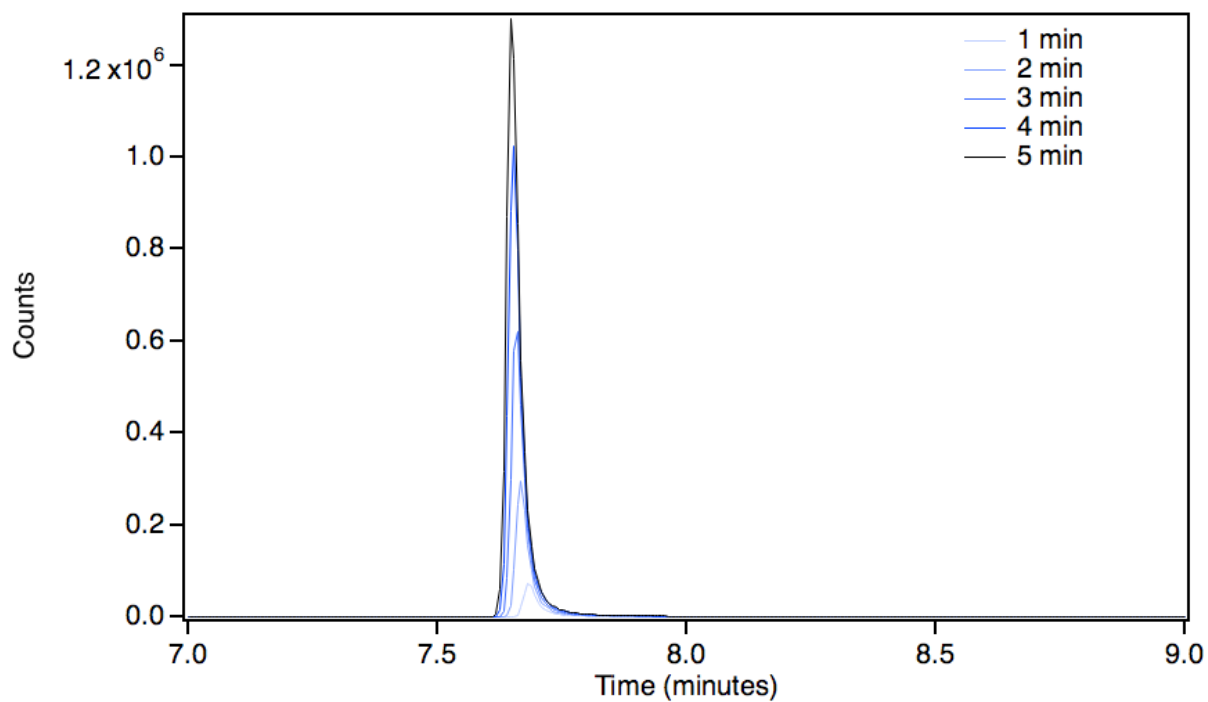


Figure C.3. Evolution of BMN over time for the third round of catalyst reuse (associated with Figure 2.11).

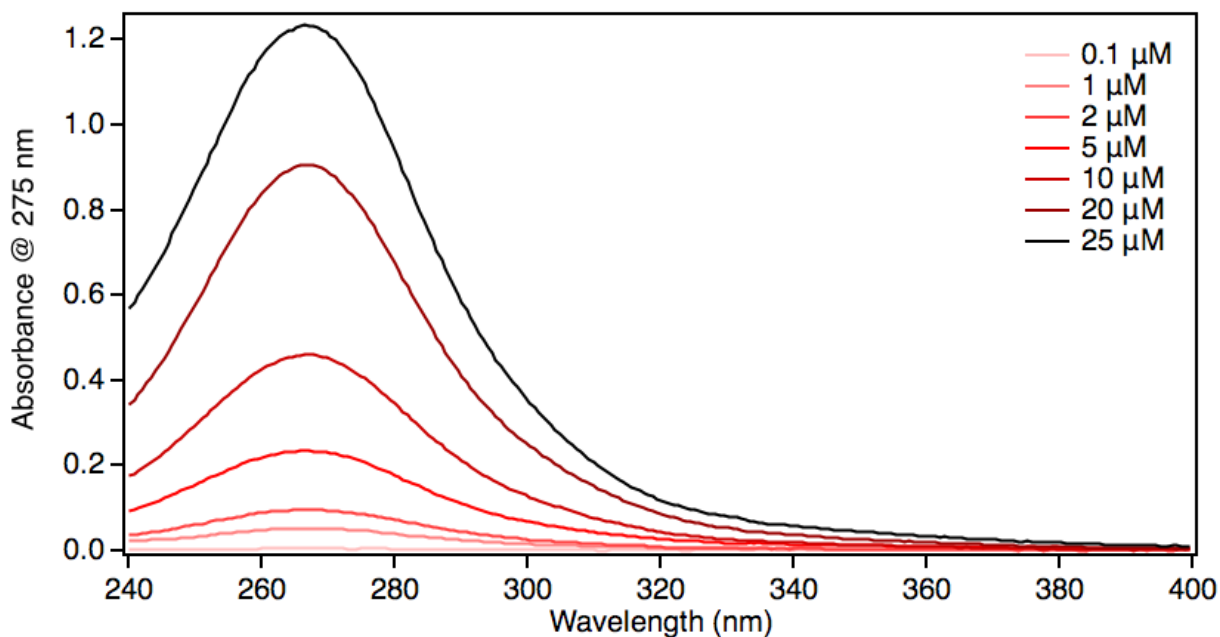


Figure C.4. Raw UV/Vis 4-nitrobenzaldehyde assay calibration curve data.

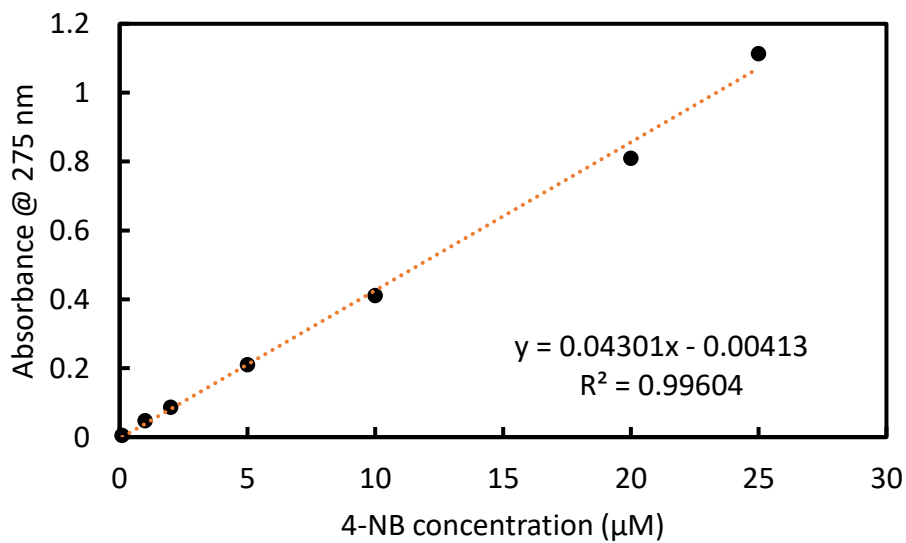


Figure C.5. Processed calibration curve for the 4-NB assay.

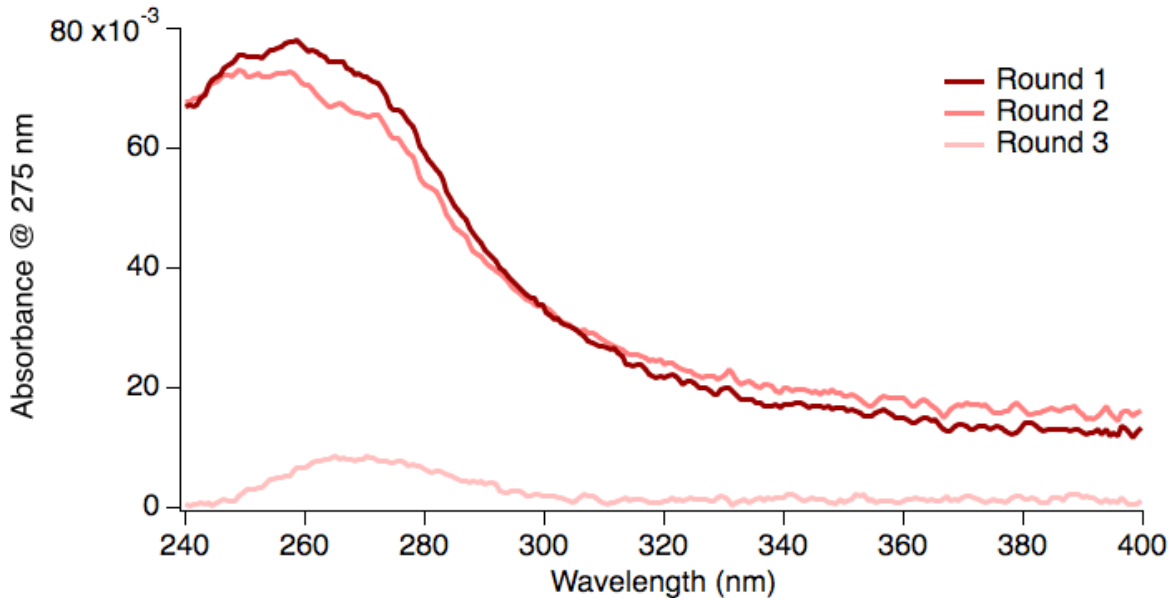


Figure C.6. Representative sample data for the 4-NB assay used to compute surface -NH_2 amounts. The absorbance difference between the 275 nm peak maximum and the baselined absorbance at 400 nm was taken to quantify 4-NB amounts present. Then, the amount detected ($\mu\text{g mL}^{-1}$) was converted into an amine density by dividing that number by the amount of material used in each trial (mg mL^{-1}) to yield accessible -NH_2 ($\mu\text{g mg}^{-1}$, $\mu\text{mol g}^{-1}$).